Revista Científica

VERITAS

Vol. 4
Nº 1 - 2016

Universidade Nacional Timor Lorosa'e (UNTL)

Edição Especial

Engenharia Ciências e Tecnologia

Versão Inglês

VERITAS

Revista Científica da Universidade Nacional Timor Lorosa'e

VERITAS

Revista Científica da Universidade Nacional Timor Lorosa'e

Index

Editorial

Message from Rector of Universidade Nacional Timor Lorosa'e

Message from Dean of Faculty of Engineering Sciences and Technology

Message from Chief Advisor for JICA-CADEFEST Project

Message from Vice Dean for Research and Cooperation

Massage from Editor Chief

Message from Technical Editor

Message from the Rector

I would like to extend my heartfelt congratulations to the inaugural issue of the Special Edition of the VERITAS by the Faculty of Engineering, Science and Technology. It is very vital for us to have the research works and dissemination to our society.

As per our Constitution of Democratic Republic of Timor-Leste, Section 59 [Education and Culture] indicates "… The State should ensure the access of every citizen, in accordance to their abilities, to the highest levels of education, scientific research and artistic creativity.", this kind of research and educational activities are relevant and should be encouraged to be conducted periodically.

According to UNTL strategic plan for 2011-2020, one of our Mission is also to accelerate scientific pursuits by creating multilateral synergies in contemporary fields to realize our vision "Centre of Excellence for Higher Education in Timor-Leste". I believe this research publication activity is in accordance with our vision.

The VERITAS plays the important role to connect the engineering research field's network in Timor-Leste and also among other nations. I expect the Faculty of Engineering, Science and Technology will continue to issue this research journal to display our ability and the latest outcomes of researches as a research oriented university in Timor-Leste.

Last but not least, I would like to express great appreciation towards the support from Japan International Cooperation Agency (JICA) to improve research activities in the faculty of engineering, science and technology. Especially, thanks to professors from Japanese universities, for reviewing the manuscripts, elevating the quality of this Special Edition of the VERITAS to a standard research journal.

Professor Doutor Francisco Miguel Martins
Rector
Universidade Nacional Timor Lorosa'e (UNTL)

Message from the Dean

On behalf of the Faculty of Engineering, Sicence and Tehnology, I am very delighted to welcome you to read the first Issue of Special Edition of the "VERITAS". I am very proud that we have the lecturers who conducted high standard quality researches. This Especial Edition of the VERITAS can illustrate our faculty's capablities as a profile.

One of our Faculty's mission is to develop research activities in the areas of technology and informatics related to ecological sustainability. Through the research activtites we can carry out the mission of our faculty to contribute to the society.

With this Especial Edition of the VERITAS we expect to exchange the researches from institutions in Timor-Leste with other international academic institutions in the world, so that people can be aware of our capablilities and the outcomes in the Hera campus of the National University of Timor-Lorosa'e. This will help us to build more close collaborations with other universities and industries to develope our nation, Timor-Leste.

To improve the quality of VERITAS, we all take maximum effort to conduct significant researches.

Your coments and advice for the Special Edition of the VERITAS are always welcome!

Mariano Renato M. da Cruz
Dean
Faculty of Engineering, Science and Technology
Universidade Nacional Timor Lorosa'e

Message from the Chief Advisor, JICA CADEFEST Project

I heartily celebrate the first publication of the Special Edition of the "VERITAS" for engineering fields from National University of Timor-Lorosa'e.

JICA, "Japan International Cooperation Agency", has supported the Faculty of Engineering, Science and Technology for capacity development since 2001. At the moment, JICA is implementing the project for the capacity development of the Faculty of Engineering, Science and Technology, National University of Timor-Lorosa'e. One of the project purposes is to improve the research abilities of the teaching staff. The researches which are conducted by teaching staff have received some support from the professors of the Japanese supporting universities. Some of the research results have been published on the international journals and proceedings of the symposium and the academic seminars. These valued outcomes are produced not only by the effect of the instruction by the Japanese professors but also by the teaching staff efforts. The motivation to conduct the research is rising among teaching staff recently, since research activity is one of their missions in the university.

Eleven papers are published on the Special Edition of the "VERITAS" for engineering fields of UNTL to reveal their research results officially. This is the publication of the first bulletin as the Faculty of Engineering, Science and Technology, and it is the first to commemorate.

In the near future, I expect that researches by many teaching staffs will be even more actively conducted, and the research level will be promoted to the international level.

Dr. Hidehiko Kazama

Chief advisor
The Project for the Capacity Development
The Faculty of Engineering, Science and Technology,
National University of Timor-Lorosa'e (CADEFEST Project)

Message from Vice Dean for Research and Cooperation

With this first issue, I am pleased to announce the launch of the Special Edition of the VERITAS for engineering fields, and extend a warm welcome to the readers and the authors. In addition, I would like to express my sincere gratitude to JICA CADEFEST project for their continuous support to the Faculty of Engineering, Science and Technology, UNTL. A special thanks go to Japanese professors as the reviewers of the papers whose advice and recommendations insured the high quality of the papers in this first issue.

The role and scope of the engineering profession are vital in Timor-Leste. Engineering researchers will be required to perform increasingly more complex tasks of creativity to develop our nation. Our VERITAS is a step towards responding to the above challenges by future directions of engineering in Timor-Leste.

The eleven articles in the first issue cover a diverse scope and a broad spectrum of topics. The first four papers are from Mechanical Engineering Department covering Computer Aided Engineering (CAE), fluid mechanics, machinery engineering and electricity industry. The succeeding three papers are focusing on concrete engineering, material engineering and road engineering from Civil Engineering Department. The last four papers are research articles dealing with aspect of solar panels, LSI, Image analysis and DC-DC converter from Electronics in Electric Engineering Department.

As the vice dean in charge of research and cooperation, I would like to thank the authors of the papers for enabling us to launch the Special Edition of the VERITAS. In addition, I would like to appreciate that the faculty recognises to endeavour to deliver the best version of VERITAS annually.

Finally, I welcome any suggestions for improving the quality and the usefulness of the next issues of VERITAS for engineering fields.

Ruben Jerónimo Freitas

Vice Dean for Research and Cooperation
Faculty of Engineering, Science and Technology
Universidade Nacional Timor Lorosa'e

Message from the Editor-In-Chief

This Special Edition of the VERITAS brings together eleven articles of researchers from Timor-Leste and Japan. It's an issue that presents the research results of researchers from the Faculty of Engineering Science and Technology. The works published here are of academic character and have their relevance to the understanding of "technical sense" of what is called "science engineer in action" with technology.

The engineering involves the application of scientific and mathematical to design and operate objects, systems and processes to help us solve problems or achieve goals. These general processes involve the development of new technologies. Although we would normally associate the technology-word things as microchip and satellites, actually, the concept is applicable to a wide variety of innovations. From the simplest tool (like the fishing rod of a chimpanzee ants), to practical problem solving (such as adding fluoride to water to help prevent tooth decay), everything we build or do, that change the natural world, to achieve our purposes is technology.

The engineering and the development of new technologies are closely linked to science. We use many technologies in scientific studies, and scientific knowledge helps engineers do their jobs and develop new technologies.

Vicente Paulino
Diretor da Unidade de Produção e Disseminação do Conhecimento
Universidade Nacional Timor Lorosa'e

Message from Technical Editor

It is my honour to welcome the Special Edition of the VERITAS for the Faculty of Engineering, Science and Technology. The publishing of the journal is not only for upgrading the quality of researchers, but also to strengthen academic networking among researchers in Timor-Leste and beyond the country.

On behalf of the Technical Editor, I thank the researchers from the Faculty of Engineering, Science and Technology, UNTL for submitting the significant outcomes of their researches. These manuscripts are our profiles and valued assets for the Faculty of Engineering, Science and Technology, UNTL.
In addition, I am very grateful to the professors from the Japanese Supporting Universities such as Nagaoka University of Technology, Yamaguchi University and Gifu University, as reviewers, for their efforts and kind contributions to edit this special edition.

Last but not least, I would also like to express my sincere appreciation to JICA CADEFEST Project which supported the Faculty of Engineering Science and Technology in the field of education, research and faculty management. Especially, this Special Edition of VERITAS was initiated by CADEFEST Project. We hope this publication will continue with and help develop the Faculty of Engineering, Science and Technology, UNTL. Thank you.

Benjamim Hopffer Martins
Technical Editor
Senior Lecturer, Department of Civil Engineering,
Faculty of Science and Technology
Universidade Nacional Timor Lorosa'e

Analysis of Stress Singularity in 2-Dimensional Structures with Edge Modification

Joviano Antonio da Costa

Department of Mechanical Engineering

Universidade Nacional Timor Loro Sa'e

Abstract: Many investigations on two-dimensional joints have been carried out theoretically and experimentally. However, interface strength in joints with straight and modified edges is focused on the comparison in this investigation. Stress singularities will be investigated and the stress singularity of straightedge is compared with that of modified edge. The microdroplet test is recommended for carrying out the push out test to estimate the interface strength and conducting the investigation in experimentally and theoretically.

1. Introduction

Many investigations on joints made of materials with different properties have been conducted in order to utilize effectively the features of each material. Joints composed of metal and ceramics have been used widely in electric devices and mechanical parts. From previous studies, it is known that failure of joints occur near the edge of interface and the reliability of the materials decreases due to the singular stress fields at the intersection point of the free surface and the interface. Many cracks exist in ceramics, and in fact, fracture and delamination occur often at the vertex of joints. Such problems cause the reduction of reliability of joints; therefore many studies on the stress singularity have been carried out theoretically and experimentally. Almost all these studies are focused on two-dimensional stress singularity ([1-5]).

2. Analysis method

Free-edge stress singularities in dissimilar material joints were illustrated in Figure 1(a). The microdroplet test was used to determine the interfacial shear strength of steel and aluminum. The microdoplet test was shown as in Fig. 3. The test specimen was set up and the force dropped down to push out the joint specimen. Significant stress concentrations (caused by the free-edge stress singularity) were observed at the corner of bi-material. It is clarified that the stress singularity is a mathematical phenomenon encountering in elastic stress solutions. On the other hand, the stress concentration is a physical phenomenon and refers to stress amplifications, which are induced by the stress singularity in this investigation. The existence of stress singularities for some specific bi-material corners or edges was shown by Bogy [1], Hein and Erdogan [3], William [6], Genested and Hallstrom [7], Klingbeil and Beuth [8], Labossiere et al. [9]. The asymptotic stress fields near the corner in bi-materials can be expressed by:

$$\sigma_{ij}(r,\theta) = \sum_{k=0}^{N} r^{-\lambda_k} K_k f_{ijk}(\theta) \quad (i,j=1,2,3) \quad (1)$$

where $f_{ijk}(\theta)$ is an angular function and K_k is also known as the "stress intensity factor". Although the fracture mechanics terminology "stress intensity factor" is used in interfacial mechanics to characterize a similar stress singularity problem. For an interfacial fracture problem (assuming initial de-bonding), it should be noticed that the stress singularity at a crack tip is intrinsic and cannot be removed. However, the stress singularity in the interfacial strength (assuming perfect bonding) can be reduced through an appropriate material design; a key issue in this investigation.

The order of stress singularity λ can be a complex number. When the value is in the range of $0<\text{Re}(\lambda)<1$, the theoretical stress values will then become infinite as r (define in 1(b)) approaches zero. This lead to a problem referred to as the "stress singularity problem". However, if λ has a non-positive real part then, the stress singularity disappears.

Bogy [1] found that the order of stress singularity was purely determined by the material properties and the two joint angles of the bimaterial corner θ_1 and θ_2 (define in Figure 1(b)). Generally, the mismatch of the material properties can be expressed in terms of the Dundur's parameters α and β - two dimensionless parameters computed from four elastic constants of two bonded materials [10].

$$\alpha = \frac{\mu_1 m_2 - \mu_2 m_1}{\mu_1 m_2 + \mu_2 m_1} \quad \beta = \frac{\mu_1(m_2-2) - \mu_2(m_1-2)}{\mu_1 m_2 + \mu_2 m_1} \quad (2)$$

where μ_1 is shear modulus of material 1, μ_2 is shear modulus of material 2, ν is the Poisson's ratio, $m=4(1-\nu)$ for plane strain, and $m=4/(1+\nu)$ for generalized plane stress. The order of stress singularity is related to the material and geometric parameters, and is determined by a characteristic equation of coefficients $A(\theta_1, \theta_2, \alpha, \beta, p)$ through $F(\theta_1, \theta_2, p)$:

$$f(\theta_1, \theta_2, \alpha, \beta, p) = A\beta^2 + 2B\alpha\beta + C\alpha^2 + 2D\beta$$
$$+ 2E\alpha + F = 0 \qquad (3)$$

Where $p = 1 - \lambda$. A, B, C, D, E, and F have been defined by Bogy [1].

In the present paper, the strength of joints with different edge angles is estimated from experiment and numerical analysis. It is shown that the failure stress of joint can be improved by applying edge angles to the material.
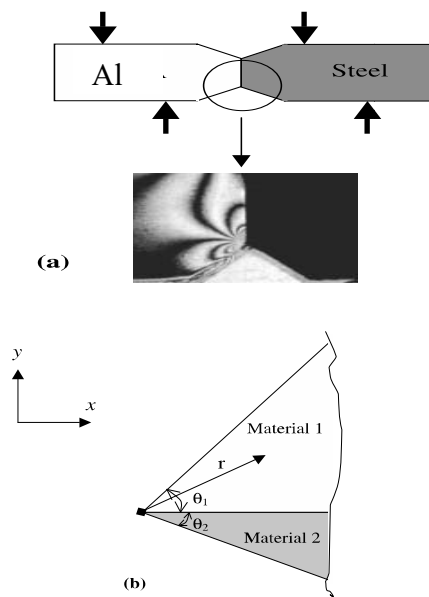

Fig. 1 (a) Bimaterial for analysis, (b) Angular definition of a bimaterial wedge

Experiment
MM~ ~m~

The purpose of this experimental study is to verify that the new edge design is effective in removing the free-edge stress singularity in joints.
Test specimen is illustrated in Fig. 2. The mechanical-digital system was used to record in situ the data during loading process, as shown in Fig. 3. The whole setup consists of a mechanical testing system, a digital caliper and a data processing software (TgAnest). The mechanical testing system includes a TGI-5kN test machine. The digital caliper was used to measure the data development during test. TgAnest software was used to process the data development and recorded it into table as shown in table 1.
Materials for specimen are aluminum and carbon steel. The nominal specimen thickness was 10 mm. A commercial epoxy was used as bonding agent. The special adhesive had two components, A and B. They were mixed before bonding and cured at temperature 100°C for at least 30 minutes. A special fixture was

designed to bond these specimens. The alignment of these specimens was carefully examined during the bonding process.
In experiment testing procedure, several testing materials were used. The average results of the experiment test then collected and determined as maximum test results as shown in table 1. Experiment results showed that the strength of material with 45° of edge angle was higher than that of straight edge.

Two types of specimens were design and prepared for comparison, as seen in Fig. 2. The straight edge specimen was treated as the baseline for comparisons. All the designs were analyzed using the finite element method (FEM). And our focus was on the modified joint specimen.
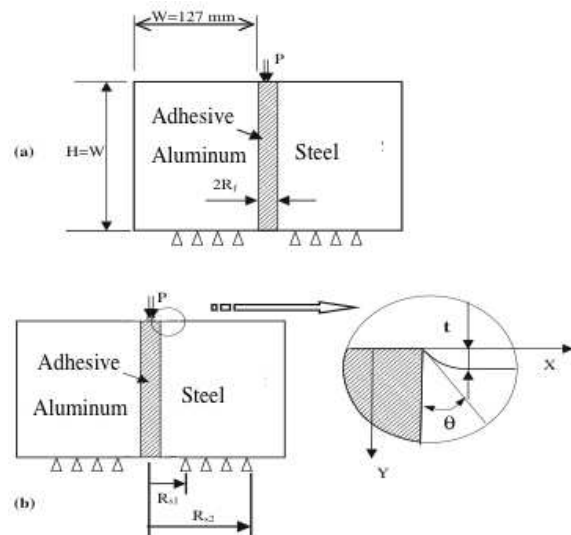
Fig. 2 Microdroplet test for push-out specimen (a) baseline straightedge, (b) matrix shaped

The main parameters that are varied in the finite element analysis are (a) the convex extension distance t and (b) the interfacial joining angles. The influence of these geometrical parameters, on the stress distribution at the interface, is illustrated in Figure 4. Owing to the stress singularity at the free edge, failure of the bimaterial specimen always initiates at the specimen edge, rather than at the center of the specimen.

For increasing the edge angle of the joint, the interfacial stress distributions are seen to be smoothening on the interface. From this analysis, we find that the free-edge stress singularity is successfully removed and convex extension distance mainly affects local stress distribution close to the free-edges.
A total of 23,090 elements were used in meshing the shape matrix of specimen and 3671 elements were

used in meshing the model of aluminum steel. Fine mesh was employed in the region where a large stress concentration was expected. The material properties were chosen as E = 71 GPa, υ = 0.33 for aluminum and E = 210 GPa, υ = 0.28 for steel. However, the proposed specimen dimensions may not be accurately machined. It could influence to the accuracy of the stress distributions.

4. Comparison of traditional Strength with Interfacial Strength Measurements

The strength is defined from the failure stress of the specimen with a uniform stress state, across the cross section.
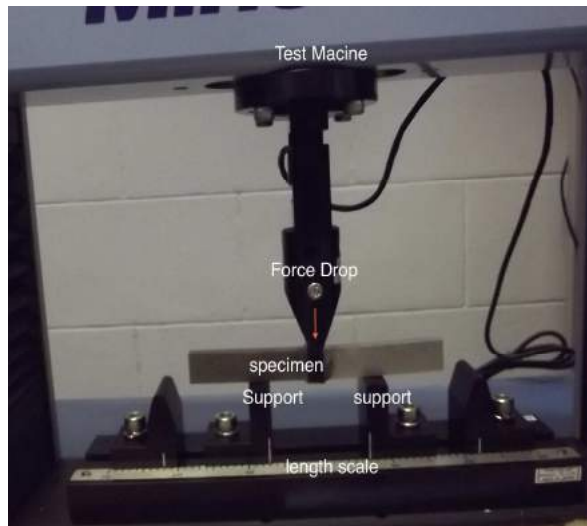
Fig. 3 Experimental setup of a mechanical system to record the stress development during loading process.

As discussed before, the measurement of the interfacial strength is quite complicated because of the possible stress singularity and the highly non uniform interfacial stress distribution. Therefore, any interfacial strength of experiment must be carefully examined.

For a specimen fabricated from two dissimilar materials shown in Fig. 2(b), the shear stress distribution across the interface is not uniform according to previous theoretical analysis and experimental verification.

The asymptotic stress field at the bimaterial corner is related to $r^{-\lambda}$.

Table 1 Push-out test of Al-Fe joint with straightedge and modified edge.

Specimen Al - Fe	Joint Angles	Max. Compression Strength (MPa)	Max. displacement (%)	Elastic Ratio (MPa)	Specimen Thickness (mm)
1	45°-45°	12.44	8.166	231	10.9
Standard deviation		2.187	1.038	33.69	
2	90°-90°	10.43	1.917	934.4	10.9
Standard deviation		8.293	1.25	31.1	
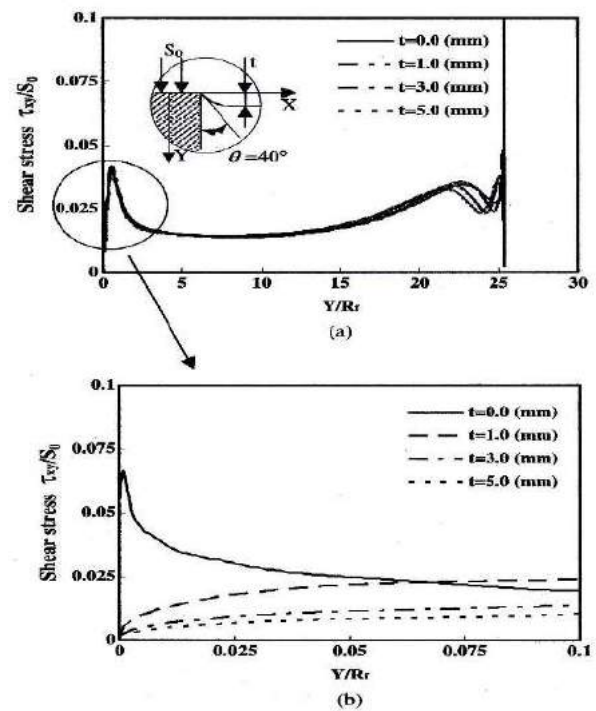
Fig. 4 Finite element analysis: the influence of various distances on the normalized interfacial shear stress distribution with two fixed joint angles (a) along the whole interface and (b) around one end of the joint (range of applied stress on the model is 5.5 mm).

Two kinds of Al-Fe bi-material specimens, with the same interface area, but different joint angles, should yield the same final failure load, if the interfacial strength is assumed to be indeed a material constant. The influence of the stress state on the failure strength is further illustrated in Fig. 4. It should be noticed that the transverse shear stress states of these two kinds of specimens are quite different.

For the specimen with straight edge shown in Fig. 2(a), the shear stress distribution will be a parabolic distribution and is not uniform. So the final shear failure will generally not initiate from the upper and lower edges of the beam specimen due to a very low shear stress. Owing to the stress singularity at the free-edge, failure of the bi-material specimen always

initiated at the specimen edge rather than at the center in all our earlier experiments [11].

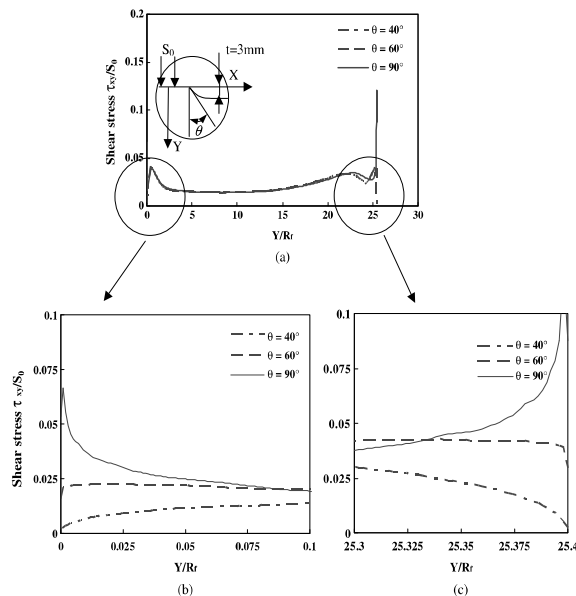**Fig. 5** Finite element analysis: the influence of the matrix joint angle on the normalized interfacial shear stress distribution (a) along the whole interface (b) and (c) around two ends of the model.

Hence, the interfacial strength from the current measurement standard is directly related to the singular stress state and taking into account all initial material defects at the whole interface. In order to measure an intrinsic interfacial strength, a uniform stress distribution across the interface should be created. Thus, all initial defects will have an equal probability of leading to a final failure (breaking the interface). This kind of strength data should be very close to intrinsic tensile strength when the interface is loaded to failure.

5. Conclusion

Experiment results show that the higher stress can be obtained from the edge angle modification of joint structures. The stress of specimen with 45° of edge modification is higher than that of straight edge (without edge modification).

FEM analysis shows that the higher stress singularity occurs for specimen with 90° of edge angle (without edge modification); otherwise the stress singularities decrease for specimen with edge modification as shown in Fig.5.

The analysis results show that both experiment and simulation, edge angles modification were effective to improve joint strength and reduced free edge stress singularities in dissimilar material joint.

References

1. Bogy, D. B. (1971). Two Edge-Bonded Elastic Wedges of Different Materials and Wedge Angles under Surface Traction, *Journal of Applied Mechanics,* 38: 377-386.
2. Dempsey J. P. (1979). Power-Logarithmic Stress Singularities at Bi-Material Corners and Interface Cracks, *Journal of Adhesion Science and Technology*, 9: 253-265.
3. Hein, V.L. and Erdogan, F. (1971). Stress Singularities in a Two-material Wedge, *International Journal of Fracture Mechanics,* 7: 317-330.
4. Koguchi, H. and Muramoto, T. (2000) . The order of stress singularity near the vertex in three-dimensional joints, *International Journal of Solids and Structures,* 37: 4737-4762.
5. Munz, D. and Yang, Y.Y., (1993). Stresses near the edge of bonded dissimilar materials described by two intensity factors, *International Journal of Fracture*, 60: 169-177.
6. William, M. L (1952). Stress Singularities resulting from Various Boundary Condition in Angular Corners in Extension, Journal of Applied Mechanics, 19: 526-528.
7. Genested, J.L. and Hallstrom, S. (1997). Crack Initiation from Homogenous and Bimaterial Corners, *Journal of Applied Mechanics,* 64: 811-818.
8. Klingbeil, N.W. and Beuth, J.L. (2000). On the Design of Debond-resistant Bimaterials, Part I: Free-edge Singularity Approach, *Engineering Fracture Mechanics,* 66, 93-110.
9. Labossiere, P.E.W., Dunn, M.L. and Cunningham, S.J. (2002). Application of Bi-material Interface Corner Failure Mechanics to Silicon/Glass Anodic Bonds, *Journal of Mechanics and Physics of Solids,* 50: 405-433.
10. Dundurs, J. (1969). Discussion, *ASME Journal of Applied Mechanics,* 36: 650-652.
11. Xu, L.R., Rosakis, A.J. and Samudrala, O. (2002). Measurements of Adhesive Tensile and Shear Strengths with the Aid of Two OpticalTechniques, In: *Proceedings of the Society of Experimental Mechanics Annual Conference.*

The Effect of the Object Shape on Drag Coefficient

Lelis Gonzaga Fraga

Department of Mechanical Engineering

Universidade Nacional Timor Lorosa'e

Abstract: The parameters that affect the process and quality of combustion applied in wood pellets boiler and other devices are presented. The objective of this paper is to enhance the understanding of the combustion quality regarding to the influence of parameters on the characteristic of wood pellet fuel and combustion. Several papers regarding to the wood pellets combustion are collected and summarized based on the fuel bed size, combustion temperature, devolatization rates, primary air flow rate / velocity and moisture content. From this paper shows that combustion temperature, devolatization rates, primary air flow rate / velocity and moisture content consider in the combustion of wood pellet have an influence on the combustion quality.

Keywords: Wood pellets, Pellets Boiler, Combustion quality.

1. Introduction

Fluid flowing through an object will be effected by the shape of the object itself. The characterization of the fluid flow will be depending on the parameter that affects the flowing itself as well. The characteristic of the fluid on the object shape will be indicated by the drag coefficient (C_D) and Reynolds number (Re). Several different shape of objects are using in this study such as sphere with different in material and diameter, and cone with different in angle and material, the fluid which is using in this research is oil, K-500.

Snyder(2000) was conducted a study on the development of A 3Dunsteady finite element/spectral incompressible Navier-Stokes solver**,** this research is referred the flow around a circular cylinder inside a channel(Re = 100) instantaneous contours of vorticity. At low Reynolds numbers, the flow is steady, but becomes unsteady at higher Reynolds number with the development of a Karman vortex street in the wake. Moreover, for the flow around a circular cylinder, but at a higher Reynolds number (Re = 200), for which 3D effects are expected to develop in the wake, with spanwise wavelengths of 3 to 4 cylinder diameters. Snyder(2000).

Helmizar (2011)was conducted an experimental study on the comparison of the flow around two circular and ellipse cylinder arranged in tandem position with their interaction on the flat wall. The existence of massif separation on the contour surface of the ellipse cylinder has contribution on the reduction of the drag force.

Rahmawati*et al*., (2012)was conducted a study on the numerical interaction of vortex-induced vibrations (VIV) among four standing flexible cylinders with the In-Line Square configuration in the uniform flow. For the same force, while the Re increased, the drag force coefficient (C_D) and lift force coefficient (C_L) will be decreased.

2. Test Materials and Procedure

The research method applied in this research is experimental and 3D flow simulation analyses. With the experimental method, the object will be dropped in the transparent tube which is filled with the oil (K-500). From this experiment then the terminal velocity will be calculated in purpose to obtain the drag coefficient (C_D) and Reynolds Number (Re), the data obtained from the experiment will be put into the computer to determine the velocity of the flow. After conducting the experiment then continued with the simulation analyses with the Solidworks3D flow simulation. For simulation analyses the value for C_D will be obtained after calculated the value of Re from the experiment. All the data obtained from the experiment and simulation will be put into the table and graph with Microsoft excel for analyzing purposes.

Several different shapes of objects are using in this study such as sphere with different in material and diameter, and cone with different in material, angle and diameter as well. Those objects could be seen as follow.

1. Cone object with 8 mm in diameter.

Fig. 1 (a) Cone 45º, (b) Cone 60º.

2. Cone object with 10 mm in diameter.
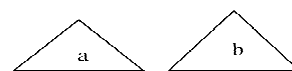
Fig. 2 (a) Cone 45º, (b) Cone 60º

3. Sphere with the diameterfrom7.95 mm-10.3 mm.

The research set up is shown in Figure 3 as follow.
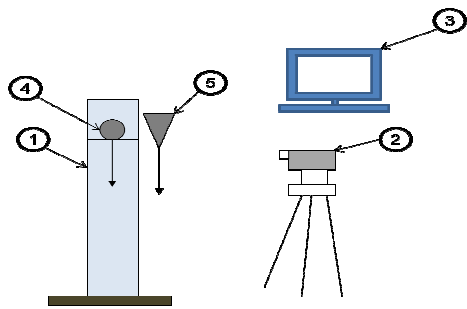
Fig.3 Research set up

Research apparatus: Research specimen:
1. Transparent tube   4. Sphere
2.Camera   5. Cone
3. TV monitor

Transparent observation tube with the diameter of $\phi100$ mm, 1000 mm in height which is filled with oil (K-500). Video camera is applied to record the data, and TV Monitor is used to do the observation.

3. Result and Discussion
1. Correlation of C_D and Re for cone (simulation & experiment)

Figure4 shows the correlation between C_D and Re of object (cone) for both simulation and the experiment, when the Re increased then the C_D will be decreased. For both simulation and experiment the highest Re=21.5 with C_D=2.19 and C_D = 2.74 respectively. This result obtained for the cone 60d10st.

Fig.4 the correlation between C_D and $Re$of cone

2. Correlation of C_D and Re for sphere (simulation & experiment)

Figure 5 shows the correlation between C_D and Re of object (sphere) for both simulation and the experiment, When the Re increased then the C_D will be decreased. For both simulation and experiment the highest Re=38.95 with C_D=1.74 and C_D = 2.07 respectively. This result obtained for the sphere with diameter 9.5mm.

Fig.5 the correlation between C_D and $Re$of sphere

3. Overall of C_D and Re correlation for sphere and cone (simulation& experiment)

Figure 6 shows the Overall correlation of C_D and Re for sphere and cone, both for simulation& experiment which have the same trend. While the Re increased then C_D is decreased.

Fig.6 The correlation between C_D and $Re$of cone and sphere

4. Correlation of L and C_D for object cone (Simulation& experiment)

Figure 7 (a and b) show the correlation between L and C_D for cone, both for simulation and experiment. It is indicated that at the same diameter and different

angle of cone, when L is increased then C_D is decreased.
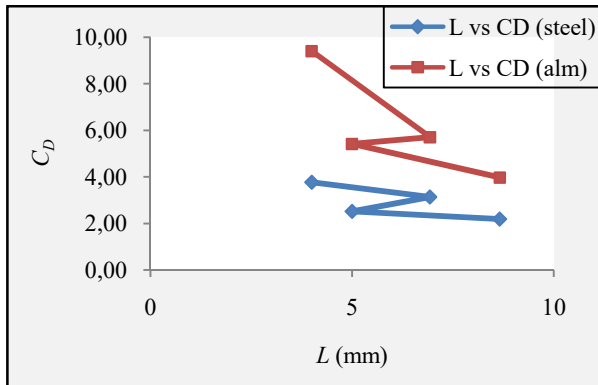
Fig.7 (a)the correlation between L and C_D(simulation)
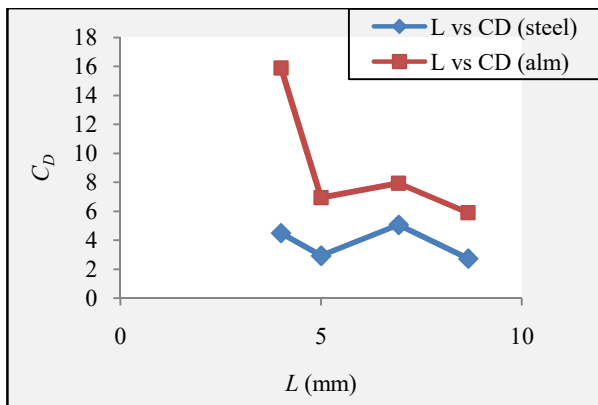
Fig. 7 (b) the correlation between L and C_D(experiment)

5. Error value for sphere and cone

Table 1 shows the error interval between the simulation and experiment analyses for C_D value both for cone and sphere. For object (cone) the error interval is between 16.42-48.71% and the smallest error is $E = 16.42\%$ for 45d10st and Re =18.52. For the object (sphere) the error interval is between 3.71-73.12% and the smallest error is $E = 3.71\%$ for sphere with the diameter is 10.05 mm and $Re = 32.74$.

Table. 1 Error interval for experimental and simulation analysis

No.	Re (cone)	Error interval for cone (%)	Re (sphere)	Error interval for sphere (%)
1	18.52	16.42	32.74	-3.71
2	10.20	19.26	25.10	12.61
3	21.50	25.07	35.54	12.83
4	5.77	28.30	26.38	16.08
5	5.39	39.27	38.95	19.17
6	8.78	48.71	35.98	19.34
7	12.31	61.15	32.78	20.54
8	2.89	69.10	10.71	30.10
9			16.14	32.30
10			30.08	33.79
11			21.83	73.12

4. Conclusions

Based on this study several conclusions are presented as follows.

The result of the object (cone) for both simulation and the experiment is indicated that when the Re is increased then the C_D will be decreased. For both simulation and experiment the highest Re=21.5 with C_D=2.19 and C_D = 2.74 respectively. This result obtained for the cone 60d10st.
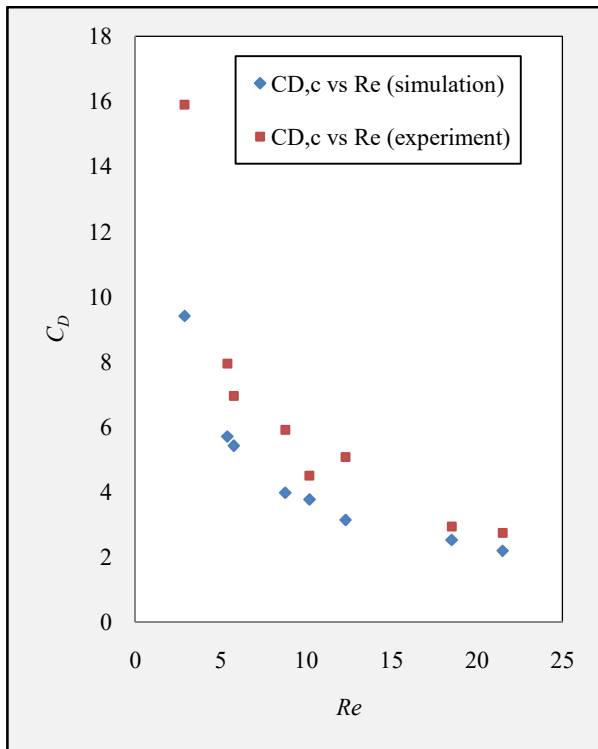
The result of the object (sphere) for both simulation and the experiment is indicated that when the Re is increased then the C_D will be decreased. For both simulation and experiment the highest Re=38.95 with C_D=1.74 and C_D = 2.07 respectively. This result obtained for the sphere with diameter 9.5 mm.
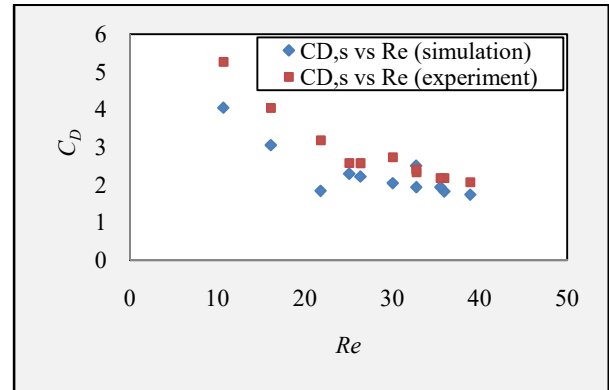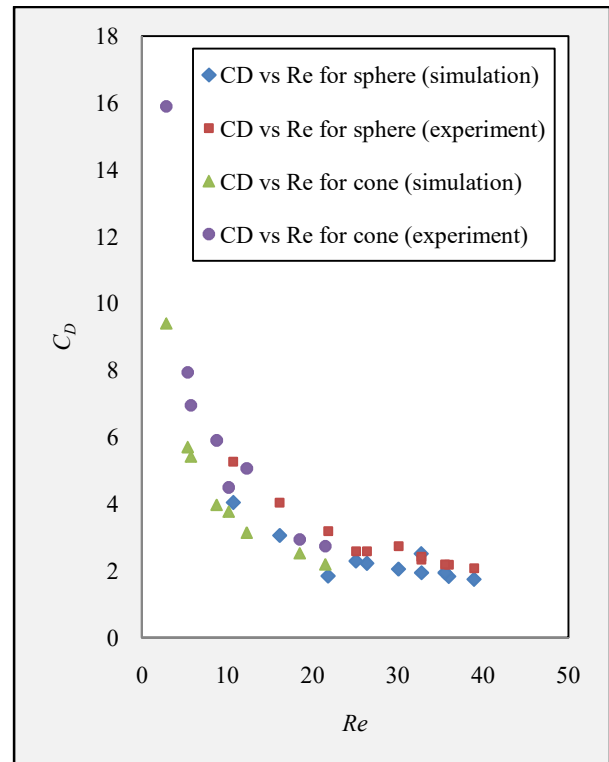
The analyses for L and C_D of the object (cone) indicated that at the same diameter and different angle of cone, when L is increased then C_D is decreased.

The error analyses between simulation and experiment for both sphere and cone indicated with the error interval of 16.42-48.71% for cone and 3.71-73.12% for sphere.

References

1. Erizal, *et al.*, Fluid Mechanics (TEP201), Bogor Institute of Agriculture.
2. Helmizar. (2011). Experimental study of the comparison of the flow around two circular and ellipse cylinder arranged in tandem position with their interaction on the flat wall.
3. Rahmawati, S., Djatmiko, E. B., & Prastianto, R. W. (2012). Numerical study on the interaction of Vortex-Induced Vibrations (VIV) among four standing flexible cylinders with the In-Line Square configuration in the uniform flow, I(1).
4. Robert W. F. and Alan T. M. 1994, Introduction to Fluid Mechanics, Fourth edition, SI version.
5. Static & Dynamic Fluids, https://salmanisaleh.files.wordpress.com.
6. Snyder. (2000). Turbulent Flowand Heat Transfer.

Development of Forced Cooling Technology on Drilling Utilizing Strong Alkaline Water With Microbubbles

[*1]Junior Raimundo da Cruz, [*2]Tanabe Ikuo

[*1] Department of Mechanical Engineering, Universidade Nacional Timor Lorosa'e
[*2] Department of Mechanical Engineering, Nagaoka University of Technology, Japan

Abstract: In machining almost all of the energy that expanded in cutting is transformed into heat. Proper selection and use of cutting fluids for cooling can help improve tool life, better surface roughness, reducing scrap and waste. In case of drilling processing, as much cutting oil has been used for lubricating and cooling, it is considered as a problem for environment when much waste are produced. Therefore in this research, the forced cooling technology on drilling using strong alkaline water with microbubbles was developed. Investigation for the corrosion resistance of the various materials were done. A through-hole drill was used and cooling effect of strong alkaline water with microbubbles was investigated. The tool life of the drill by drilling utilizing strong alkaline water with microbubbles was also evaluated by experiment. It is concluded from the results that; (1) Cooling of strong alkaline water with microbubbles was very effective, (2) Heat transfer coefficient of drilling using strong alkaline water with microbubbles was higher than conventional wet drilling, (3) Tool life of drilling using strong alkaline water with microbubbles was improved compared to the conventional wet drilling.

Keywords: Drilling, strong alkaline water, through-hole drill, cooling, heat transfer coefficient

1. Introduction

The drill tip normally becomes extremely hot and easily to wear out as it drills deeper into workpiece which is considered severe in drilling process. Heat that is caused during drilling can increase tool wear, reduce tool life, and cause poor surface finishing. For this reason, various type of drills with high heat resistance[1),2),3)] and cooling methods[4),5)] to reduce heat have been introduced to minimize heat, however they were still not sufficient enough. In addition, through-hole drills[6)] by supplying high pressure cutting fluid was also introduced to fast remove cutting chips and improve cooling effect; however the cooling effect is still insufficient.

Thus, in this study, the forced cooling by using the phenomenon of evaporation effect[7)] of water to achieve force cooling by supplying water to the through-hole drill was developed. Microbubbles were added to strong alkaline water (pH 12.5) in order to accelerate an evaporation cooling effect. First, the optimal specification of strong alkaline water was clarified by experiments, then the heat load of the drill was reduced by supply the strong alkaline water with microbubbles through the through-hole drill and the effectiveness of the forced cooling method was evaluated by experiment. Moreover, the effectiveness of this method for the industrial application was evaluated by drilling experiment.

2. Corrosion resistance of machine elements in strong alkaline water

Water is a good conductor of heat but has drawbacks as a cutting fluid. Although the effectiveness of water evaporative cooling is very large compare with the use of cutting fluid, there are still only few applications being used in industries because it corrode any steel material around it. This corrosion can be inhibited by higher water pH to pH 12.5 (Alkaline water) in order to use as cooling during machining. Therefore, in this research, corrosion resistance of materials in the strong alkaline water which are being widely used in industries is clarified by experiment. The strong alkaline water was firstly measured to define the change of pH over 2 month by leaving in the ambient condition of 20°C, 40°C and 12°C as shown in **Table 1**. It is confirmed from the result shows in **Fig.1** that the pH only decrease from pH12.5 to 12.0, therefore it can be used for long period of time. Based on the corrosion properties of strong alkaline water[8)] in the case of steel, the corrosion will not occur when the pH of strong alkaline water is more than 10.0. Some materials like titanium alloys cannot withstand corrosion when the water pH is below 10.0, therefore the pH values of strong alkaline water between pH 10.0 - pH 13.0 are considered appropriate for this application.

Table. 1 Test condition for changes of alkaline water pH

Medium in container	Strong alkaline water
Ambient condition	20±1°C, 40±1°C and 12±1°C Humidity: 60%
Quantity of water	10 ℓ
Size	Ø250×230 mm

Table. 2 Condition of the corrosion test

Medium in the vessel	Strong alkaline water (pH 12.5)
Ambient condition	Room temp.: 20±1˚C, Humidity: 60%
Period	Two months
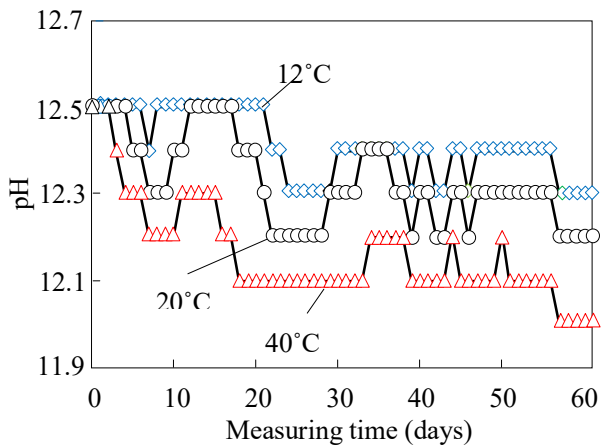
Fig. 1 Variation of pH values at different temperatures

The corrosion resistance of various cutting tools and materials used in industries on strong alkaline water were observed. The test were performed by immersing all test materials inside the strong alkaline water of pH 12.5 with condition shown in Table 2 at constant room temperature of 20±1ºC and 60% humidity for two months. The experimental results of the durability of materials inside strong alkaline water are shown in **Table 3**. The results show that the materials, except aluminum and aluminum alloys, show no corrosion after kept in the strong alkaline water for 2 month. Copper, brass, some electrical element and some coating of material tools such as TiAlN and TiAlCr show only discoloration. However, when the amount of Al element contained in these coated materials increase, the possibility for corrosion to occur is large. It was also observed that other machine elements did not corrode except the screws. Therefore, it is considered machining used strong alkaline water as cooling source is possible. However, it is not applicable for cutting aluminum because the use of alkaline water exhibits corrosion.

Table. 3 Results of the corrosion resistanceof machine elements tested for two month inside alkaline water with pH12.5

	Material types	Observation	
Machine tool stracture	S45C	✓	
	SUS304	✓	
	Cast iron	✓	
Work piece	Ti	✓	
	Ti6Al4V	✓	
	Inconel 718	✓	
	S45C	✓	
	Copper	✓	Discoloration
	Brass	✓	Discoloration
	Aluminum	×	Corrode
Tool	HSS	✓	
	Carbide	✓	
	Cermet	✓	
	Diamond	✓	
	CBN	✓	
	Ceramic	✓	
Coating material of tool	DLC	✓	
	Ti AlN	×	Discoloration
	TiAlCr	×	Discoloration
Machine element	V-belt	✓	
	Drive belt	✓	
	Timing belt	✓	
	O-ring	✓	
	Bearing	✓	
	Linear guide	✓	
	Ball screw	✓	
	Oil pump	✓	
	Oil seal	×	Only screw corrode
	Wire hose	✓	
	Excel hose	✓	
	Tube fitting	✓	
	Oil level gauge	✓	
Machine Element	Rubber bushing	✓	
	Exhaust cleaner	×	Corrode and discoloration
	Thinned cylinder	✓	Only screw corrode
	Air check	✓	
	Check valve	✓	Only screw corrode
	Lubricator	✓	
	Regulator	✓	Only screw corrode

Electrical element	Push-button switch	✓	Only screw corrode
	Command switch	✓	Only screw corrode
	Optoelectronic switch amplifier	✓	Only screw corrode
	Servomotor	✓	Only screw corrode
	Box terminal	✓	
	Electromagnetic contactor	✓	Corrode
	Solenoid valve	✓	Discoloration
	Solenoid valve base	✓	Discoloration
	Flat cable	✓	
	Cable connector	✓	
	Direct acting two port solenoid valve	✓	Corrode and discoloration
Basic material	Acrylic acid resin	✓	
	Vinyl chloride	✓	
	Nylon	✓	
	Polyurethane	✓	
	Polycarbonate	✓	
	Nitrile rubber	✓	
	Polyurethane rubber	✓	
	Fluoro rubber	✓	
	Chloroprene rubber	✓	
	Chlorosulfonated Polyethylene rubber	✓	
	Oil proof vinyl mixture	✓	
Paint	Lacquer paint	✓	
	Urethane resin paint	✓	
	Epoxy resin paint	✓	

NB: ✓ : Not corrode ×: Corrode

3. Forced cooling using strong alkaline water and microbubles

In this research, life time of microbubbles inside the alkaline water was observed by releasing microbubbles into strong alkaline water. It is considered that large cooling efficiency can be achieved by supplying strong alkaline water with microbubbles to cutting point. Therefore, the experiment was done by supplying microbubbles (the distribution of the microbubbles sizes are various[9]) with flow rate 8 ℓ/min for 10 minutes into

30 ℓ of strong alkaline. The time from the cloudy strong alkaline water (pH 12.5) becomes clear was measured and the result is shown in **Fig.3**. The measurement was also performed for big bubble sizes (1-2 mm and 3-5 mm) which supplied to the strong alkaline water with flow rate 32 ℓ/min. The result shows that microbubbles was retained for about 4 minutes in strong alkaline water, and therefore it is considered that, strong alkaline water mixed with microbubbles can be transported through pipe until reaching to cutting point which is possible to be used for a forced cooling. However, when the sizes of bubbles inside strong alkaline water were 1-2 mm or 3-5 mm, it only retained for a few second in strong alkaline water. Thus, supplying strong alkaline contained those sizes of air bubbles is considered to be very difficult. Therefore in this paper, it is decided to supply only microbubbles to the strong alkaline water for the experimental evaluation.
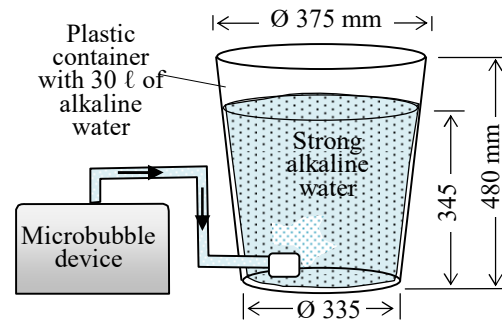
Fig. 2 Experiment setup for measurement of the life time of microbubbles
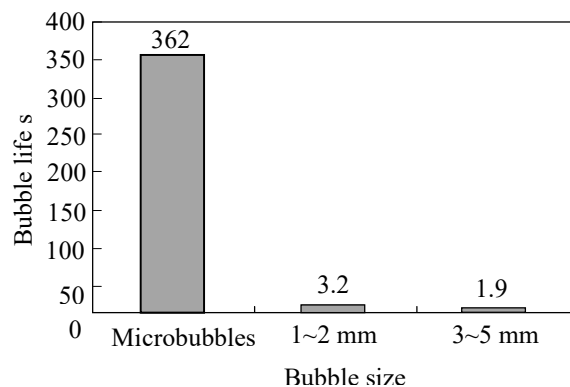
Fig. 3 Relation between bubble size and its life in strong alkaline water

The suitable amount of supplied microbubble and the flow rate to the work piece needed to be optimum in order to achieve large cooling effect. Therefore, the optimum microbubbles capacity in the strong alkaline water and the amount of water flow rate was investigated by measuring heat transfer coefficient. The experimental setup to

evaluate optimum amount of microbubbles and the optimum supplied flow rate is shown in **Fig.4**. In this setup, a rubber heater (100×100×2 mm) was sandwiched between two steel plates and was hanged in the center of vessel filled with strong alkaline water. The temperature of steel plate was measured at 10 points using thermocouples during experiment and the average was calculated.
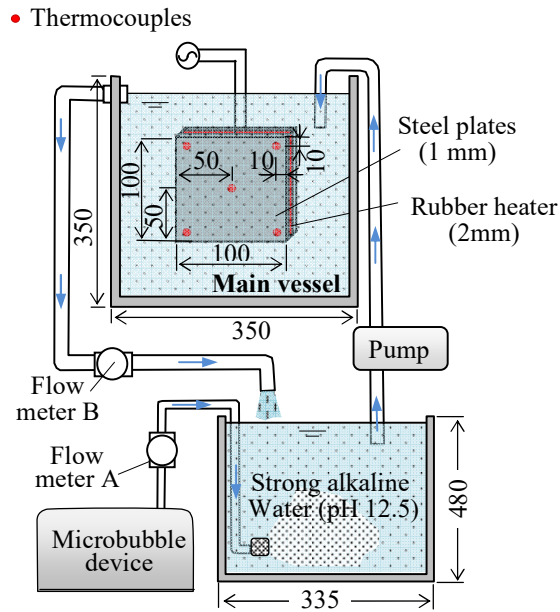
Fig. 4 Experimental setup for measuring heat transfer coefficient of alkaline water with bubbles
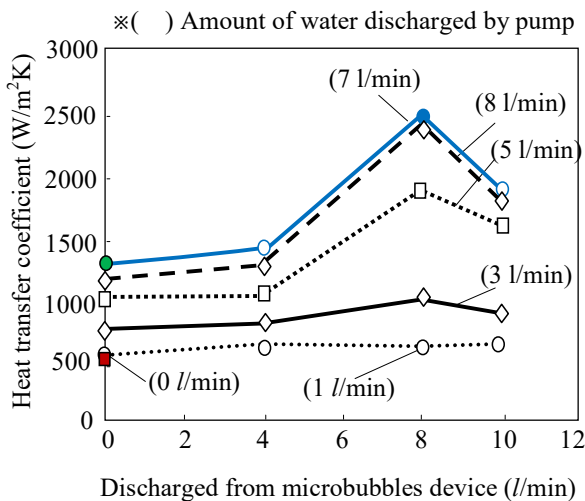
Fig. 5 The reletaionship between amount of microbubble and the flow rate of the pump

The heat transfer coefficient was calculated from the average temperature of steel plate surfaces and the strong alkaline water. Theflow meter A was used to measure the

flow rate of microbubble, while the flow meter B was used to measure the water flow discharged from pump. Notice that flow meter B was not placed at the output of the pump but at the output of the main vessel. This is because the used of high discharged pressure 2.1 MPa from pump can damage flow meter which has only 1.0 MPa maximum allowed pressure. In case of flow meter A was directly placed at the output of microbubble device because of the maximum discharged pressure of microbubble device only 0.7 MPa. Using this setup, then the difference in convection heat transfer coefficient was measured. In order to obtain the optimum water flow rate pumped out by pump, various flow rates were taken as parameter for the experiment. As the amount of microbubbles in the strong alkaline water can also affect the efficiency of the cooling capacity, thus different flow rates discharged from microbubbles device was also taken as experimental parameters. By these, a main vessel with a through-hole drill was selected and the relative evaluation was made on forced cooling effect when supplying with strong alkaline water mixed with microbubbles. The measurement result of heat transfer coefficient shows in **Fig.5**. The calculation result shows that the optimum discharged flow of microbubbles from the microbubbles device is at 8 ℓ/min and the optimum flow rate discharged by pump is at 7ℓ/min. It can be seen that in the case of without using water flow by pump (Only cutting in strong alkaline water and without microbubbles), heat transfer coefficient is about 500 W/m^{2}K. In the case of supplying only strong alkaline water at 7ℓ/min, the heat transfer rate improve to 1200 W/m^{2}K and increase up to 2500 W/m^{2}K when using strong alkaline water of 7ℓ/min containing microbubbles (at 8ℓ/min). As large amount of microbubbles was containing in the strong alkaline water, heat transfer coefficient improved and the effectiveness of cooling by water evaporation was also improved with supplying air. From this result, it is confirmed that large cooling effect can be generated by circulating the strong alkaline water containing microbubble.

4. Evaluation by real drilling for the effectiveness of the proposed cooling method

(1) Evaluation of drill temperature
The drill tip temperature at the time of supplying strong alkaline water mixed with microbubbles was investigated by experiment. As it is difficult to measure the drill temperature during drilling because of the rotation condition, another experiment setup shown in **Fig.6** was used for the drill temperature measurement. In this setup, two small ceramic heaters were bonded on the tip of cutting edges of the drill (Ø15mm, with through hole) and two T-type thermocouples were also fitted on the groove (3 mm from the cutting edge) in 2 places near cutting edge using silicon bond with 2 mm of thickness until solidify.

Then load of 20N was applied to the thrust direction of a drill in experiment so that the hole on the work piece and the drill tip was contacted tightly together. In this experiment, Ti6Al4V types of workpiece was used and max 260°C temperature was supplied to ceramic heaters with consideration to the measurement limitation of T-type thermocouple and applicable limitation of silicon bond. In dry condition, the steady state temperature of the cutting edge of drill reached to 260°C when supplied with 29.8V, 0.12 kW electricity power (for each ceramic heater), therefore those conditions were fixed to be used. The outside surfaces of the workpiece were insulated with the polystyrene foam of 5 mm thickness to prevent the influence of cooling from the side surfaces. The experiment was conducted using 3 conditions; dry condition, only strong alkaline water was supplied (7ℓ/min) via through-hole, and by supplying strong alkaline water (7ℓ/min) mixed with microbubbles (8ℓ/min) via through-hole. The measurement results of the temperature on the edge of the drill for Ti6Al4V are shown in **Fig.7**. The measured temperature shows that, the cooling effect of the strong alkaline water is 3.1 times larger compared with dry condition and for strong alkaline water mixed with microbubbles was 3.5 times larger than dry condition. Because of the Ti6Al4V type of the   are the material with low thermal conductivity, thermal load on the tool become much larger during the deep hole processing for this material, it is considered that the proposed method by supplying strong alkaline water with microbubbles is very effective for forced cooling to the drill.

Fig. 7 Temperatures on the edge of the drill for different cooling conditions

(2) Evaluation of processing surface roughness and the tool life

In this section, real cutting experiment was performed and the effectiveness of the forced cooling method using strong alkaline water mixed with microbubbles was evaluated by measuring the surface roughness of the cut surface. The experimental setup to evaluate our proposed cooling method is shown in **Fig. 8**. The conventional
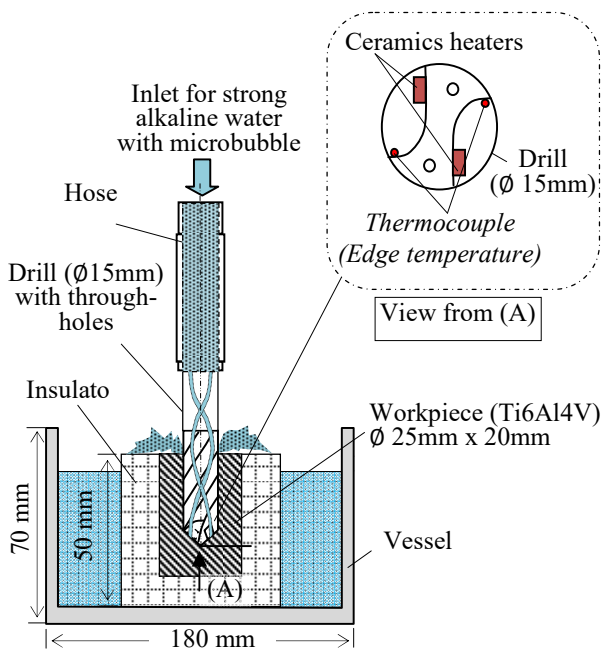

Fig. 6 Experimental setup and position of thermocouples for measuring temperature on the edge of the drill

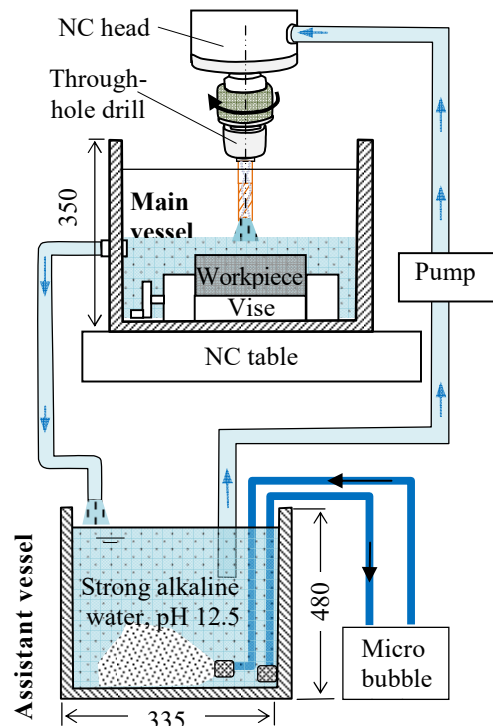**Fig. 8** Experimental setup for drilling evaluation

Table. 4 Drilling condition for evaluation of the forced cooling of alkaline water with microbubbles

Specification of the drill	
Diameter	Ø 15 mm
Length	150 mm
Material	Carbide with TiN
Through hole	Ø 5mm×2 holes
Specification of the cooling medium	
Medium	Strong alkali water (pH12.5)
Microbubbles	8 ℓ/min in 40 ℓ alkaline water
Drilling condition	
Spindle speed	500 rpm
Cutting speed	24 m/min
Feed speed	40 mm/min
Depth of drilling	From 0 to 25 mm
Workpiece	Ti6Al4V

Fig. 9 Photograph of experiment setup for drilling using proposed method

Fig. 10 Result of tool life regarding the drill using the forced cooling of alkali water with microbubbles

drilling condition shown in **Table 4** was used for drilling Ti6Al4V material using Ø15 mm of the drill tip. In the experiment, the surface roughness was measured at the surface on starting time of the processing and on the time just before drill life was reached. The drill considered reaches its tool life when the flank ware is reach 0.15 mm.

The measurement was done by taking average value from 9 points in the positions of three places at depths of 5 mm, 15 mm and 25 mm. In this experiment, 4 conditions; the dry cutting, the conventional wet cutting, cutting by supplying only strong alkaline water (7 ℓ/min), and cutting in 40ℓ of strong alkaline water vessel supplying with 8 ℓ/min of microbubbles via through hole were performed. In order to prevent the obstruction caused by some cut pieces on the hole of trough-hole drill, high pressure pump with discharge pressure 2.1 MPa was used. The tool life for drilling with supplying strong alkaline water mixed with microbubbles was measured and evaluated. As stated earlier, for the judgment of the tool life, the tool life is defined to be reached by the time when flank wear of the drill edged reach to 0.15 mm. The measurement result of a tool life is shown in Fig. 10. The result shows that the tool life using forced cooling by strong alkaline water mixed with microbubble was 12 times compared with dry cutting, 2.3 times compared with wet cutting using cutting oil and about 1.5 times using only strong alkaline water respectively. By using forced cooling effect of strong alkaline water mixed with microbubbles, the drill is effectively cooled and the reducing in hardness of the drill

became lesser. Since the thermal conductivity of Ti6Al4V and chip are lower, the generated cutting heat is intensively conducted to the drill and therefore the drill temperature becomes higher and the hardness of the drill also becomes lower.

The measured result of Arithmetical mean roughness (Ra) and ten-point mean roughness (Rz) of surface after drilling experiment on Ti6Al4V is shown in **Fig.11**. In this process, the previous experiment setup (**Fig.8**) and drilling condition (**Table 4**) was used for processing. Again, for this experiment, 4 conditions; the dry cutting, the conventional wet cutting, by supplying strong only alkaline water (7ℓ/min), by cutting in 40ℓ of strong alkaline water vessel supplying with microbubbles via through-hole (7ℓ/min) were performed. The result (**Fig.11.a**) shows that by using forced cooling of strong alkaline water mixed with microbubbles on drilling Ti6Al4V, Ra surface roughness was improved about 31% compare with dry

cutting and about 21% compared with wet cutting in the initial cutting. At the end of tool life, Ra surface roughness improved about 61% compared with dry cutting and 40% compared to using cutting oil. The result of measured Rz surface roughness (**Fig.11.b**) also shows that surface roughness was improved about 41% compare with dry cutting and about 33% compared with wet cutting in the initial cutting. At the end of tool life, Rz surface roughness improved about 56% compared with dry cutting and 40% compared to using cutting oil. Since the cooling effect of evaporation of strong alkaline water mixed with microbubbles is large enough to suppress the thermal deformation of drill, the loss in hardness and strength of the drill is lower, the loss of drill sharpness is lesser and also the reduction in rigidity of drill is lower resulting the small vibration amplitude and smooth surface roughness. From these results it can be considered that longer tool life on drilling processing of difficult to cut materials with low thermal conductivity is possible by using proposed forced cooling of strong alkaline water mixed with microbubble.

5. Conclusion

In conclusion, the results of this study are summarized as follow;

(1) Cooling of strong alkaline water with microbubbles was very effective without corroding most of the processing materials except for the aluminum based materials.

(2) By adding microbubbles to the strong alkaline water, it produces extremely large forced cooling effect with higher heat transfer coefficient value about $2500W/m^2K$.

(3) By using the proposed method of supplying strong alkaline water mixed with microbubble to the drill via through-holes, the rise of the temperature on the tool tip can be reduced about 71.6%, and the work surface roughness was improved about 60% at the end of the tool life.

(4) Tool life of drilling using strong alkaline water with microbubbles was improved 12 times compared to conventional wet drilling.
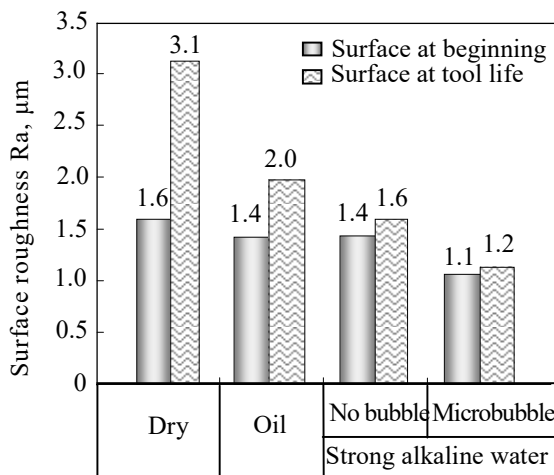
(a). Ra surface roughness
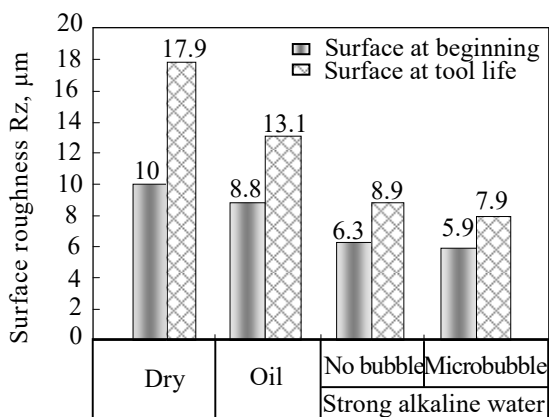
(b). Rz surface roughness

Fig. 11 Measured surface roughness of drilling on Ti6Al4V workpiece

References

1. SUNG L.,NOTOYA H.,YAMADA S.,TAKANO N., OYAMA T.,TSUKUDA I. : Drilling of Al-17%Si alloy(T6 treated) with the coated and carbide drills, *Institute of Light Metals*, Vol. 47, No.6, pp. 311-316, 1997.
2. Yoshikawa M. : Diamond Technical Overview, NGT, pp.137-400, 2007.
3. Sekiguchi T. :Trend and Next Development of Cutting Tool for Eco-machining, *The Japan Society of Precission Engineering*, Vol. 75, No.1, pp.123-125, 2009.
4. Tasdelen B. Wikblom T., Ekered S. :, Studies on minimum quantity lubrication (MQL) and air cooling at drilling, *Journal of Materials Processing Technology*, Vol. 200, Issues 1-3, pp. 339-346,2008.
5. A. Sönmez, M. V. Kök, R. Özel :Performance analysis of drilling fluid liquid lubricants, *Journal of Petroleum Science and Engineering*, Vol. 108, Pages 64-73, 2013.
6. ARAI M., OHNO T., OGAWA M., SATO S. : Driling of High Hardness Steels with the High Pressure Supply of Coolant, *The Japan Society of Precission Engineering*, Vol. 62, No. 9, pp. 1310-1314, 1996.
7. TANABE I., TRUONG HONG Mihn, YOSHII K. : Turning with Environment-Friendly Cooling Method Using Water Evaporation : 1st Report, Cooling Effect of Water Evaporation and Its Applicability to Tool Tip Cooling, *Transactions of the Japan Society of Mechanical Engineers*, Series C, Vol. 66, No. 643, pp.1026-1030, 2000.
8. SHIMOHIRA S. : Material Science of Corrosion and Corrosion Protection, Agne Gijutsu Center, pp.30-32, 255-257, 287-288,1995.
9. Pressurized high-density micro-nano bubble carbonated spring generator, Micro and Nano Bubble Generation Capacity, Giken Co. Ltd, http://www.idea-techno.com/pd/microbubbles/naturan/kaatuyoukai-kounoudo.html

10. TANABE I., TRUONG HONG M., SUGAI H., INOUE M. : Cutting with Heating of Work Piece and Cooling of Tool Regarding Cemented Carbide Mould and Die(Machine Elements and Manufacturing), *Transactions of the Japan Society of Mechanical Engineers*, Series C, Vol. 73, No. 727, pp.885-2630, 2007.

11. NACHi Cutting tool 2011 Catalogue : NACHi Co. Ltd, 2010.

12. YAMADA Y., IKEDA T. :Coated Cutting Tools : Drills, Endmills (Special Issue on Recent Trend of Development of Cutting Tools), *Journal of Precision Engineering*, Vol. 61, No. 6, pp778-782, 1995.

Electricity Industry Development in Timor-Leste

Paulo da Silva
Department of Mechanical Engineering
Universidade Nacional Timor Lorosa'e

Abstract: Providing a reliable electricity services to 1.2 million people is challenging. This study therefore conducted to evaluate whether the evolution of the sector has laid proper foundation for the securing the electricity policy or not. An intensive discussions and interviews with actors from related institutions were conducted to obtain all data and information. Timor Leste Electricity Industry (TLEI) experienced several changes in the last few decades during its development starting power origin, power restoration until power consolidation. It was found that important aspects including laws, regulations and frameworks are remaining in government portfolio. There are no dedicated institutions to manage the industry independently. The key aspects for guaranting the long term power supply are less acknowledged in its policy settings.

Keywords: Electricity Industry, Electricity Police, Goverment Portopolio, Timor-Leste, TLEI,

1. Introduction

Timor-Leste electricity industry (TLEI) has gone through several changes during its development. It was much developed during Indonesian Administration compare to Portugues though destroyed in 1999.Enourmous efforts were done to accelerate the serviceyet it is challenging.

Some studies on electricity development sector have been conducted yet it does not discuss the important aspects of the industry. Therefore this study is conducted to review the development of electricity industry in the country, by looking at three stages: 1). Power Origins (Portugues and Indonesia), 2). Power Restauration, and 3). Power Consolidation.The main aim of this paper is to understand the policy and actions which being implemented in the last couple of years. It also tries to review whether these policies are adequately in place to guarantee the long term power services that the IV constitutional government introduced. The methods of this study are reviewing the past and current studies.The electricity authors who involved directly on electricity industry operation in Timor Leste were interviewed.

2. Evolution of electiricty industry

Power Origin (Colonialism till 1998): During Portugues occupation, most Timorese consider electricity as one of the luxurious productsthat only accessed by those economically capable[1]. Dili was only single town in Timor with power supply and other basic infraestrucutres such as sealed road which believed constructed in late 1962. Meanwhile, other districts in Timor Leste, communities were heavily relying on biomass to full fill their energy requirements. Traditional energy sources such as firefood, candlenuts, rubber were used for the lighting, cooking and heating needs.

Alves stated that the central electric Kaikoli and the electricity poles in the main capital were constructed in late 1960s, however accessing to the power was in 1962/63. He explained the centre produced a 6000KV transmission capacity and 230 Volts distribution capacity through 6 sub stations in Dili to morethen100 customers.The trained locals who worked for the electricity industry were 20 people including Mr. Alves. He was the first senior person who worked in Kaikoli generating centre. Meanwhile the industry was managed by government through municipal administration (Camara de Municipio). Alves explained, there were no regulatory authorities, board members who responsible specifically on electricity issue, no laws for protecting customers' right and also no subsidy policy for social aspects.

Apart from its brutality, the Indonesian developed the electricity far better than Portuguese regime. In 1983/4, the power was extended to all sub district level at least two to three villages were access to electricity. In 1998, Timor-Leste was known as Timor Timur hadabout 28MW of power capacity from 58 isolated power generations. Each centre has capacity between 50KVA and 100KVA. Half of this was used to supply energy to Dili customers. There were about 43,000 clients and 90% of them were residential[2]. In 1985, the central governmentintroduced electricity reform based on decree law No. 15/1985 to allow private sector to step in, especially the transmission and distribution components [3]. However, this reform was

only occurred inJava and other provinces. The industry in the island was continued to be managed by a single utility called PLN (National Electricity Company).

The managerial positions were only occupied by Indonesian and the local Timorese were only assigned for basic services. On the other hand the extention of electricity which was known as "listrikmasukdesa" or community electrification program was introduced with specific purpose. The authorities could easily desiminate information about the political issue and also try to convince the Timorese through media.The basic infrastructure was built to facilitate this aim.

Power Restoration (1999 – 2007): When Timor-Leste separated from Indonesia in 1999, all the power stations suffered enormous damage. The transmission and distribution lines were destroyed and wires were stolen. Power utility management capacity systems, computer recording centres were removed and destroyed. All PLN qualified managerial and technical staffs departed.

The United Nations Transitional Authority in East Timor (UNTAET) started putting efforts on power sector in 1999. About39 power stations(50KW to 100KW) in major towns in the country were fixed. The project wasfunded by several donors (*ADB under TFET, Japan and Portugal*) with overall cost of $6.8 million [4]. In April 2002, repairing medium voltage and introducing new low voltage distribution lines were conducted including upgrading 50 kW to 100kW in Betano. In 2005, funds from Japan, Portugal and TFET were used to upgrade the 16MW Comoro power plant. It is estimated about $12,490,590 million executed for the power station between 2000 and 2005. In October 2002, Norway Government through Norway Aid Development (NORAD) supported 6x1MW diesel generators at estimated price of $1.8 million. During transitional period, $2.59 million from both TFET and Japanese donors was used to strengthen EDTL through procurement of equipment for Dili power station, staff reassignment and recruitment. The Comoro power station serves more than 26,500 customers with total generating capacity of 19 MW [5].

Power Consolidation (2008 - 2012): TheGusmao government recognizes that access to *electricity is a basic right and the foundation for country's economy.* [5]. Building new generating stations, upgrading the old electricity transmission and distribution systems and introducing renewable energy alternatives are the actions to respond this principal.It invested on250MW power plants in 2008. This national electricity grid is the largest infrastructure that the country ever built. The first power plant with capacity of 119.5MW which situated in Hera is shown in the figure 1.

Fig. 1 Sites of 250MW Power Generating Plants[5]

The second power plant was built in Betano (figure 1) with overall capacity of 136.6MW. This average generating capacityis produced by 8 x 17MW generators. As same as the 1st plant, it has own fuel storage facilities and a sub-station that raises the voltage to 150KVA for the objective of connection with the transmission line.

These plants are completed with nine substations(10MVA - 63MV) to reduce power voltage that allows connection to the existing 20KV distribution lines in the districts.

Electricity Generating Capacity: There was no power supply in 1999 as most of the generating stations were destroyed. In 2012 the generating capacity reached 120MW as Hera Power plant built. In 2014, the total generating capacity for the country was250MW. In addition, 17MW diesel base power plant was completed in November 2015 in Oequsi.
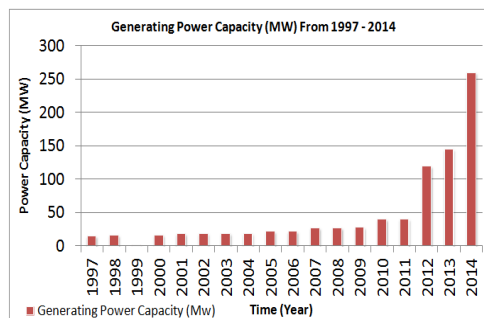
Fig. 2 growth of generating power capacities [5]

Meanwhile the transmission and distribution capacity in the current systems are 150kVand 20kV respectively.

Investment on Electricity Industry: About $200 million was used for electricity industry development between 2005 and 2006. Although it declines in year 2007 due to military crises, the investment increases dramatically when introduced 250MW power plant project in 2008. Until 2011, the public investment on electricity infrastructure reached $1 billion.
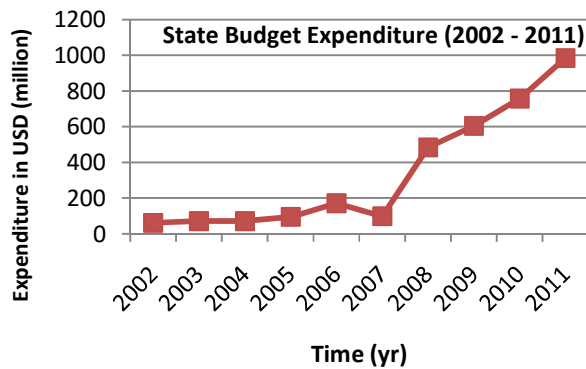
Fig. 3 State Investments on TLEI [5], [6] & [7]

3. Electrical Governance

Electricity Price (1997 – 2012): According to ADB (2000/1) the price charged to residential customers for every 25kWh was $1.57 including 10% tax during Indonesian time. Meanwhile, there is no available data for industrial and commercial customers. The current electricity tariff in Timor-Leste is set based on decree law no.1/2003 [4]. The social needs of Timor-Leste are highly considered in the structuring of the current electricity rates which charged to customers without tax and it is a flat rate system. According to EDTL [8], the initial monthly cost for residential customers for the first 20 kWh is 5 cents per kWh. The upper strata residential rate of 12 cents / kWh is a good compromise between the ability to pay and cost of production. The rate that charged to business customers divided into three types including: 15 cents/kWh for 0-1000kWh/mth, 20cents/kWh for 1000-3600kWh/mth and 24cents for over 3600kWh/mth[8].Currently the annual revenue from electricity selling below $15 Million, meanwhile over $120 Million is spent on diesel. Da Silva [5] stated that approximately 30% - 35% of electricity is to be recorded. EDTL [8] indicates that almost 70% - 80% is not recorded due to illegal connection, not paid and transmission losses.

Ownership & Structure: The TLEI was owned by a public utility company during colonialism. It was specifically managed by municipal body in Portuguese time and by a public utility called PLN during Indonesian time. Meanwhile structure of electricity industry was monopoly model which is also known as vertical integrated model. This model does not allow for competition.All components of the industry from generation, transmission and distribution thus are managed by a single utility. However in early 2015, morethan 10 private businesses are contracted to sell electricity to customers in Dili. In addition, supliers are invited to compete in supplying fuel.

Policy and regulations: There was no specific energy policy developed between 2002 and 2007. The policy for electricity industry development got much emphasised in the national strategic development plan that the IV Constitutional Government issued. It is called "Timor-Leste Strategic Development Plan 2011 – 2030". Thisnational strategic development plan targets that all houses will be electrified either from conventional or renewable energy sources of energy by 2030. However, the core aspects of energy and electricity sector to support the goal is fail to be taken into account in its policy settings. The mains aspects which should be highlighted:

Political and Policy Issues: different government have different views and strategies in developing the industry. For example, the first government (FRETILIN) supports for renewable energy options, by allowing the study on Iralalaro hydro power that the Norway Government expertise carried out. It was planned to start the construction in 2007. However, when the AMP government took office in 2007, the study put aside and introduced instead HFO (now diesel base power plant). Therefore, it overrides the core objective of providing electricity to improve societal welfare. In ministerial level, electricity issue is often ignored in their policy plans though it is essential for the normal operations of services. This is because the country is considered as not an energy intensive country at present situation. Decision makers solely focus on their own department priorities without taking into account the importance of electricity. One thought that the electricity is considered as lesser importance by ministries since it is driven demand and in itself, it cannot be used to generate income thus it is not reflected in the majority annual plans of each ministry.

Lack of integrated planing is resulting in overlaping policy settings. For example, Estatal implemented Solar PV for 442 village offices instead of secretary of state for energy[10].However, the policy could be an effective and efficient one; if electricity is understood in its proper context by all key decision makers especially in the ministerial levels and that there are more productive uses of electricity in the country. Also, integration of bottom up and tob down policy would serve better.

Institutional Arrangements: although EDTL is the main responsible for electricity sector, its responsibility is only limited to the basic operation and maintenance aspects. The sector lacks of proper utility regulator authority to handle legal issues and frameworks and sector development planning. At the same time, there is absence of managerial structure in municipalities level although there are some EDTL local recruited staffs to overseing day to day activities.

Regulation and Legislation: EDTL was established during the power restoration period based on the GovTL decree no.13/2003. This law also defines the roles of EDTL, the industry ownership and the government role as regulatory authority. However before this law was established, in the late 1999, the transitional Government-UNTAET created an initial regulation (1999/1 of UNTAET). This regulation sets the overall legal principle and states that since there is no new regulation in place, the law and regulation prior to 25 October 1999 would continue to apply. Then, in 2001, UNTAET created tariff directive which gives right to EDTL to charge customers. Meanwhile there is no proper regulation to regulate fuel prices. Lack of act and regulations is considered as one of the contributing factors to the weak performance of the electricity industry in the country.

Community issue: the culture of "pay for use" is still far from the usual best practices among Timorese electricity customers. Some families even do not pay their bills and they continue access to power without any penalty from provider. Government[4] indicates that in Dili the capital city itself, estimated only 40% of businesses pay their electricity bills.

Resources Issues: human resource is the major issue, currently the electricity sector has less than 50 people who have engineering background in electricity discipline. They have very limited capacity and experiences. According to EDTL officials, as of 2010, there were only 410 people working in the electricity sector. Only one to two people are assigned in each isolated generating stations (districts). The industry currently lack of qualified personals that capable to handle the 150KV transmission. Up until now, the country still relies on international experts to handle heavy electricity industry tasks and central power plant controlling systems.

4. Conclusion

Originally, the Timorese was heavily relying on bimass for its cooking, heating and lighting needs. Although the basic electricity infrastructure extended to sub district level by Indonesian Administration, it was destroyed in 1999. Meanwhile all qualified staffs left for Indonesia. With international aids, the majority of diesel base generating stationswere reoperated at the late of 1999 and beginning of 2000. TLEI got more attention as 267MW power plants constructed in Hera, Betanoand Oequise. The industry is public owned. The industry still needs to have proper institution with proper authority. The taken policies should reflect the local social, political, economical and environmental structure that in line with ecological modernization approach. From the TLEI development stages, it shows that the foundation for its sustainability development still needs to be considered in order to guarantee the long term energy services in the future.

References

1. Alves, V., The Senior of Kaikoli Electricity Generating Station Staff from 1962-1974, Interviewed in Quintal Bo'ot – Dili, Timor-Leste in July 2014.
2. ADB, Technical Assistance-Power Sector Development Plan-Phase I, 2001, Dili – Timor-Leste
3. Sharma. D., Electricity Reforms in the ASEAN A Panoramic Discourse, Economic and Political Weekly, 2005, Vol XL, No 50, AH Wheeler Bookstalls, US.
4. GovTL, POWER: Priorities and Proposed Sector Investment Program, Ministry of Transport, Communication and Public Works, 2005, Dili, Timor-Leste. Available at: http://www.laohamutuk.org/Oil/Power/PowerSIP 2005.pdf<accessed on 3 Feb 2012>.
5. Da Silva, P., A Comprehensive Review of Electricity Industry Development in Timor-Leste, Energy Planning and Policy Department – University of Technology, Sydney (UTS), Master Thesis for Energy Planning and Policy Course, 2012, Sydney, Australia.
6. GovTL, Budget Overview Book 1, State 2011 Budget, Ministry of Finance, 2011, Dili Timor-Leste
7. Lao Hamutuk, Notes for the "Allocation of the 2012 State Budget" graphic*FromLa'oHamutuk*, 2011,Dili, Timor-Leste
8. Electricidade de Timor-Leste (EDTL) – Department of Comercial, Data and information were collected on several occosion from December 2011- April 2012.
9. UNTAET, Electricity tariffs directive law for Timor-Leste, 2001, Dili-Timor-Leste
10. Mercy Corps, Addressing Energy Poverty in Timor-Leste, 2009, Dili-Timor-Leste. Available at: http://www.energyforall.info/site/wp-content/uploads/2011/08/Timor-Energy.pd f<accessed on 23 Feb 2012>

Bond Strength of Reinforced Concrete using Stainless Slag as Fine Aggregate

[*1]Leandro Madeira Branco, *[2]Katsuhiko Takami

[*1]Department of Civil Engineering, Universidade Nacional Timor Lorosa'e

[*2]Department of Civil and Environmental Engineering, Yamaguchi University, Japan

Abstract: It is important to reduce the consumption of sea sand as fine aggregate due to subvert the environment issue by using alternative waste material such as stainless slag.   Stainless slag is a by-product in producing stainless steel, In Japan, that amount of stainless slag is estimated approximately 30,000 tons per year. Many experimental studies have been conducted to use this stainless slag as fine aggregate. In this study, pulling out tests are carried out in order to make sure that the concrete using stainless slag as fine aggregate has sufficient bond strength against reinforcing bars in comparison with normal concrete. The bond strength is one of essential factors which form the reinforced concrete structure. The slippage between concrete and reinforcing bar and the bond strength are measured for two test specimens. One is stainless slag concrete and the other is normal concrete. As results, the slippage and bond behavior of two test specimens are quite similar.

Keywords: Waste material, Bond strength, Reinforced concrete, Stainless slag, Fine aggregate

1. Introduction

It is important to reduce consumption of sea sand as fine aggregate due to subvert the environment issue by use alternative waste material such as stainless slag. Stainless slag is a waste material produced by production of stainless steel, approximately one ton of stainless steel waste is generated when producing three tons of stainless steel. In Japan, the amount of stainless slag is   estimated approximately 30,000 tons per year in producing stainless steel. The previous experimental studies[1] have clarified the basic physical properties of stainless slag concrete, and revealed the possibility to be efficiently used as fine aggregate. And also, long term properties of the concrete are investigated[2].

In order to promote stainless slag as fine aggregate on the structural purpose, authors investigated the behavior and performance of bond behavior for reinforced concrete (RC) containing stainless slag as fine aggregate.

Bond strength, defined chemically as the strength with which a chemical bond holds two atoms together, has been conventionally measured in terms of the amount of energy it required to break the bond. In engineering field, it is measured in terms of the stress needed to separate the bonded layers from each other. The amount of adhesion between bonded surfaces is measured in terms of the stress required to separate a layer of material from the base to which it is bonded, the stress acting parallel to the bonded material along the interface is called bond stress.

The utility of reinforced concrete as a structural member is derived from the combination of concrete that is strong and relatively durable in compression with reinforcing steel that is strong and ductile in tension. In order to keep the composite action, the transmission of load without loose between the concrete and steel is necessary. This load transmission is referred to as bond and is ideal as a continuous stress field that develops in the area of the steel-concrete interface. The transmission of axial force from reinforcing steel bar to the surrounding concrete produced from the development of tangential stress components along the contacting surface.

In this paper, the bond behaviors around a steel reinforcement of reinforced concrete specimen using stainless slag as fine aggregate have been investigated.

2.   Material of experiment

2.1 Concrete materials

Table 1 shows the properties of concrete materials. Sea sand as fine aggregate (S) is extracted from the Sea of Genkain located in Fukuoka prefecture, and that has dry density 2.57 g/cm^3, water absorption 1.62% and fineness modulus 2.85. Stainless steel slag (NSS) which is a by-product stainless steel production, with physical properties oven-dry density 3.04 g/cm^3, surface dry density 3.08 g/cm^3, water absorption 1.53%, and fineness modulus 2.95 including 1.96% amount of finer material. Two of AE water reducing agent (Frolich SV 10 and SV 100) in admixture is 0.1% total amount of cement, respectively

Table.1 Description concrete material

Material	Surface Dry Density (g/cm^3)	Water absorption (%)	Fineness modulus	Maximum particle size (mm)
Sea Sand (S)	2.57	1.62	2.85	-
Stainless Slag (NSS)	3.08	1.53	2.95	-
Crushed Gravel (G)	2.70	1.00	-	20
Ordinary Cement (C)	3.15	-	-	-
Water (W)	1.00	-	-	-
AE (Frolic SV-100)	0.1 % of total cement			
AE (Frolic SV 10)	0.1% of total cement			

Table. 2 Description Reinforcement bar

Mark	Type	Diameter measurement (mm)	Length (mm)	Elastic modulus (N/mm^2)	Yielding strength (N/mm^2)
D25	SD295A	25.4	500	2×10^5	295

Table. 3 Mix proportion

Type	W/C	Unite weight (kg/m^3)					
		W	C	NSS	S	G	AE
Slag 0	50	170	340	0	696	1097	3.40
Slag 60	50	170	340	500	278	1097	3.40

2.1 Reinforcement steel

Description of reinforcement steel bar has been shown in the Table 2.

3. Experiment Procedure[3]
3.1 Concrete mix proportion

Table 3 shows the mix proportions. The two cases of replacement of sea sand with stainless slag are designed as shown 0% and 60%. Every concrete has w/c ratio of 50%. The procedure of mixing using twin-screw mixer with the maximum capacity 50 liters, insert fine aggregate and cement mixing during 30 second, then

The next step is mixing water and AE insert inside the mixer, running again mixer for 1 minute, finally add the coarse aggregate for 2 minutes mixing. The total time of mixing is 3 minutes 30 second. After that, pull out the concrete to the basket and performed slump design and air content. The procedure of Slump test and air content based to JIS A 1101 and JIS A 1128, with the design of slump 10±2.0 cm and air content 4.5 ±1.5 cm. After finishing slump and aur content tests, pouring fresh concrete into a cylinder mold for compressive strength, tensile strength and modulus elastic tests, including cube mold for bond strength test.stop the mixer.

3.2 Casting Specimen for bond strength test

The reinforcement attached by strain gauge at area with distance four times of diameter not including free distance at outside, the attachment with the difference 2 cm between strain gauge. Then another are 2 times diameter is a free zone as a balance to the performed stress during testing as shown in Fig. 1 and fix the reinforcing bars vertically at the center.

The concrete specimens were cast in 3 layers of 150x150x150 mm cube molds with embedded reinforcing bar (D25). Deform bar place in the center of cube as shown, at the end left about 3 cm free. The concrete pouring to mold by use method of cast was divided by 3 layers, each layer was compacted by 25 blows using the standard compacting rod and later the concrete surface was smooth. After 24 hours, the molds were removed and the concrete specimens were cured in a water tank for testing date, testing for 0 % stainless slag was 21 days and for 60 % stainless slag 16 days. This is condition occur because of the changing of temperature rapidly.

3.3 Measurement and loading equipment

The experiment of bond strength, conducted by using method "Test Method for bond strength between reinforcing steel and concrete by pull-out test (JSCE-G-503-2007)", the principle and setting of testing as shown. After setting the specimen on the support base, fixed and connected with the displacement meter under support base hole and spacer plate, put in the upper of the specimen. Laden was performed by using a manual hydraulic jack, tensile strength machine was used defined in JIS B 7721. Overall view of setting of measurement and equipment was used shown in Fig. 2.

The measurement method by setting the degree of tensile stress to 50 N/mm^2 and applied the load, the bond stress was then calculated and recorded at intervals of 0.01mm of average loaded end slippage.
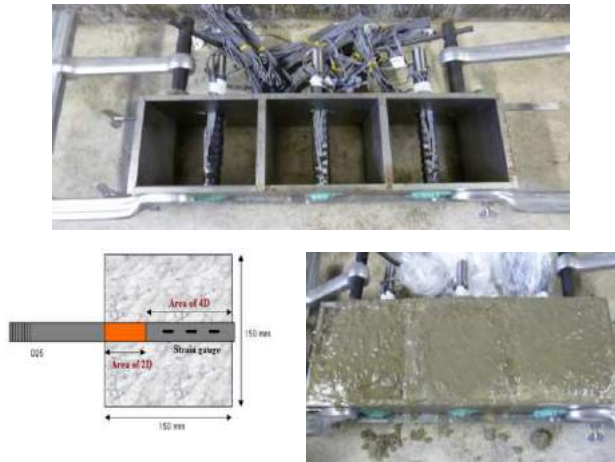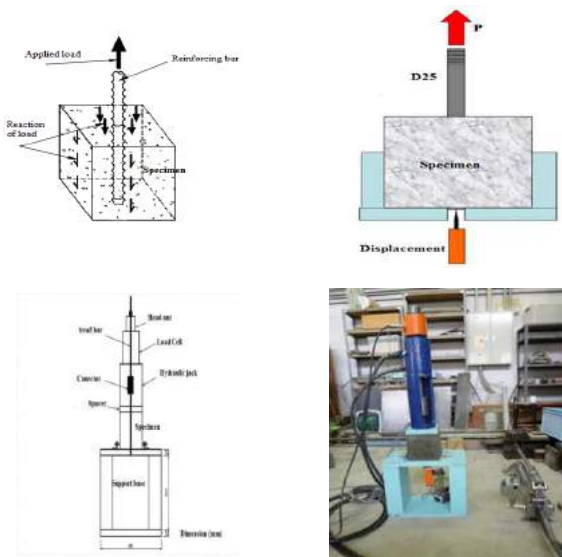

Fig. 1 Preparation of test specimens

Fig.2 Overview of testing and loading method

3.4 Bond strength calculation

The calculation for bond strength of Reinforced concrete is based by "Test Method for bond strength between reinforcing steel and concrete by pull-out test (JSCE-G-503-2007)". The result took from the measurement during the experiment. The result, as the expression of bond stress can be formulated as shown below

$$\tau = \frac{P}{4\pi D^2} \times \alpha \qquad (1)$$

Where, τ : Bond Stress (N/mm^2)

P : Load (N)

D : Diameter of rebar (mm)

α : The correction factor of compressive strength

$$\alpha = 30 / f'_C$$

f'_C : Compressive strength of concrete (N/mm^2)

The detail of Formula above,

Circumference of rebar $= \pi D$

Attachment length $= 4D$

Surface area of compressive A $= \pi D \times 4D = 4\pi D^2$

Bond stress $\tau = \dfrac{P}{A} \times \alpha = \dfrac{P}{4\pi D^2} \times \alpha$

3.5 The property of concrete specimen

The cylindrical specimens were prepared for the compressive strength, split testing (tensile strength) and elastic modulus test. **The** specimens were cured in the water pool, with temperature and moisture control until the testing day. The testing methods are based on Japanese industrial standard (JIS), namely JIS A 1108 for compressive strength test, JIS A 1113 for Split tensile testing and JIS A 1149 for elastic modulus at the age 21 and 16 days, for the concrete contains a stainless steel slag (NSS) with the replacement of sea sand with 0 % and 60 %, respectively.

Table. 4 Result of Slump and air content

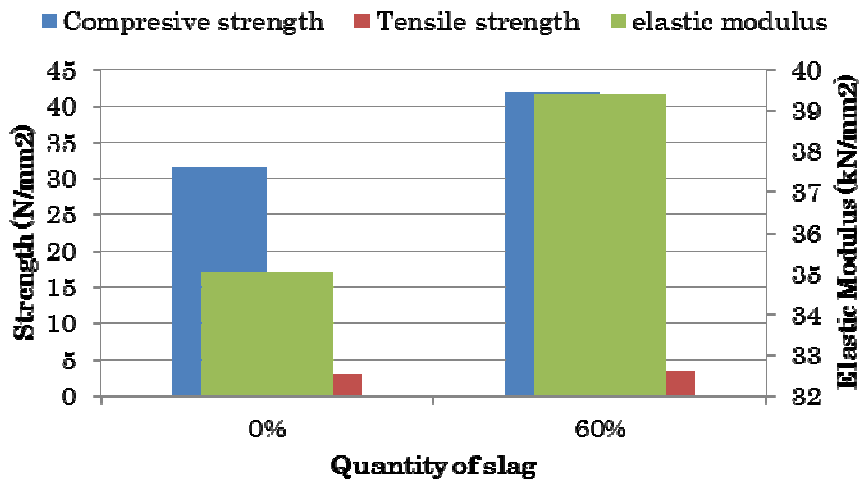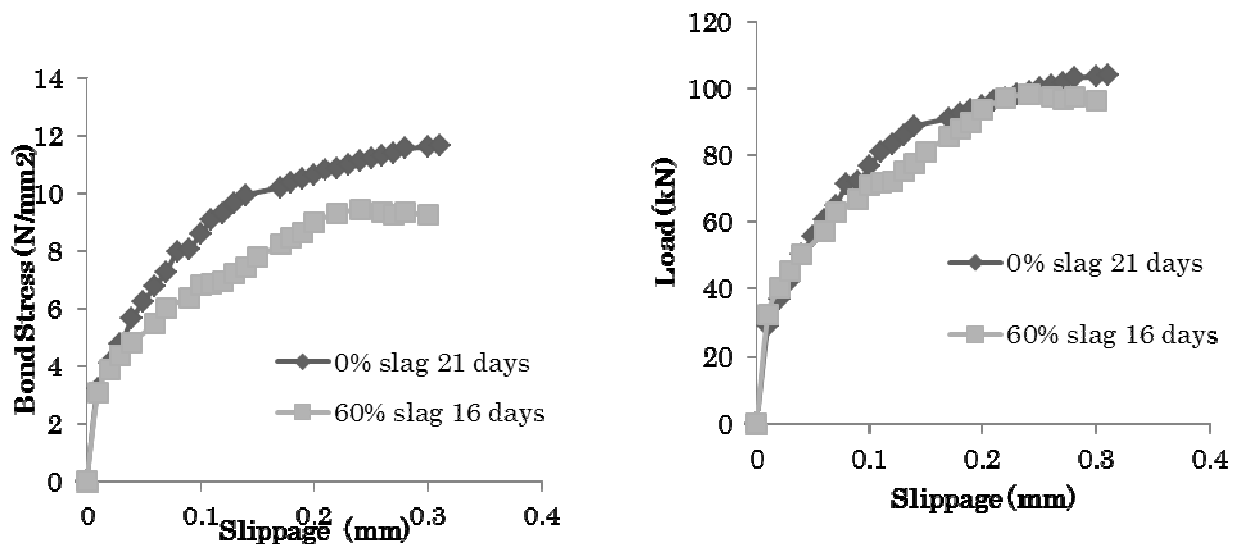| Slag	Slump (cm)	Air content (%)
0 %	14	6
60 %	8	3.5

Fig.2 Results of properties of concrete

A) Relationship between Bond stress and Slippage

B) Relationship between Load and Slippage

Fig. 4 Result of Pull-out test

0 % of stainless slag   60 % stainless slag

Fig. 5 Behavior of specimen after crack and failure

4. Result and discussion

4.1 The property of concrete

The results are shown in Table 4. The performance of mechanical properties of fresh concrete is within the design criteria. Fig.3 shows the result of the properties of hardened concrete. The compressive strength of the concrete containing 60 % of stainless slag which tested at 16 days is higher than that of the concrete containing 0 % stainless slag. In the previous study[2], the strength of the concrete containing the stainless slag up to 30% is almost same with that of the normal concrete without stainless slag. This time, the concrete with high volume stainless slag may have high strength and large elastic modulus in comparison with normal concrete.

4.2 Bond strength

Fig. 4 shows the relationship between pull-out load and slippage and the relationship between bond stress and slippage. The result shown applied load for both of concrete specimen, shows not a significant difference. There is no significant difference in the result of pull-out load at each slippage between the specimen with 0% NSS after 21 days curing and 60% NSS after 16 days curing. However, the result of bond stress shows that the concrete containing only sea sand owned the quiet higher or almost similar bond stress result compared with the concrete containing 60 % of stainless slag. It can be said that the concrete with higher compressive strength should show the higher bond strength.

4.3 Crack behavior

Fig. 5 (a) shows the cracks condition observed both on the specimens containing 0% stainless slag and 60% during the proses of test then, after the sample failure and the when measurement of crack using crack meter measurement.. Cracks occurred rapidly in the concrete to in the bond of concrete and steel in the test specimens.

The crack behaviors in both specimens were similar. This is condition causes applied tensile stress in the concrete itself. The specimens were broken into two pieces in order to observe the condition at the cross section including the reinforcement bar. It finds the specimen with contain stainless slags which showed the larger in the compressive strength however it shows more bubble inside the specimens (it cause by weak in compacted and preparation sample) than the one with no stainless slag as shown in Fig. 5 (b).

5. Conclusion

The bond strength behavior of reinforced concrete containing stainless slag was investigated in this paper. The method conducted to analysis by using the pullout test method was taken in order to analyze the bond strength of reinforced concrete. From this series of the experiments, the following conclusions can be drawn.

The compressive strength and elastic modulus of concrete with 60% stainless slag are higher in comparison with the normal concrete.
1. Bond behavior of reinforced concrete depends on testing age and consistency of the concrete.
2. The bond strengths of both tested concrete are almost same.

References

1. Oka, Y. Takami, K. Uraki, D and Matsui, E.; Study on Concrete using Stainless Slag as Fine Aggregate, Proceedings of the Japan Concrete Institute Vol.35, June 2014.
2. Tokushige, Y. Matsuo, E. Takami, K. and Tasaka, A.; Fundamental study on the properties of concrete using stainless slag as fine aggregate, Proceedings of West Branch of Japan Society of Civil Engineers, March 2013.
3. JSCE Guideline for Concrete no. 15 (2007) Standard Specification for concrete structure-2007 "design" English version

Preliminary investigation of physical properties of river aggregate in Timor-Leste

[*1]Leandro Madeira Branco, [*1]José Maria Ximenes

[*1] Department of Civil Engineering, Universidade Nacional Timor Lorosa'e

Abstract: Aggregate typically occupies 70 to 80 % of concrete and 70 to 95 % for road pavement. Considering that dominant composition,stable material properties of aggregate are required.Therefore attention to the quality of aggregate should be prayed, because it will determine the limitation of concrete strength, durability and performance of concrete and it´s structures. The main purpose of this studyis to make clear the material properties of aggregate in Timor-Leste for deciding the mix-proportion of desired concrete. From this research, several conclusions and recommendations for practical use of aggregate were derived. And it is emphasized to accumulate test data on aggregate for producing reliable concrete.

Keywords: Physical properties, river aggregate, Timor-Leste

1. Background

Aggregate typically occupies 70 to 80 % of the total volume for normal concrete and 70 to 95 % for road pavement. Considering that dominant composition, stable material properties of aggregate are required. Therefore attention to the quality of aggregate should be prayed, because it will determine the limitation of concrete strength, durability and performance of concrete and itsstructures. This study is a preliminary investigation for basic information and the starting point to grasp the quality of river aggregate in Timor-Leste.

Generally, river sand and gravel are used as fine aggregate and coarse aggregate for producing concrete in many construction sites for housing, Material qualities of aggregate for concrete are regulated by specifications, for example, AASHTO in U.S.A, and SNI in Indonesia. However, in private construction use, river sand and gravel are directly used for concrete without strict quality confirmation by tests.

This study is regarded as a preliminary research providing the basic information for societies to recognize the quality of river aggregate, and that also can be used for construction. The result may show adequate places to take the river aggregates.

2. Basics information

2.1 Environment condition

Timor-Leste is a tropical island, and has two seasons (dry season and rainy season)forwhole years. The rainy season starts October to March, and the dry season startsApril to September.

The topography of the country is mountainous, and that condition creates many riversconsequently. But there is nodams (water banks) in the basins. In the rainy season, rainfall directly flows from the mountain or hill area to the flat area and sometimes makes flood and sedimentation.Actually, several rivers only run in the rainy season, and dry up perfectlyin the dry season.

2.2 Sampling location

Seven locations are chosen for sampling of river aggregate as shown in Table 1. Sampling locations are selected evenly around Timor-Leste. In these locations, practical extractions of aggregate for construction are carried out.

Table. 1 Location of sampling

No.	Location	River Name	Condition of sample
1	District Aileu	Mantane	dry
2	District Liquisa I	Maumeta	wet
3	District Liquisa II	Comluli	wet
4	District Liquisa III	Aipelu	wet
5	District Manatuto I	Manatuto	wet
6	Distric Manatuto II	Laleia	dry
7	District Dili	Comoro	dry

Sampling works last through the rainy season to the dry season, so the water content of aggregate is deferent in each sample. Those conditionsare added to Table 1.

Sampling of aggregate is carried out in accordance with ASTM D 75[1]. Examples of sampled river fine aggregate are shown in Fig.1.

Fig. 1 Examples of sampled fine aggregates

3. Test for aggregate

3.1 Sieve analysis (ASTM C136[1])

According to ASTM C 136, coarse aggregate is defined as all material of aggregate retained in sieve

4.75mm, and fine aggregate is all material of aggregate passing sieve 4.75 mm. Fineness modulus is calculated with the results of sieve analysis for fine aggregate and coarse aggregate, respectively

3.2 Density and water absorption test (ASTM C127[1]), (ASTM C128[1])

Test methods for density and water absorption for coarse aggregate and fine aggregate are described in ASTM C 127 and ASTM C 128, respectively. At the tests for density and water absorption of both aggregate, saturated surface dry condition is the norm. So each sampled aggregate which was in wet or perfect dry condition, was adjusted to saturated surface dry condition

Generally, aggregate is classified to three ranges in density, lightweight aggregate is under 2.5 g/cm^3, normal aggregate ranges between 2.5 g/cm^3 and 2.7 g/cm^3, and heavy weight aggregate is above 2.7 g/cm^3.

3.3 Amount of material passing test sieve 75 μ m (ASTM C117[1]) and Los Angeles abrasion test (ASTM C131[1])

The abrasion loss value by Los Angeles abrasion test indicates toughness of aggregate. This time, Los Angeles abrasion test was carried out in the National Laboratory.The abrasion value depends on the rock type of aggregate. The limit abrasion loss values from 40% to 45% are adopted in most of states and agencies in U.S.A.

4. Result and Discussion

4.1 Sieve analysis

Fig. 2 shows the results of sieve analysis for coarse aggregate. The maximum size of coarse aggregates among collected aggregate is 31.5 mm. It is recognized that the coarse aggregate in District Liquisa II consists of smaller size particles, whereas the coarse aggregate in District Aileu consists of comparatively larger size particles.
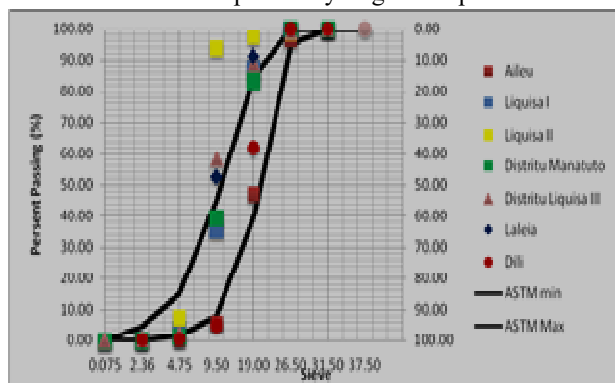

Fig. 2 Grading of rivers coarse aggregates

Fig.3 shows the results of sieve analysis for fine aggregate. The grading of investigated river fine aggregate indicates that as a whole, particle size of aggregate in sampled locations is larger excluding in Distric Manatuto II. Some grading curves are out of the grading recommendation in ASTM.
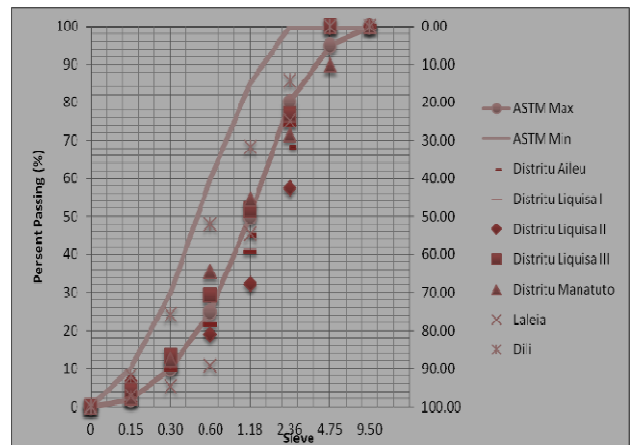

Fig. 3 Grading of rivers fine aggregates

Fineness modulus calculated with the result of sieve analysis is also shown in Table 2.

Table. 2 Fineness modulus of aggregates

No	Location	River Name	Fineness modulus	
			Fine Aggregate (%)	Coarse Aggregate (%)
1	District Aileu	Mantane	3.46	4.50
2	District Liquisa I	Maumeta	3.53	3.73
3	District Liquisa II	Comluli	3.73	3.02
4	District Liquisa III	Aipelu	3.24	3.51
5	District Manatuto I	Manatuto	3.33	3.76
6	District Manatuto II	Laleia	3.60	3.54
7	District Dili	Comoro	3.59	3.32

4.2 Density and water absorption

Table3 shows the measured density and water absorption for fine aggregate and coarse aggregate. Densities of fine aggregate and coarse aggregate in District Manatuto are a little lager than those of aggregate in other districts. Also, water absorptions of fine aggregate and coarse aggregate in District Manatuto I and Manatuto II are fairly low. This means that the aggregates at two locations are extremely solid. On the contrary, from that point of view, fine aggregates in District Aileu, District Liquisa III and District Dili have voids inside of particle. Water absorption of coarse aggregate in District Aileu is comparatively high.

4.3 Fineness particle passing 0.075 mm sieve and Los Angeles abrasion

Table 4 shows the results of fineness particle passing test 0.075mm sieve and Los Angeles abrasion test. Fineness particle passing 0.075mm sieve ration of the aggregate in District Aileu is extraordinary high. Concrete using aggregate with high volume fine particle tends to become sticky and low workable.Los Angeles abrasion loss values of all aggregate are below 41%.

Table. 3 Density and water absorption of fine and coarse aggregates

No	Location	River Name	Density (g/cm³)		Water absorption (%)	
			Fine	Coarse	Fine	Coarse
1	District Aileu	Mantane	2.58	2.51	2.13	3.04
2	District Liquisa I	Maumeta	2.66	2.62	1.95	1.66
3	District Liquisa II	Comluli	2.63	2.64	1.43	1.87
4	District Liquisa III	Aipelu	2.62	2.62	2.32	1.98
5	District Manatuto I	Manatuto	2.74	2.70	0.99	0.88
6	DistricManatuto II	Laleia	2.67	2.64	0.89	1.15
7	District Dili	Comoro	2.58	2.66	2.35	1.90

Table. 4 Fineness particle passing 0.075mmsieve and Los Angeles abrasion

No	Location	River Name	Fineness particle passing 0.075mm sieve (%)	Los Angeles abrasion (%)
1	District Aileu	Mantane	14.30	33.83
2	District Liquisa I	Maumeta	7.50	39.08
3	District Liquisa II	Comluli	6.64	37.51
4	District Liquisa III	Aipelu	2.82	35.08
5	District Manatuto I	Manatuto	1.80	26.97
6	District Manatuto II	Laleia	1.26	37.14
7	District Dili	Comoro	6.26	40.82

5. Conclusion

From this preliminary investigation, several conclusions and recommendations for practical use of aggregate are derived in Table 5.

Table. 5 Conclusion and recommendation

No.	Location	Conclusion
1	District Aileu (Mantane)	- It has to be washed. - Be careful to adjust to surface dry condition of coarse aggregate. - Not recommended to use directly if not washing
2	District Liquisa I (Maumeta)	- Could be used directly during mixing concrete without washing, however need to investigate concrete strength in the future
3	District Liquisa II (Comluli)	- Could be used directly during mixing concrete without washing, however need to investigate concrete strength
4	District Liquisa III (Aipelu)	- Could be used directly during mixing concrete without washing, however need to investigate concrete strength
5	District Manatuto I (Manatuto)	- Recommended for use in practical construction, however need to investigate concrete strength
6	DistricManatuto II (Laleia)	- Recommended for use in practical construction, however need to investigate concrete strength
7	District Dili (Comoro)	- Grading is good. - It has to be washed. - Need further investigation for the concrete strength

This time, sampling point for one river is only one location. Practically, collecting aggregate for construction is conducted along the river. So, continuous investigations of physical properties of aggregate along the river are necessary. It is important to accumulate test data on aggregate for producing reliable concrete in Timor-Leste.

References

1. ASTM Annual Books 2004.
2. Irving Kett "ENGINEERED CONCRETE Mix design and Test Method "ISBN 0-8493-2277-4 TA442.5K48 1999

The application of a evaluation of road surface in Timor-Leste by using Ippo-campo system

[*1]Aleixo Sarmento, [*1]Hugo da Costa Ximenes, [*2]Ayaho Miyamoto, [*2]Hisao Emoto
[*1]Department of Civil Engineering, Universidade Nacional Timor Lorosa'e
[*2]Department of Civil and Environmental Engineering, Yamaguchi University, Japan

Abstract: Recently, road pavement surfaces have seriously deteriorated due to aging and the increasing number of heavy vehicles. Therefore, appropriate maintenance is required for the road to provide service over a long time. Many efforts have been made by road experts for maintenance of the road pavement surface. However, there are some problems due to cost performance and vehicle running costs. Therefore, we have tried to develop a more rational assessment system using the latest information and technology. This paper is about the practical application of a road condition assessment system applied in Timor-Leste road networks to evaluate the serviceability of existing road pavement surfaces. The system will evaluate the condition of pavement surfaces using video recording and motion sensor to obtain Z-axis (vertical) acceleration data. This system was developed using the Visual Basic Application.

Keywords: Road surface, Timor-Leste, Ippo-campo system, Visual Basic Application

1. Introduction

Timor-Leste is one of the least developed countries in the region. Its nonoil economy is characterized by slow and unstable growth, although there has been recent strong growth in urban centers, particularly in the capital city. The economy is essentially agriculture-based, with about 72% of the total population of 1.1 million living in rural areas. Subsistence farming provides the main source of livelihoods for the large majority of rural people with limited production of agricultural products, mostly coffee, for cash income. The Asian Development Bank (ADB) has announced that agricultural productivity Timor-Leste is low compared with other countries in the region. Despite development efforts in recent years, the poor condition of basic infrastructure in general and the road network in particular remains a key constraint (Government of Timor-Leste, 2011)[1),2), 3)].

According to the Ministry of Public Works (Mo-PW) of the Democratic Republic of Timor-Leste (RDTL), Timor-Leste has a relatively dense road network, with a total estimated length of 6,036 km. It includes 1,426 km of national roads, 869 km of district roads, 716 km of urban roads, and 3,025 km of unpaved rural roads. Overall, the road network is in a bad condition. A recently completed study funded by the European Commission surveyed 730 km of rural roads accessible by vehicle and found about 69% of these to be in a bad or very bad condition. It is, therefore, estimated that 90% of the total rural roads network is in a bad or very bad condition. National and district roads are also in a poor condition.

Roads constitute the primary mode of transport in Timor-Leste, carrying 70% of freight and 90% of passengers. The ADB study affirmed that, due to the poor condition of rural roads, rural people face increased travel times and transportation costs and are isolated in terms of access to social and economic facilities and services, such as local markets, schools, health facilities, job opportunities, government services, and banking services (Asian Development Bank of Timor-Leste, 2013).

Indication of road pavement damages addresses to ultimate causes; one example is the overloading of a heavy vehicle at an exponential rate of the average power fourth. In addition, most roads in Timor-Leste do not receive proper maintenance, especially in rural areas. It is, therefore, desired to analyze the main factors causing the lack of maintenance and, therefore, to propose means by which they can be improved. Particular emphasis will be placed on the provision and maintenance of road pavement systems, the failure of which is probably the main reason for the poor performance of Timor-Leste's roads.

This paper introduces a road condition assessment system to evaluate the serviceability of existing road pavement surfaces in Timor-Leste. The system is suitable to the condition of Timor-Leste as a developing country because it is a rational system that uses the latest information and technological devices at a relatively low cost.

2. Methods and procedure for road condition assessment[4)-7)]

For road pavement, the Maintenance Control Index (MCI) has used in Japan as indexed road pavement damage by using cracking, rut depth, and smoothness as a parameter of ratio.

(1) Method purposed and application system

In this study, the apply to evaluate road pavement system in Timor-Lest is proposed. This system is using motion sensor, which have function as GPS, a gyro sensor and acceleration sensor. Fig. 1 shows the installed equipment in a vehicle that used for measurement. The speed of the car is at 50 km/h to 60 km/h. The motion sensor data, records video data, audio data, subtitle data, and GPS data are acquired by the system. Especially, GPS and acceleration data are getting from motion sensor as shown in Fig.2. And then by analyzing these data, the output of the evaluation of the road surface can be obtained.

(2) Determination of Threshold in Timor-Leste

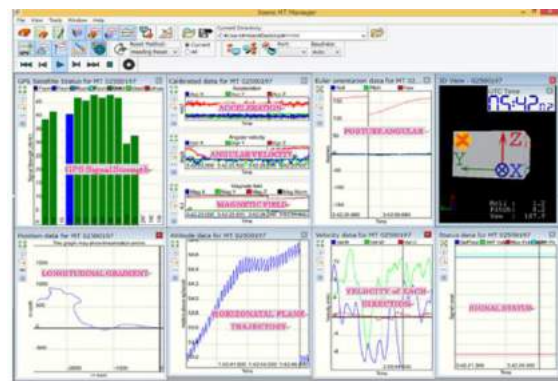**Fig.1** Arrangement of equipment (Ximenes, 2014)

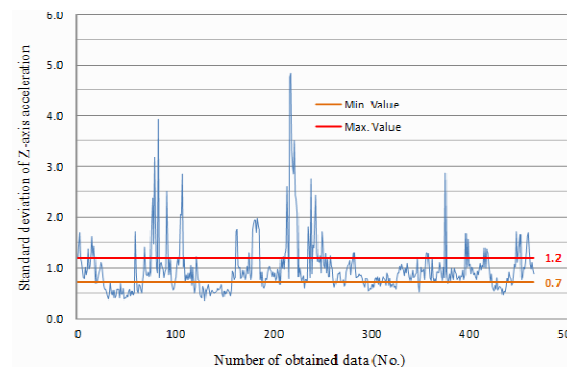**Fig.2** Display on signal system (Ximenes, 2014)

Fig.3 Threshold value (Ximenes, 2014)

This application system can be obtain standard deviation by the objective to determine value of threshold. It was decided that the good condition ranged 0~0.7, the moderate ranged 0.7~1.2, and bad condition was more than 1.2[7)].

Fig. 4 Road network and target route (Ximenes, 2015)

Table 1 The route number and destination

No	Route number/ Line colors	Destination	Roundtrip distance (km)	Remarks
1	I/ Dark purple	Dili-Maubisse-Dili	70 x 2	Succeed
2	II/ Yellow	Dili-Maliana-Dili	149 x 2	Succeed
3	III/ Red	Dili-Baucau-Dili	122 x 2	Succeed
4	IV/ Dark blue	Baucau-Com-Lospalos-Baucau	67 x 2	Succeed
5	V/ Purple	Manatuto-Natarbora-Manatuto	81 x 2	Succeed
6	VI/ Reddish yellow	Baucau-Viqueque-Baucau	60.7 x 2	Succeed
7	VII/ Pink	Dili-Ermera-Dili	59.6 x 2	Succeed
8	VIII/ Brown	Maubisse-Same-Maubisse	42.5 x 2	Succeed
9	IX/ Dark yellow	Fleicha-Ainaro-Suai-Fleicha	88.5 x 2	Succeed
	Total Distances		740.3 x 2	Done

3. Experimental study in Timor-Leste

The target experimental road pavement network measurement by using ippo-campo system in Timor-Leste is shown in Fig.4 and Table 1.

4. Result

(1)Compare with March 2014 and September 2015 at Dill to Maliana

The video data as shown in Fig. 5 on March 2014 of initial measurement compare with the road condition on September 2015. As result, it is founded that clearly the road condition.

(2) Data comparison

Table 2 is shown in compared with thresholds in routes of the Timor-Leste road network. Table 3is shown in a list of evaluating the road conditions in Timor-Leste by using the Ippo-Campo system [8].

March 2014

September 2015

Fig. 5 The video data comparison

Table. 2 Comparison condition using the both thresholds

Route's number	Evaluation results							
	Japanese Thresholds				Timor-Leste Thresholds			
	Good	Moderate	Bad	Total	Good	Moderate	Bad	Total
I	48	881	16222	17151	1563	7021	8567	17151
II	635	3802	18985	23422	5923	6507	10992	23422
III	94	1955	16743	18792	3533	9324	5935	18792
IV	132	2849	9384	12365	4189	4664	3512	12365
V	1052	2372	15383	18807	5130	5204	8473	18807
VI	154	459	12574	13187	973	2705	9509	13187
VII	388	1714	12785	14887	2766	2679	9442	14887
VIII	233	540	11351	12124	1156	2727	8241	12124
IX	394	426	18846	19666	1221	3611	14834	19666

Table. 3 Evaluation result of road condition in Timor-Leste using Ippo-Campo system

Route's number	Percentages of each conditions(%) (Japanese thresholds)				Percentages of each conditions(%) (Timor-Leste thresholds)				Comparative changes using both thresholds (%)			
	Good	Moderate	Bad	Total	Good	Moderate	Bad	Total	Good	Moderate	Bad	Total
I	0.28	5.14	94.58	100	9.11	40.94	49.95	100	8.83	35.80	-44.63	0.00
II	2.71	16.23	81.06	100	25.29	27.78	46.93	100	22.58	11.55	-34.13	0.00
III	0.50	10.40	89.10	100	18.80	49.62	31.58	100	18.30	39.21	-57.51	0.00
IV	1.07	23.04	75.89	100	33.88	37.72	28.40	100	32.81	14.68	-47.49	0.00
V	5.59	12.61	81.79	100	27.28	27.67	45.05	100	21.68	15.06	-36.74	0.00
VI	1.17	3.48	95.35	100	7.38	20.51	72.11	100	6.21	17.03	-23.24	0.00
VII	2.61	11.51	85.88	100	18.58	18.00	63.42	100	15.97	6.48	-22.46	0.00
VIII	1.92	4.45	93.62	100	9.53	22.49	67.97	100	7.61	18.04	-25.65	0.00
IX	2.00	2.17	95.83	100	6.21	18.36	75.43	100	4.2	16.20	-20.40	0.00

5. Conclusions

The Ippo-Campo system was designed as road surface pavement maintenance—a system based on a running vehicle to obtain data from a motion sensor, video record, sound, subtitle, and GPS. In the initial plan, it was designed for the condition of Japan's roads, where it has been established as a good system on IT-based works. Through the IT-based works, the system can accordingly obtain output data of the result easily in various formats that are effective and efficient. Therefore, the system can also be applied in other countries. In developing countries, there are some problems relating to road maintenance work because there is a limitation to the budget used for a good system for maintaining a road network. This condition results in many roads remaining damaged, which is affected by the economic loss of a country. Hence, the use of the Ippo-Campo system in a developing country is necessary because it is relatively low-cost. The application of Ippo-Campo to a road network in Timor-Leste has confirmed the effectiveness and workability of the system. As a result, the conclusions are summarized as follows:

a) An IT-based road condition assessment system (called "Ippo-Campo"), which has been developed based on a digital movie, vehicle vibration, sound with GPS, and low-cost constraint, can be applied in Timor-Leste's road network with a different threshold.

b) The proposed (Ippo-Campo) system tried to apply a few actual road networks in Timor-Leste to evaluate its effectiveness. As a result, it has confirmed that the road surfaces in the target routes, as shown in Figure 5, are in a not-so-good condition compared with the condition of the Japanese rural area road network.

c) Timor-Leste, as a developing country, needs a simple and rational system for a road condition assessment system. Therefore, the Ippo-Campo system can contribute to the making of a rational maintenance strategy in Timor-Leste's road network in the future.

References

1. Asian Development Bank of Timor-Leste: Democratic Republic of Timor-Leste: Road Network Upgrading Project, ADB LOAN No. 2857-TIM, 2013.
2. Government of Timor-Leste: Timor-Leste Strategic Development Plan 2011–2030, 2011.
3. Ximenes, H. C., Emoto, H., Miyamoto, A., Sarmento, A.,: Practical application of road condition assessment system to road networks in Timor-Lest, Proc. of 2014 Asia-pacific computer science and applications (CSAC2014), 27-28 Dec., Shanghai China, CRC Press, 2014.
4. Miyamoto, A., Yoshitake, T.,: Development of a Remote Condition Assessment System for Road Infrastructure," International., 2009.
5. ECCE Conference, EUROINFRA, Current State and Challenges for Sustainable Development of Infrastructure, Symposium 1, Helsinki, Finland, pp. 21–22, 2009.
6. Miyamoto, A., Nakano, T., and Yoshitake, T.,: Development of a Road Condition Assessment System Using Digital Movies, Vehicle Vibration and Sound, Proceedings of the Fourteenth International Conference on Civil, Structural and Environmental Engineering Computing, Civil-Comp Press, Paper No.195, pp. 1–22., 2013.
7. Sayers, M. W., Gillespie, T. D., and Paterson, W. D. O., The International Road Roughness Experiment," World Bank Technical, p. 45, 1985.
8. Ximenes, H. C., Development of a road condition assessment system (IPPO-CAMPO) and practical Use of analytic hierarchy process (AHP) in decision making of road maintenance in Timor-Leste, Master thesis , Yamaguchi-University, 2015.09

The Impacts of Ambient and Panel's Temperature on the Output Performance of Commercial Solar Panels in Timor-Leste

[*1]Ruben Jerónimo Freitas, [*2]Hiroki Yoshida
[*1]Department of Electrical and Electronics Engineering, Universidade Nacional Timor Lorosa'e
[*2]Department of Electrical, Electronic and Computer Engineering, Gifu University, Japan

Abstract: The study was carried out to investigate the impacts of ambient and panel's temperature on the output performance of commercial crystalline and amorphous solar panels in Timor-Leste. The study shows that the high temperature does not favor high performance of the photovoltaic modules.

Keywords: Photovoltaic, polycrystalline, monocrystalline, amorphous, ambient and panel's temperature

1. Introduction

Timor-Leste is a country located in tropical area that receives a lot of sunshine through the year. As a consequence of its location, technically it is very potential to utilize photovoltaic technology in order to produce electrical energy. Technologies of photovoltaic system, started from commercially well-known brands to unknown brands have been widely available in Timor-Leste nowadays. People can simply distinguish those panels through the specification information available on the rear side of panels. Generally, available technologies of PV panels are made from polycrystalline (PC), monocrystalline (MC) and amorphous include thin film with different characteristics and efficiencies. Therefore, it is very important to know the output performance of such panels due to the impact of ambient and panels' temperatures.

To be operated on its maximum power point tracking (MPPT) is one factor that might affect the output performance of a PV panel. Meanwhile, MPP itself varies with factors such as; solar insolation, PV's cell temperature and operating voltage which are strongly influence the output current and power characteristics of PV. This correlation can be shown from well-known simplified equivalent PV circuit model bellow.[1-3]

$$I = I_{ph} - I_s \left[\exp\left(\frac{qV}{kT_cA} \right) - 1 \right], \qquad (1)$$

where, k is Boltzmann's constant, T_c is the cell temperature, A is the ideal factor, I_S is cell saturation of dark current in ampere, I_{ph} is the photocurrent, q is electronic charge.

The operating temperature of a solar cell can be estimated by the ambient temperature, wind velocity, the characteristics of the module and also by the intensity of sunlight falling on the module.[4] To calculate cell operating temperature can be estimated by using the approximation given by Ross and Smokler[1,4] as ;

$$T_{cell} = T_{air} + \frac{\text{NOCT} - 20}{800} \times S \ [°C], \qquad (2)$$

where the *nominal operating cell temperature* (NOCT) is defined as the temperature reached by open-circuited cells in a module under the following representative conditions: Irradiance on cell surface 800 W/m^2, air temperature 20 ℃, wind velocity 1 m/s and S is the insolation in W/m^2.

At last, the output performance of any PV panel can be obtained by using common electrical output formula and efficiency of the PV panel as;

$$Power[W] = Volt[V] \times Current[A] \qquad (3)$$

$$\text{Efficiency } \eta = \frac{\text{Power of PV Panel } P \times 100\%}{\text{Area of PV Panel } A_{\text{PV}} \times S} \qquad (4)$$

2. Materials and procedure

The study was conducted in the Laboratory of Power and Energy of Electrical and Electronic Engineering in Hera. Several of PV panel technologies from PC (SUNTECH 30 W), MC (JIS 100W) and amorphous (SHARP 120 W) were utilized. PV panels were put in the tilt angle of 10 degree facing north and connected to MPPT controllers to measure their output voltage and current. The precision weather station model Vantage pro2, was used to investigate environmental impacts, such as; the temperature of the environment and wind speed. The pyranometer model MS-602 was used to measure solar insolation. All data were recorded automatically on the data logger and computer by using special weather station software.

3. Results and discussion

Let us start with a brief review of results on studies conducted in other tropical region i.e. in Nigeria.

Sanusi,Y.K. et.al[5] measured the photovoltaic system

that consisted of three amorphous silicon solar modules in parallel configuration for the monthly average values of ambient temperature T_A ℃ and power output of the system for the year of 2006, 2007 and 2008 were compared. Among the results, it shows that there is a direct proportionality between the power output produced by the system and the ambient temperature of the locality.

Omubo-Pepple,V.B. et.al[6] measured MC type of panel by using digital multi meter. The data was measured every 30 minutes, started from 6 AM – 3 PM for one day off. Among the results: the group confirmed that the ambient temperature has no direct effect on the solar panel temperature rather solar flux does have effect. Indication of the operating temperature of the commercial photovoltaic module was about 43 ℃.

The study in Hera was conducted by using three different type of PV panels such as; PC, MC and amorphous. The results of the measurement are shown in the following tables.

Table. 1 PC Panel

Condition						
Date	20-11-2013			P max		30 W
Location	Hera			η at STC		10.36 %
Measurement						
Time	PV Panel				Amb. temp.	Wind speed	Inso-lation
	V [V]	I [A]	P_o [W]	T_m [℃]	T_a [℃]	v [m/s]	S [W/m²]
13:05	15.2	1.6	24.5	57	32.3	1.3	1002.8
13:10	15.4	1.6	25.3	57	32.3	2.7	1044.6
13:15	15.1	1.7	25.0	58	32.3	3.1	1016.7
13:20	15.1	1.6	24.8	59	32.4	0.4	1002.8
13:25	15.3	1.6	24.7	57	32.4	1.3	1002.8
13:30	15.3	1.6	25.0	59	32.4	0.4	1030.6
13:35	**15.3**	**1.7**	**25.7**	**60**	**32.6**	**1.7**	**1072.4**
13:40	15.2	0.7	10.2	57	32.6	1.3	487.5
13:45	15.8	1.5	24.3	55	32.3	0.4	919.2
13:50	15.8	1.5	23.6	57	32.4	0.9	961.0
13:55	15.9	1.5	23.3	58	32.6	0.4	947.1
14:00	15.7	1.5	23.3	59	33.0	0.9	947.1
Avg.	**15.4**	**1.5**	**23.3**	**58**	**32.5**	**1.2**	**952.9**

Table. 2 MC Panel

Condition						
Date	26-11-2013			P max		100 W
Location	Hera			η at STC		15.3 %
Measurement						
Time	PV Panel				Amb. temp.	Wind speed	Inso-lation
	V [V]	I [A]	P_o [W]	T_m [℃]	T_a [℃]	v [m/s]	S [W/m²]
11:05	15.2	2.6	39.5	48	31.3	0.0	501.4
11:10	14.6	2.6	37.3	50	31.4	1.8	459.6
11:15	14.4	4.8	68.8	51	31.5	0.0	1002.8
11:20	14.6	4.8	70.0	52	31.5	0.9	1044.6
11:25	14.5	5.1	73.7	52	31.6	0.4	1183.8
11:30	13.5	5.0	67.2	58	31.9	0.0	1100.3
11:35	16.5	1.4	22.2	55	32.3	0.4	348.2
11:40	15.0	1.5	21.9	49	32.1	0.3	278.6
11:45	15.4	2.0	30.1	43	31.5	1.8	376.0
11:50	**15.0**	**5.0**	**74.5**	**44**	**31.2**	**1.3**	**1142.1**
11:55	14.3	2.5	36.3	49	31.3	0.0	515.3
12:00	14.3	2.7	37.9	51	31.7	0.9	557.1
Avg.	**14.8**	**3.3**	**48.3**	**50**	**31.6**	**0.7**	**709.2**

Table. 3 Amorphous Panel

Condition						
Date	28-11-2003			P max		128 W
Location	Hera			η at STC		8.94 %
Measurement						
Time	PV Panel				Amb. temp.	Wind speed	Inso-lation
	V [V]	I [A]	P_o [W]	T_m [℃]	T_a [℃]	v [m/s]	S [W/m²]
11:05	41.2	0.7	28.0	45	31.6	1.3	222.8
11:10	43.0	0.7	31.0	42	31.3	3.6	250.7
11:15	44.0	2.7	120.5	44	31.1	0.4	1030.6
11:20	**42.2**	**3.0**	**126.3**	**50**	**31.3**	**0.9**	**1100.3**
11:25	41.6	2.6	108.9	54	31.8	0.9	947.1
11:30	41.1	1.3	52.2	54	32.2	0.0	445.7
11:35	43.6	2.6	113.3	55	32.4	0.4	1044.6
11:40	45.7	2.2	101.9	59	32.8	0.9	1072.4
11:45	39.4	0.9	34.3	54	32.9	0.4	278.6
11:50	40.3	0.7	29.8	51	32.8	0.0	236.8
11:55	41.2	0.8	31.7	48	32.6	0.4	264.6
12:00	42.7	0.9	38.4	45	32.1	0.4	320.3
Avg.	**42.2**	**1.6**	**68.0**	**50**	**32.1**	**0.8**	**601.2**
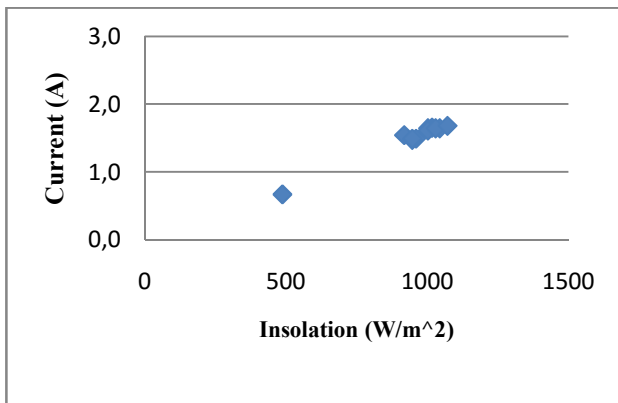
Fig. 1 Current vs. Insolation in PC
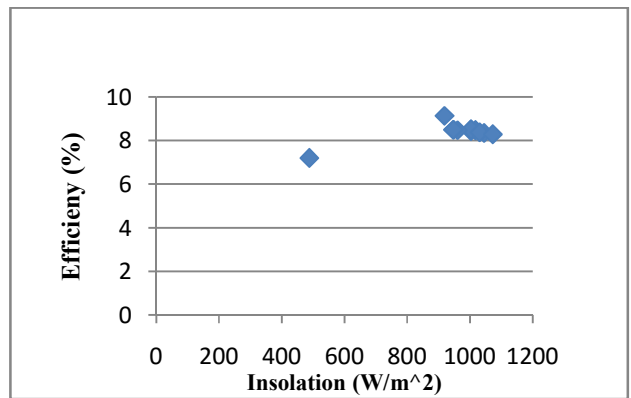
Fig. 2 Current vs. Insolation in MC

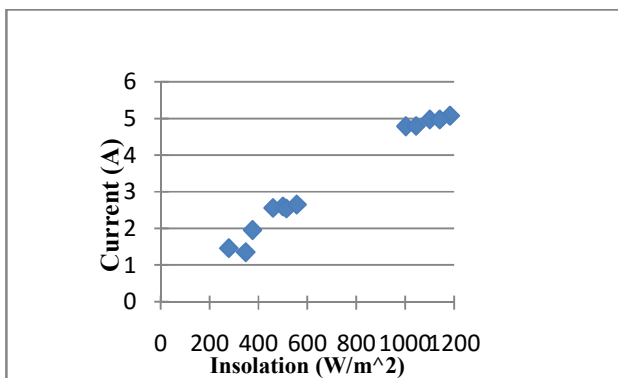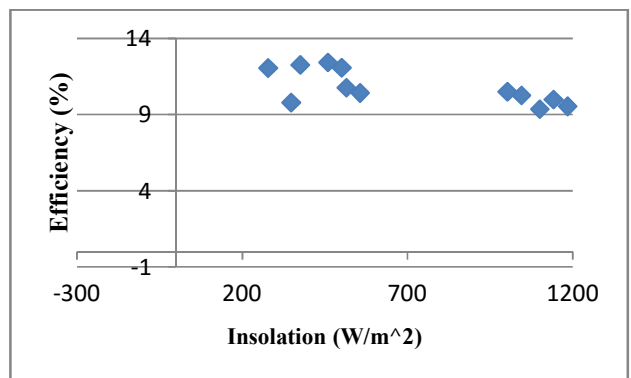**Fig. 3** Current vs. Insolation in Amorphous
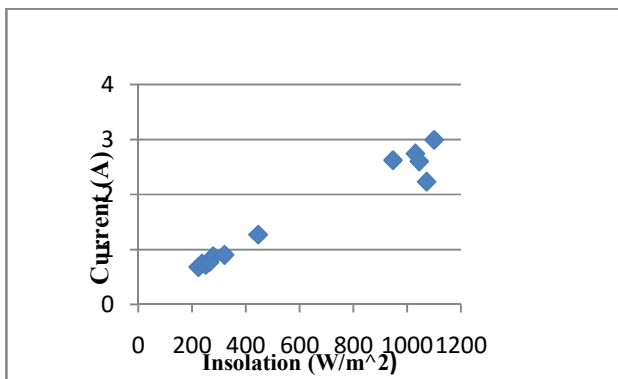

Fig. 4 Efficiency vs. Insolation in PC

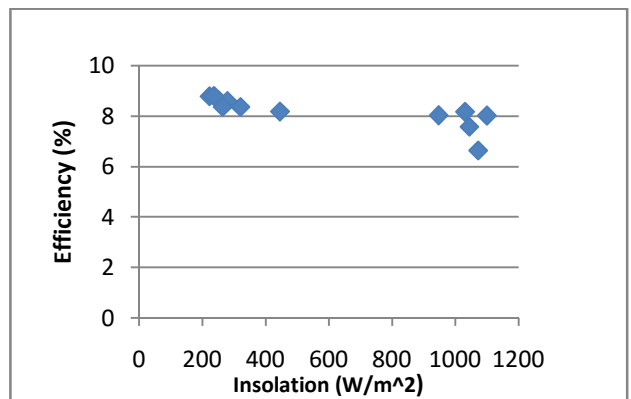**Fig. 5** Efficiency vs. Insolation in MC

Fig. 6 Efficiency vs. Insolation in Amorphous

It can be seen from Figs. 1-3 that there is a direct proportionality between current and irradiance. It is understandable as the current is depending on solar insolation that absorbed by the panel as formulated in equations 1 and 4. When the insolation is increasing, it increases the number of carriers in the cell junction thus the current is also increased and resulted in high current of the panel as well. Figures 4-6 show the relation between efficiency and insolation, where the efficiency is relatively constant against the insolation although it may have a weak dependency on insolation. The average efficiency of MC, PC and amorphous panel are: 10.8%, 8.4%, and 8.2% respectively.
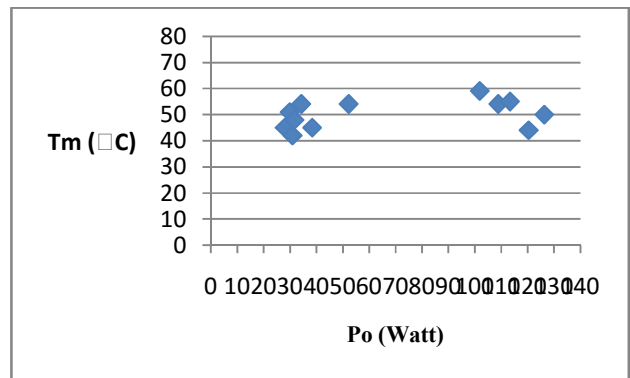
Fig. 9 T_m vs. P_o in Amorphous
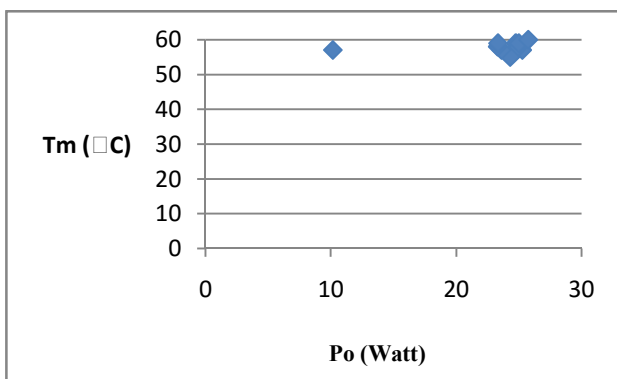
Fig. 7 T_m vs. P_o in PC
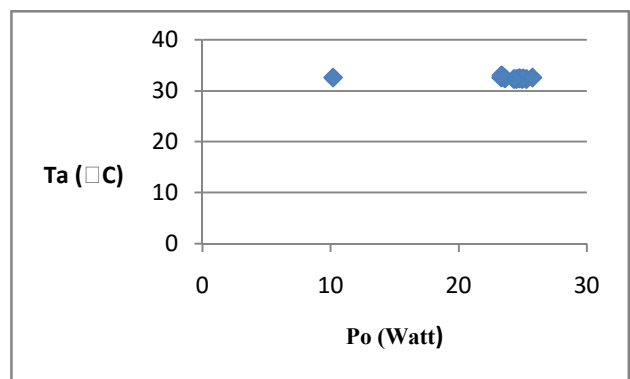
Fig. 10 T_a vs. P_o in PC
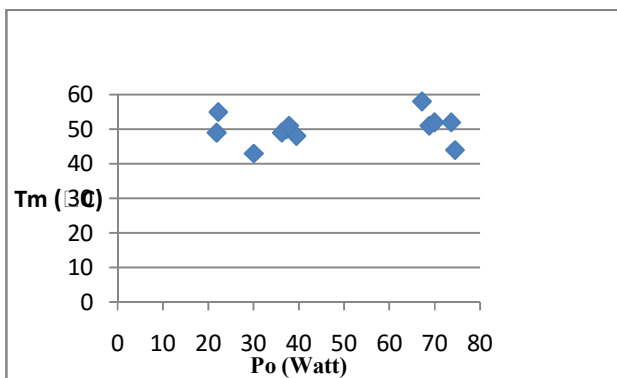
Fig. 8 T_m vs. P_o in MC
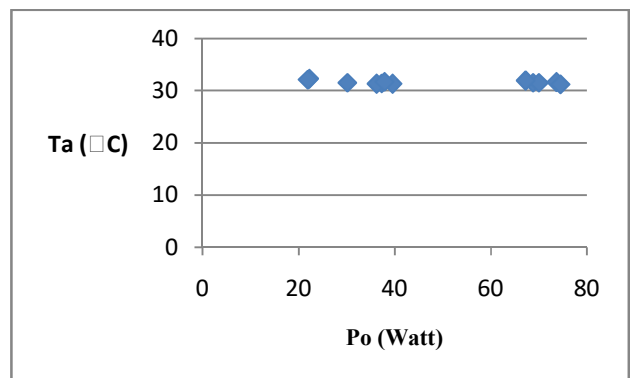
Fig. 11 T_a vs. P_o in MC
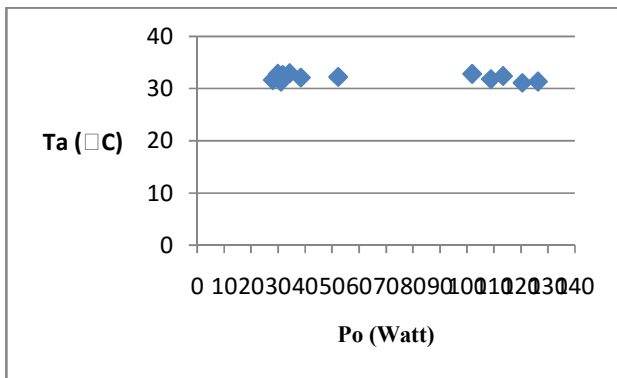
Fig 12: T_a vs. P_o in Amorphous

In Figs 7-12 are the relation between the output power of the panels and the module temperature T_m and the ambient temperature T_a. There is no drastic change in ambient and panel temperature during short interval time. The scatter of the data in the figures is due to sudden change of the weather (cloudy) and hence irradiance decrease.

The panels produce highest output when the T_a was at 32.6°C, 31.2°C and 31.3°C for PC, MC and amorphous panel respectively, while the T_m was at 60°C, 44°C and 50°C. The operating panel temperature for MC i.e. 44°C in this study is not different much with the result from Omubo-Pepple,V.B. et.al, i.e. 43°C.

4. Conclusion

The present study shows that there is a direct proportionality between solar irradiance, output current and efficiency of the PV module. Higher temperature does not always contribute to the higher performance of the photovoltaic module in the present condition.

References

1. Tsai, H.L.: Insolation-oriented model of photovoltaic module using Matlab/Simulink, Elseiver, Solar Energy 84, 2010.
2. Gonzales-Longatt,F.M.: Model of Photovoltaic Module in Matlab[TM], II CIBELEC 2005, 2005.
3. Petreus, D., Farcas, C., Ciocan, I.: Modelling and Simulation of Photovoltaic cells, Acta Technica Napocensis, Vol.49, no.1, 2008.
4. Wenham, S. R., Green, M.,A., Watt, M. E., and Corkish, R.: Applied photovoltaics, 2nd ed., pp. 3-21, 2007.
5. Sanusi, Y.K., Fajinmi, G.R. and Babatunde, E.B.: Effects of ambient temperature on the performance of a photovoltaic solar system in a tropical area, The pacific journal of science and technology. Vol. 12, No. 2, pp. 176-180, 2011.
6. Omubo-Pepple, V.B., Israel-Cookey, C. and Alaminokuma, G.I.: Effects of temperature, solar flux and relative humidity on the efficient conversion of solar energy to electricity, European Journal of Scientific Research., Vol. 35, No. 2, pp. 173-180, 2009.

License Plate Recognition Using Image Processing

[*1]Olga Maria de Sousa, [*2]Hiroki Yoshida

[*1]Department of Electrical and Electronics Engineering, Universidade Nacional Timor Lorosa'e

[*2]Department of Electrical, Electronic and Computer Engineering, Gifu University, Japan

Abstract: License plate detection is an important task that has application in various areas, especially in traffic and security applications. In this research, morphological filtering, template matching and character recognition are used to detect and recognize the license plate in image. Image reconstruction is also used to reconstruct and enhance the image in order to obtain the higher accuracy of detection rate. The output of this research is to record all the history of visitors and travel time of vehicles in a database. Based on this recording data, we can control the entry and exit time of a car, especially a car of an institutions.

Keywords: License plate recognition, morphological filtering, template matching, character recognition

1. Introduction

The research of license plate recognition (LPR) have been done and implemented in many countries, especially in advanced countries. This work has applications in various areas such as: for traffic controlling, automation access control, law enforcement and security system. Since the vehicles number plate of every country is different, it is always challenging to deal with this task.

In recent years, the applications of LPR have been developed and invented for a lot of purposes. Most applicable LPR research purpose is on vehicle controlling, monitoring and management system. It can be used to control and monitor the date and time of vehicle entry and exit, counting incoming and outgoing vehicles into a workplace.

A number of algorithms for License plate recognition have been proposed by many researches [1-4]. Morphological operation [5-7] is one of simple and useful method. The work of LPR based on morphology analysis was presented by Phalgun Pandya and Mandeep Singh [8] to recognize number plate in India. Morphological opening and closing, skew correction and template matching were used for character extraction and recognition. Another work of LPR was also presented by M. M. Rashid et al. [9]. In this work LPR was implemented for automatic parking management system and parking fee collection based on vehicle number plate. The parking and billing system are operated based on image processing of recognizing number plates.

In dealing with license plate number recognition and detection, template matching and optical character recognition [13-14] are two well-known methods that widely use for LPR researches. Divya gilly and Dr. Kumudha raimond [10] used template matching for license plate recognition. This system is only used to detect license plate at front view and rear view.

Another efficient technique of license plate recognition was introduced by Suprokash Dey, et al., [11] recently. The license plate was recognized by using morphological edge detection and character matching algorithm. This system was mainly designed to detect real time license plate in India.

Automatic license plate recognition system was also designed by Ms. Ankita Lad and Mr. Dhaval Patel [12]. This proposed method used optical character recognition method based on image processing to detect, segment and recognize vehicle license plate. The system is implemented in MATLAB and focuses on Indian standard number plate.

In this paper, a number of existing methods are evaluated to be used for designing a license plate recognition system. Edge detection, morphological analysis, character recognition and template matching are used to detect and recognize license plate in image. This study is done to be implemented on entrance and exit gate of an office or university (campus). The implementation plan is illustrated in Fig. 1.
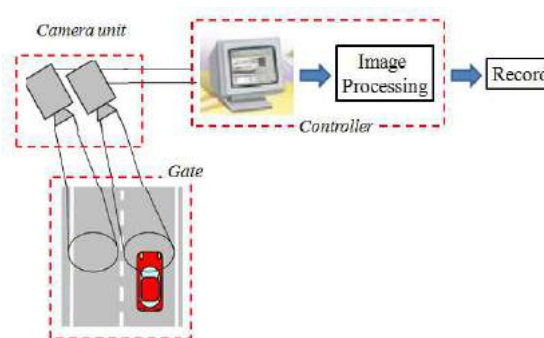

Fig.1 Implementation illustration

The rest of the paper is organized as follows. Section II describes the method of license plate recognition used in this research. The experimental result and discussion is given in section III and the paper is concluded in section IV.

2. Method

In this research, morphological filtering, optical character recognition and template matching are used to recognize license plate in image. The system uses unit camera to take the image of the front or rear of the vehicle. The captured image will be applied preprocessing step to obtain a better image. Then image processing is used to analyze the images and extracts the plate information. After the plate's numbers are extracted, character recognition is applied to get the result or output. At final step, the result is recorded or storage in database including the time of entry and exit of a car. The frameworks of this work is shown in Fig. 2.
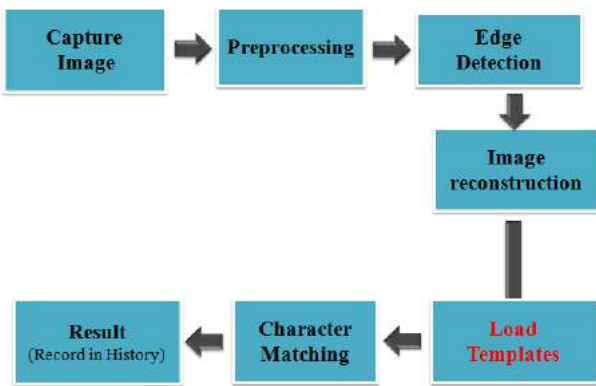
Fig.2 The LPR system framework

(1) Capture image

This research uses input image that captured by camera. The captured image is RGB image, then it is converted into grayscale image before applying preprocessing. One sample of used images is shown in Fig.3.

(a)   (b)
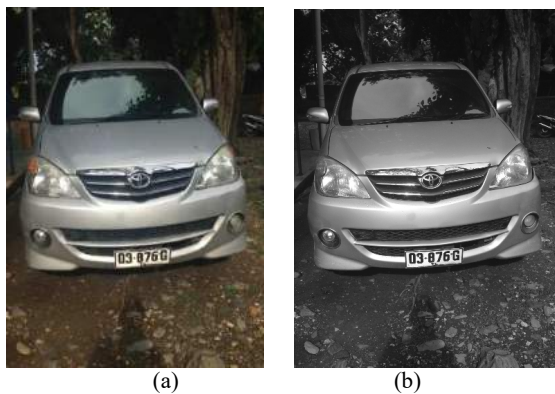
Fig.3 Sample image, (a) Original, (b) Grayscale
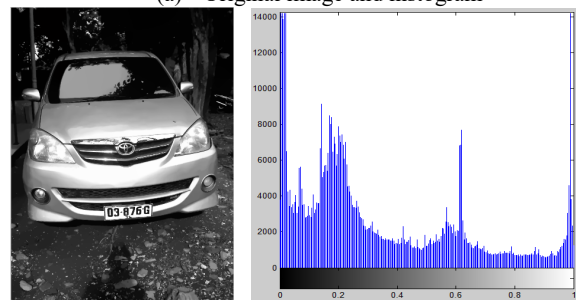
(2) Preprocessing

In preprocessing step, a few process were performed in order to obtain a good recognition result. The important tasks that are done in this stage are: image enhancement, image filtering and smoothing. The image is enhanced by adjusting its contrast and equalizing its histogram. After enhancement, filtering and smoothing is performed to

obtain a better image. In this case, wiener filtering and L0 smoothing [15] are used.
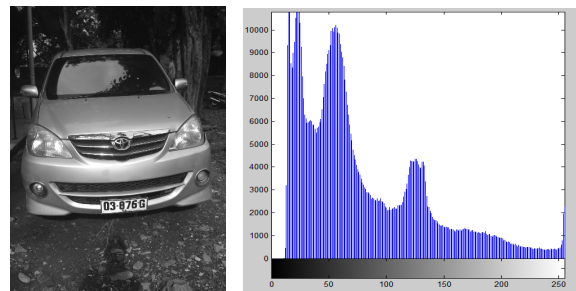
(a) Original image and histogram

(b) Preprocessed image and histogram

Fig. 4 Preprocessing result

(3) Edge detection

Canny operator is one of edge detection techniques that is widely use in image processing. This method uses two thresholds to detect strong and weak edges. In this research, in order to detect the edge of object in image, the threshold is set to low threshold: 0.2 and high threshold: 0.4. Fig.5 shows the result of canny edge detection.

Fig. 5 Canny edge detection

(4) Image reconstruction

In this step morphological analysis is used to reconstruct the image. Region filling, object labeling and dilation operation are performed to obtain desired region only and eliminate undesired object.

- Region filling: is to set 0 regions inside connected component with 1.

- Object labeling: is to label every connected component
- Dilation operation: is used to thick labeled region referred on structuring element.

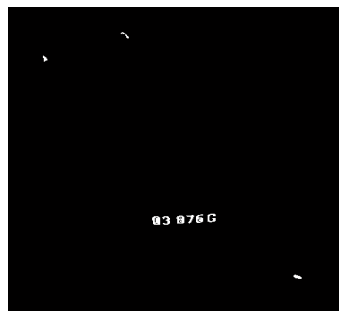In order to obtain a better result, the reconstruction is repeatedly done for few times.

1. **Step 1**:
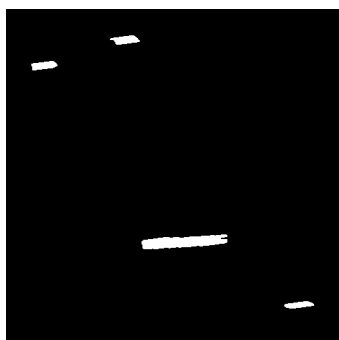
Region filling → object labeling → dilate image

In this step, the connected component area less than 100 and greater than 500 are eliminated. The result of this process is shown in Fig.6.
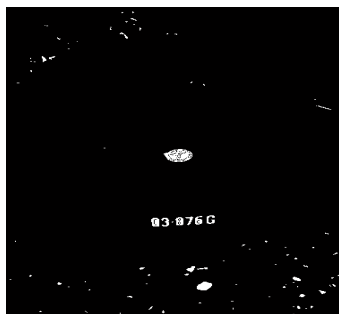
(a)Filled region

(b)Elimination undesired region

(c)Dilated image

Fig 6 The result of first reconstruction step

2. **Step 2**:

In this step, the same process in step 1 is done and the areas greater than 3200 are eliminated. The remained region is the location of plate number (Fig. 7).

Fig. 7 The result of reconstruction step 2

3. **Step 3**:

Object labeling → crop plate location → erode

The step 3 performs object labeling that will label the remained region in image. Then image is cropped to keep only the labeled region. Erode operation is applied to return the binary image as shown in Fig. 8.

Fig. 8 Eroded image

4. **Step 4**:

In order to obtain good shape of license plate character, region filling and dilate operation are performed again in this step. The result of reprocessed is shown in Fig. 9.

Fig. 9 Result of step 4

(5) Character matching

The character is matched based on template matching method. Fig.10 shows samples template of some alphabet and number that are manually prepared from threshold image with 42 x 24 sizes of template images.

Fig. 10 Samples of template images

Based on template, the license plate will be recognized. To match the prepared template, the plate number image is resized into 42 x 24 as shown in Fig. 11.

Fig. 11 Resized image

3. Experimental results

In this research, the experiments is done using MATLAB. The result of character recognition is shown in Figures bellow (Fig. 12).
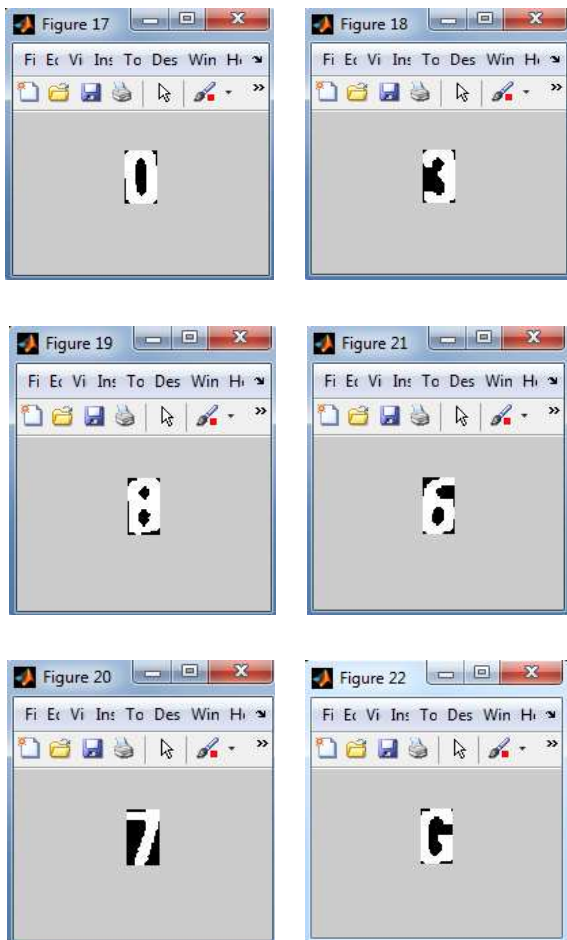

Fig. 12 Character recognition results

After the characters are recognized, then the matrix of image is converted into word to be saved. The result of the word is stored in word file. This storage data consist of vehicle plate number and travel time of entry and exit time vehicles into office or campus. This information will be stored in database and easily to collect when it is required

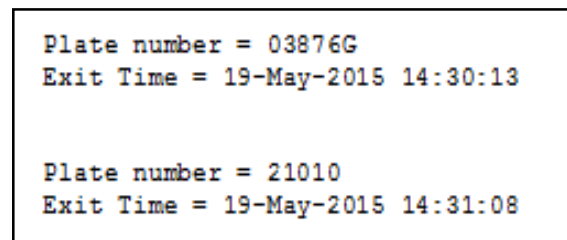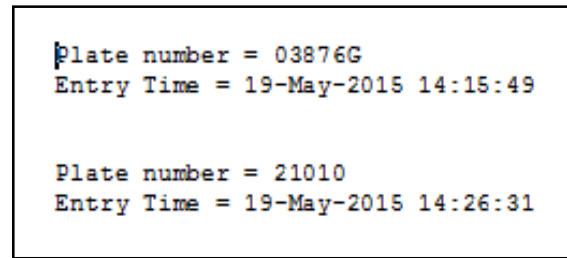to be analyzed. Fig. 13 shows the result of stored information in word file.


```
Plate number = 03876G
Entry Time = 19-May-2015 14:15:49


Plate number = 21010
Entry Time = 19-May-2015 14:26:31
```

```
Plate number = 03876G
Exit Time = 19-May-2015 14:30:13


Plate number = 21010
Exit Time = 19-May-2015 14:31:08
```

Fig. 13 result of stored information in word file.

4. Conclusion

This research is used simple method to recognize license plate number. By using edge detection, morphological analysis, character recognition and template matching can design a vehicle monitoring and recording system. This system is simple but it has an important application. It can be used to control the driver behavior and regulate indiscipline driver.

In this research, the experiments is done on still images. For future plan, this system will be developed to be implemented for real time video monitoring.

5. Acknowledgement

Reference

1. Leonard G. C. Hamey, Colin Priest, 2005. Automatic number plate recognition for Australian conditions, *Proceedings of the Digital Imaging Computing Techniques And Applications (DICTA)*.

2. Karishma K. Jage, Gauri D. Joshi, and Shradhadevi S. Nair, (2013). Algorithm for automatic license plate recognition applied to parking section, *International Journal of Eng. Research & Tech. (IJER)*, vol. 2.

3. Shishir Kumar, Shashank Agrawal and Kumar Saurabh, (2008). License Plate recognition system for indian vehicles, *International Journal of Information Technology and Knowledge*, vol. 1.

4. Prathamesh Kulkarni, Ashish Khatri, Prateek Banga, and Kushal Shah, (2009). A Feature Based Approach for Localization of Indian Number Plates, *IEEE International Conference on Information Technology*, pp: 157-162.

5. Velappa Ganpathy and Wen Lik Dennis LUI, (2008). A Malaysian Vehicle License Plate Localization and Recognition System, *Journal of Systemics, Cybernetics and Informatics*, vol. 6.

6. C.Nelson Kennedy Babu, Krishnan Nallaperumal, (2008). A License Plate Localization using Morphology and Recognition, *In Proceedings of India Conference*, vol. 1, pp.34 – 39.

7. P. V. Suryanarayana, Suman K. Mitra, Asim Banerjee and Anil K. Roy, (2005). A Morphology Based Approach for car license Plate, *IEEE Indian 2005 Conference, Chennai, India*, pp. 24-27, 11-13.

8. Phalgun Pandya, Mandeep Singh, (2011). Morphology based approach to recognize number plates in India, *International Journal of Soft Computing and Eng. (IJSCE)*, vol.1, pp. 107-112.

9. M. M. Rashid, A. Musa, M. Ataur Rahman, N. Farahana and A. Farhana, (2012). Automatic parking management system and parking fee collection based on number plate recognition, *International Journal of Mach. Learning and Computing*, vol. 2, pp. 93-98.

10. Divya gilly and Dr. Kumudha raimond, (2013). License plate recognition – a template matching method, *International Journal of Eng. Research and Applications (IJERA)*, vol. 3, pp. 1240-1245.

11. Suprokash Dey, Amitava Choudhury and Joydeep Mukherjee, (2014). An efficient technique to recognize license plate using morphological edge detection and character matching algorithm, *Int. Journal of Comp. Applications*, vol. 101, pp. 36-41.

12. Ms. Ankita Lad and Mr. Dhaval Patel, (2015). Automatic license plate recognition using optical character recognition based on image processing, *IJARIIE*-ISSN(0)-2395-4396, vol. 1, pp. 65-70.

13. Er. Kavnet Kaur and Vijay Kumar Banga, (2013). Number plate recognition using OCR technique, *Int. Journal of Research in Eng. And Technology*, vol. 2, pp. 286-290.

14. Ng Simin and Florence Choong Mei, (2013). Automatic car-plate detection and recognition system, *EURECA*, pp. 113-114,

15. Li Xu, Cewu Lu, Yi Xu and Jiaya Jia, (2011). Image smoothing via L0 gradient minimization, *ACM Transanction on Graphics,* vol. 30.

Robust Digital Control of DC-DC Converter at Laboratory Electronic and Electrical Department

Tarcisio Freitas Savio

Department of Electrical and Electronics Engineering, Universidade Nacional Timor Lorosa'e

Abstract: Robust DC-DC Converter is required torespond extensive load variation and input voltage variation. We proposed an approximate 2DOF digital control, which realizes the start-up response and dynamic load response independently. It makes band width wider and the output voltage more stable for variation of load and input voltage. It is actually implemented on a DSP connected to a DC-DC converter.

Keywords: Robust Digital Control, 2DOF digital control, DSP

1. Introduction

Robust DC-DC converter for extensive variationof load and input voltage is needed. Then demand to suppress output voltage changes becomes severer. We proposed an approximate 2 DOF digital controller, which realizedstartup response and dynamic load response independently. Ithad wide control bandwidth and variations of the output voltage fortheir sudden changes. In this study,the approximate 2DOF digital control system has additional zeros.The third-order differential transfer characteristics were applied for equivalent disturbances and output voltages.This controller is implemented on a DSP with connection to a DC-DC converter. Experimental results demonstrate that this type of digital controller can satisfy severe requirementsat low samplingfrequency.

2. Design Of Dc-Dc Converter

2.1 DC-DC converter

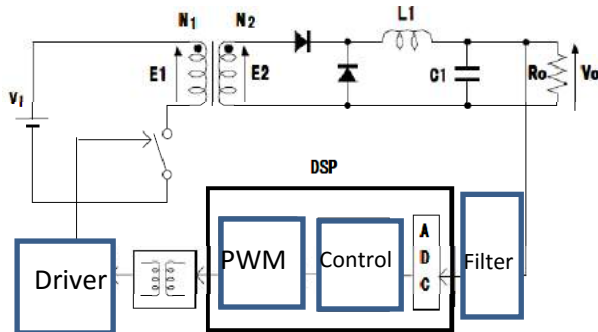The block diagram of the approximate 2DOF controller with a DC-DC converter is shown in Fig.1.

Fig. 1 Brock **diagram of a** DC-DC converter

To realize the controller, we used aDigital Signal Processor (DSP), TMS320F28335 manufactured by Texas Instruments. It has a built-in AD converter and a Pulse Width Modulation (PWM) switching signal generator attriangle carrier frequency of 100[KHz].The discrete-time state equation of the systemwith a zero-order hold is express as

$$\dot{x}(t) = A\ x(t) + b\ u(t) \quad y(t) = C\ x(t) \quad (1)$$

where

$$x = \begin{bmatrix} Vo \\ i_{L1} \end{bmatrix}, \quad A = \begin{bmatrix} -1/R_o(C_1 + C_0) & 1/(C_1 + C_0) \\ -1/L_1 & -R_1 L_1 \end{bmatrix},$$

$$B = \begin{bmatrix} 0 \\ Gp/L1 \end{bmatrix}, \quad C = \begin{bmatrix} 1 & 0 \end{bmatrix}, \quad G_p = \frac{R_L}{R_0 + R_L} \times \frac{V_{in}}{TBPRD}$$

and total resistance of coil and driver FET R_o.

$$x_d(k+1) = A_d x(k) + B_d v(k) \quad (2)$$

$$y_d(k) = C_d x_d(k) \quad (3)$$

$$A_d = \begin{bmatrix} e^{AT} & \int_{T-L}^{T} e^{A\eta} bd\eta \\ 0 & 0 \end{bmatrix}, B_d = \begin{bmatrix} \int_0^{T-L} e^{A\eta} bd\eta \\ 1 \end{bmatrix}$$

$$C_d = \begin{bmatrix} C_c & 0 \end{bmatrix} x_d = \begin{bmatrix} x & \xi_1 \end{bmatrix}^T \xi_1 = u$$

The third-order differential characteristics from disturbances qu and qy. Connected four series delays considering input delay time, conversion of current feedback and additional zeros as shown in Fig. 2.
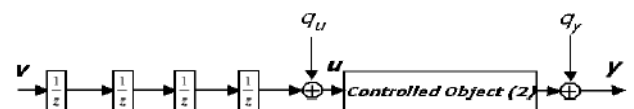

Fig.2 Control object with 4 input delay elements

2.2 The model matching system

We consider transfer function between thereference input r and the output y specified as

$$W_{ry} = \frac{(1+H_1)(1+H_2)(1+H_3)(z-n_1)(z+n_2)(z+H_4)(z+H_5)(z+H6)}{(1-n_1)(1-n_2)(z+H_1)(z+H_2)(z+H_3)(z+H_4)(z+H_5)(z+H6)} \quad (4)$$

Robust system is constituted with inverse system and filter as shown in Fig.**3.** If an equivalent conversion of the controller is carried out, the approximate 2DOF digital integral-type control system will be obtained as shown in **Fig.4**. The transfer functions of itis shown in Fig.4are

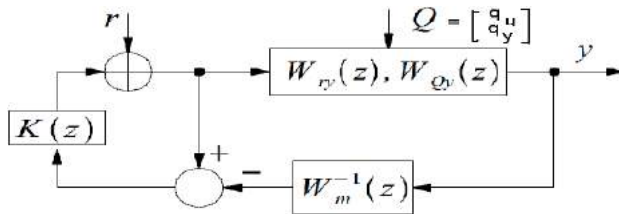$$y \approx \frac{1+H_2}{Z+H_2}r, \quad y \approx \frac{(z-1)^3}{z-1+k_z}\overline{W_{Qy}}Q \quad (5)$$
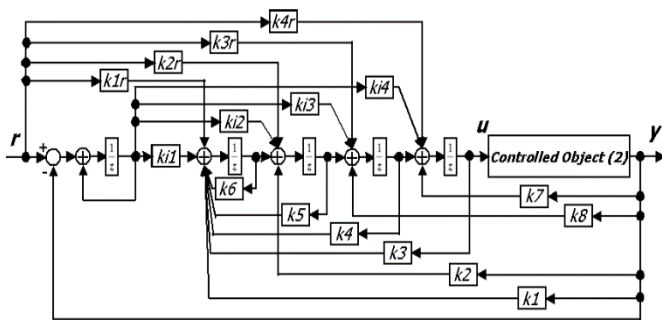

Fig.3 Robust system with filter

Fig.4 Approximate 2DOF digital control system

2.3. Experimental results

The sampling period T is set 10[us]. The nominal value of RL is 0.33[ohm].The control system satisfiedthe specificationsof the rising time of the startup transient response.The sensitivity function of second-order differential disturbance plotted in Fig.5is -40[db/dec] as averaged over frequency disturbances characteristics.
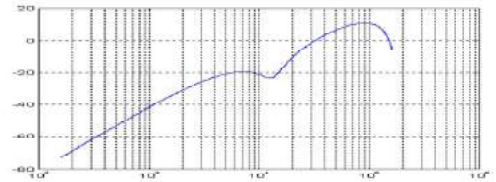

Fig.5 Sensitivity function of second-order differential disturbance characteristics.

The experimental results of startup response are shown in Fig.6. The dynamic load responses are shown in Fig.7 and Fig.8. The output voltage change of the second-order differentiation with Fs= 100[KHz] is suppressed within about 40[mV]. The output voltage change of the first-order differentiation with Fs= 400[KHz] is suppressed within about 50[mV]. This means that using low frequency Fs, the output voltage changes can be suppressed.
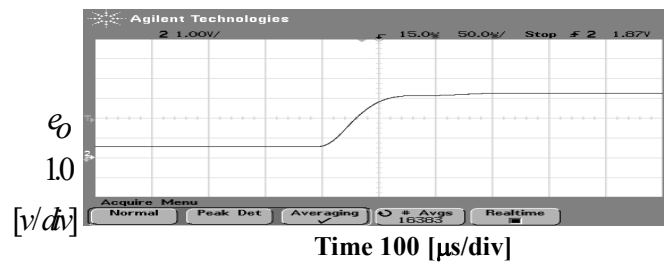

Time 100 [μs/div]

Fig.6 Experimental results of the startup responseof the second-order differential disturbances characteristics with Fs=100[KHz]

Time 200 [μs/div]
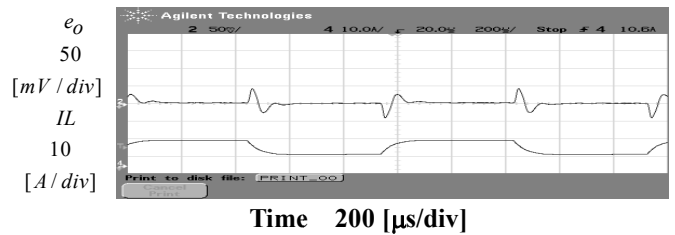
Fig.7 Experimental results of dynamic load responseofthe second-order differential characteristics with Fs=100[KHz] .
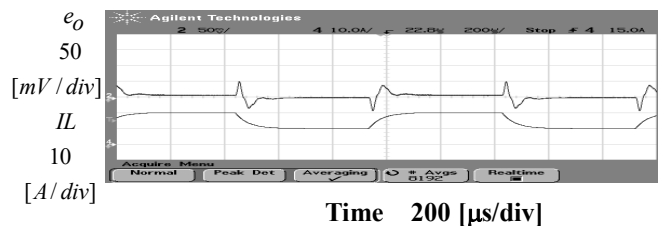

Time 200 [μs/div]

Fig.8 Experimental results of dynamics load response ofthe first-order differential disturbances characteristics with Fs=400[KHz].

Fig.9 The Manufactured new quarter brick DC-DC Converter

3. Conclusion

In this research, the design of the robust control system with the differential characteristics transfer functions of disturbances was shown. By the simulation and experimentalresults,a robust digital control system can be realizedatlow sampling frequency.

References

1. E. Takegami, K. Higuchi, K. Nakano, K. Watanabe, S. Tomioka, "The Method For Determined Parameters of Approximate 2DOF Digital controller for Robust Control of DC-DC Converter," ECTI-CON2005,pp.593-596, 2005.

2. H.Fukuda and M. Nakaoka, state-vector Feedback Controlled-based 100KHz Carrier PWM Power Conditioning Amplifier and its High Precision Current-Tracking Scheme" IEEE IECON' 98,pp.1105/1110 (1993)

3. H.Guo, Y. Shiroshi and O. Ichinkura," Digital PI Controller for High frequency Switching DC-DC Converters Based on FPGA" IEEE INTELEC' 08,536/541(2003)

LSI Implementation of a Secure Low-Power CSSAL Cellular Multiplier

[*1]Cancio Monteiro,[*2]Yasuhiro Takahashi,[*2]Toshikazu Sekine

[*1]Department of Electrical and Electronics Engineering, National University of Timor Lorosa'e
[*2]Department of Electrical, Electronic and Computer Engineering, Gifu University, Japan

Abstract In this paper, a secure and low-power charge-sharing symmetric adiabatic logic cellular multiplier over $GF(2^4)$ implemented in LSI using 0.18 μm CMOS process is presented. The verification of the logic functionality and the operating speed of the implemented LSI in adiabatic switching technique will be discussed. The correlation of LSI output logic function and the supply current trace are measured in order to analyze the current-to-data dependency in respect to the given input transitions. Maximum power clock frequency for chip measurement is 5 MHz, whereas the post-layout simulation is up to 50 MHz and the pre-layout simulation reaches 125 MHz using the same individual logic.

Key words adiabatic, bit-parallel multiplier, SCA, cryptographic

1. Introduction

Finite field arithmetic plays an important role in modern coding theory and practical application of cryptographic system [1],[2]. From the view point of the cryptographic hardware implementation, one of the main issues is related to the security of processed information by side-channel analysis (SCA) attacks. The SCA attacks, such as differential power analysis (DPA) [3] and differential electromagnetic analysis (DEMA) [4] have become a crucial challenge for cryptographers and hardware engineers to maintain the secrecy of private information in cryptographic implementation, such as in smart card. The main factors of aforementioned attacks are related to the occurrence of CMOS logic power consumption when input data flip, and required operational time of cryptographic hardware itself. In counteracting to the SCA attacks, the various novel works on the cell level have been implemented, and the strongest among those logic circuits is the three-phase dual-rail pre-charged logic (TDPL) [5]. The TPDL was implemented in a conventional CMOS logic operation that causes the high spike current occurrence and huge energy consuming. Consequently, the DPA and DEMA attacks are a bit difficult to avoid. Hence, the authors of this paper have designed a secure logic with low peak current transition and low energy consumption by employing an adiabatic switch principle [6]. Few papers on secure adiabatic logic have been published which referred to this work, such as 2N-2N2P [7], and symmetric adiabatic logic (SyAL) [8]. The SyAL has achieved low power and high resistance

to DPA attacks as stated, however, the throughout evaluation in the pre-layout simulation level [9] found out that the SyAL still perform certain different current values for every input transition. In this work, the fabricated LSI multiplier over $GF(2^4)$ in 0.18 μm CMOS process using the proposed charge-sharing symmetric adiabatic logic (CSSAL) is measured. The comparison of the circuit speed of the pre-layout, post-layout and the fabricated chip are also discussed in the following chapters.

2. Adiabatic Logic Approach in a Secure Logic Implementation

2.1 Imperfection in Existing Logic Style

As shown in Fig. 1(a), Static Complementary CMOS (sc-CMOS), which the simplest and default inverter logic in the standard cell library used for security IC's only consumes energy from the power supply when its input has a 1–0 transition. At this transition, a high instantaneous supply current occur, as can be observed in Fig. 1(a). During the 0–1 input transition, the energy previously store in the output capacitance is dissipated, and it supposes to be no supply current flow, but there are still some small current flowing because of the short circuit during input state transition of PMOS and NMOS simultaneously. Moreover, there is no supply current profile during 1–1 and 0–0 transitions. Hence, scCMOS performs data dependence, because current signal is drawn only at pull-up network (PUN), means circuit is connected to power supply which we consider as current-to-data dependency. Solution for current-to-data dependency against
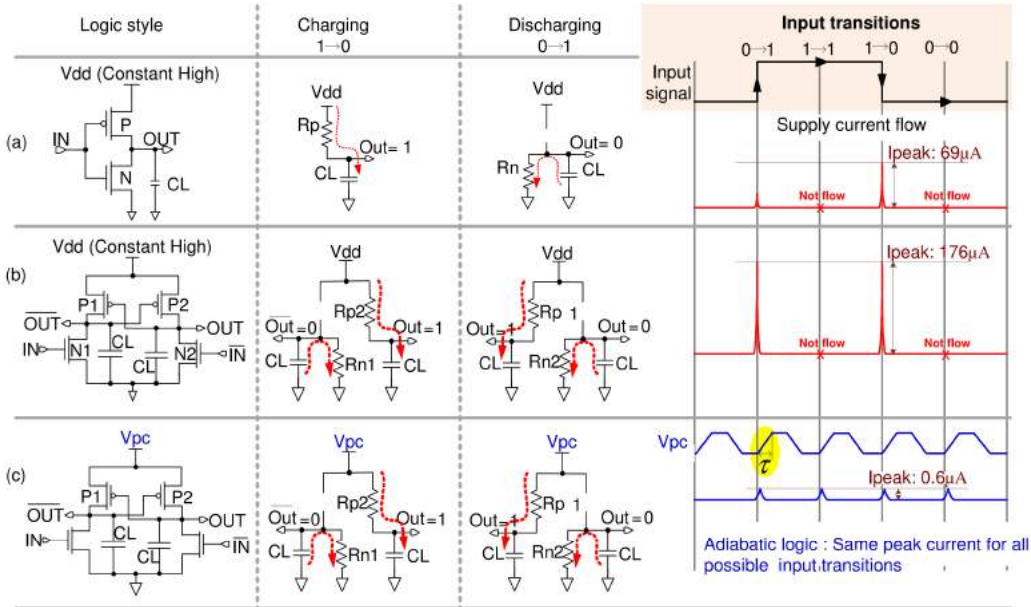
Fig. 1   Comparison of the transitional supply current traces; (a) scCMOS, (b) DR CMOS
logic, and (c) DR adiabatic logic.

SCA attacks, most of the recent secure logic styles are implemented in a complementary dual-rail (DR) logic style in order to balance charging and discharging loads as depicted
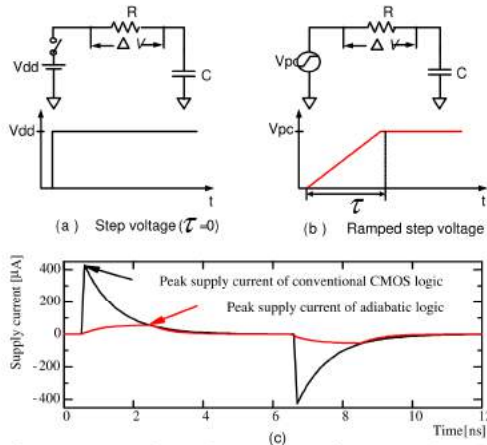

Fig. 2   Comparison of supply currents for equivalent RC models of CMOS logic ((a) step voltage) and adiabatic logic ((b) ramped step voltage). (c) The peak supply current of adiabatic logic is significantly lower than the conventional CMOS logic under the same parameters and conditions.

in Fig. 1(b). Subsequently, both of the 0–1 and 1–0 transitions produce balanced supply current trace. However, either the scCMOS or the complementary DR logic consumes no power during 1–1 and 0–0 transitions. Consequently, the Hamming distance model always possible. Hence, in order to make all output transitions become invisible from the view point of the peak current differences, we then implement our proposed logic in adiabatic logic technique by supplying trapezoidal power clock signal instead of constant V_{dd} in

DR CMOS logic style. By doing this, all possible input transitions produce similar and very low-peak supply current as shown in Fig. 1(c).

2.2   Adiabatic Logic Technique

The principle of adiabatic charging can be understood by contrasting it with the charging of a capacitor in an equivalent RC circuit for the conventional CMOS method. In the conventional CMOS circuit, the load capacitance C is charged from 0 to V_{dd}, where V_{dd} is the voltage of the constant DC power supply. During the charging period of the conventional CMOS in Fig. 2(a), the energy charged into the capacitor is:

$$E_{charge} = \frac{1}{2}CV_{dd}^2. \tag{1}$$

From the perspective of energy conservation, a conventional CMOS logic emits heat and thus wastes energy with every charging–discharging cycle with the following equation:

$$E_{total} = E_{charge} + E_{discharge} = \frac{CV_{dd}^2}{2} + \frac{CV_{dd}^2}{2} = CV_{dd}^2. \tag{2}$$

If the logic is driven with a certain frequency $f(= 1/T)$, where T is the period of the signal, then the power consumption of the CMOS gate is determined as

$$P_{total} = E_{total}/T = CV_{dd}^2 f. \tag{3}$$

The power consumption of the conventional CMOS is proportional to V_{dd}^2, thus, one of the most effective ways to reduce its power consumption is to lower the power supply voltage V_{dd} or reducing the load capacitance.

Adiabatic switching is commonly used in minimizing the energy lost during a charging or discharging period. The

main idea of adiabatic switching is shown in Fig. 2(b), which indicates a transition that is considered sufficiently slow that heat is not significantly emitted. This is made possible by replacing the DC power supply with a resonant LC driver or a trapezoidal power-clock voltage waveform. If a constant current source delivers a charge $Q = CV_{dd}$ during the time period τ, the energy dissipation in the channel resistance R is given by:

$$E_{Adiabatic} = \xi P\tau = \xi I^2 R\tau$$
$$= \xi \left(\frac{CV_{dd}}{\tau}\right)^2 R\tau, \qquad (4)$$

where I is considered as the average of the current flowing to C, and ξ is a shape factor that is dependent on the shape of the clock edges. Observing the adiabatic switching equation, the charging period τ is indefinitely long, and therefore energy dissipation is ideally reduced to nearly zero [6].

From the logic's security view point, it assumes that, if the individual logic, such as AND and XOR are able to consume an uniform and low-peak current, regardless of the input logic transitions, then, their implementation in a more complex digital circuit will be more secure against leakage of information processed to DPA or DEMA attacks. We make this assumption become possible by adopting the adiabatic logic technique as shown in Fig. 2(c). This figure shows a comparison of peak supply current for equivalent RC models of the conventional CMOS logic and the adiabatic logic. The instantaneous peak supply current of the adiabatic logic is significantly lower than that of the conventional CMOS logic style.

3. Investigation of the Proposed CSSAL and its Implementation in a Bit-Parallel Cellular Multiplier over $GF(2^4)$

3.1 Secure Logic Investigation

Evidently shown in Fig. 1(c) that, the DR inverter logic with trapezoidal power clock supply produces similar and lowest peak current. However, with the extension of the gate structure for AND or XOR functions using universal DR pull-down network (DR-PDN) tree will cause a predictable of input data regarding to the visible different supply current trace per input transition. Therefore, the input gate of CMOS structure should be put into the proper design for balancing the energy consumed for all possible input-output transitions. The proposed CSSAL achieves this goal by (a) implementing a secure logic in an adiabatic operating mode and by (b) implementing a proposed logic with special charge-sharing in symmetric pull down network tree, which more detail logic operation can be found in Ref. [9].

For verification of the proposed CSSAL in secure logic implementation, we investigate and compare with other con-

ventional secure logic styles, such as 2N-2N2P, TDPL, SyAL from the point view of equivalent RC model at PDN when input condition of (A,B) is (1,1), (0,1), (0,0), and (1,1). The conventional 2N-2N2P and the TDPL are implemented in universal DR-PDN tree which remain some floating internal charges as depicted in Figs. 3,4; consequently, various energy consumption occur for every transitional of input function. Moreover, the SyAL was implemented in symmetric input logic style with charge-sharing technique, however, during the active evaluation phase, floating charges exist as shown in Fig. 5.

In the proposed CSSAL, the logic operation starts by setting all internal node capacitances to ground level when the discharge ($Dischg$) and Input signals are such that $V_{Dischg}, V_{In/\overline{In}} \geq V_{THN}$ before the power clock signal arrives. This makes our proposed logic balances the low-peak supply current traces, which a unique different from SyAL technique. We prove it by the pre-layout and the post-layout simulation for NAND/AND individual logic in all dual-input 16-possible transitions that, the proposed CSSAL exhibits only a single line with low-peak current trace for 16 different data as depicted in Fig. 7.

3.2 Secure Logic Implementation

The targeting logic cell in this work was proposed in a cellular architecture [1] which has explored the inner-product multiplication algorithm to compute the function of AB+C into a low-complexity and less computation time cellular architecture in a class field $GF(2^m)$. There are several definitions described and arithmetic calculation have been done to define cellular array multiplication of $GF(2^m)$ where $m = 4$ to calculate the function block of the bit-parallel multiplier over $GF(2^4)$. Similar architecture proposed in [2] for computing AB^2+C which is also suitable for LSI implementation for cryptosystem; however, it has the drawback of high circuit complexity and requires more computation time per cell.

The multiplier circuit architecture is depicted in Fig. 8. The complexity of inner cell includes one 2-input AND gate and one 2-input XOR gate with the logic depth from each primary input line to the output line is symmetrically $m + 1$ basic cells. The complexity of cellular multiplier over $GF(2^m)$ includes $(m + 1)^2$ identical cells.

For the purpose of comparison study, we have implemented the proposed CSSAL logic and the 2N-2N2P, SyAL and the TDPL into the multiplier circuit in Fig. 8. Each circuit layout has designed in a full custom design using cadence virtuoso IC6.1 as shown in Fig. 9.
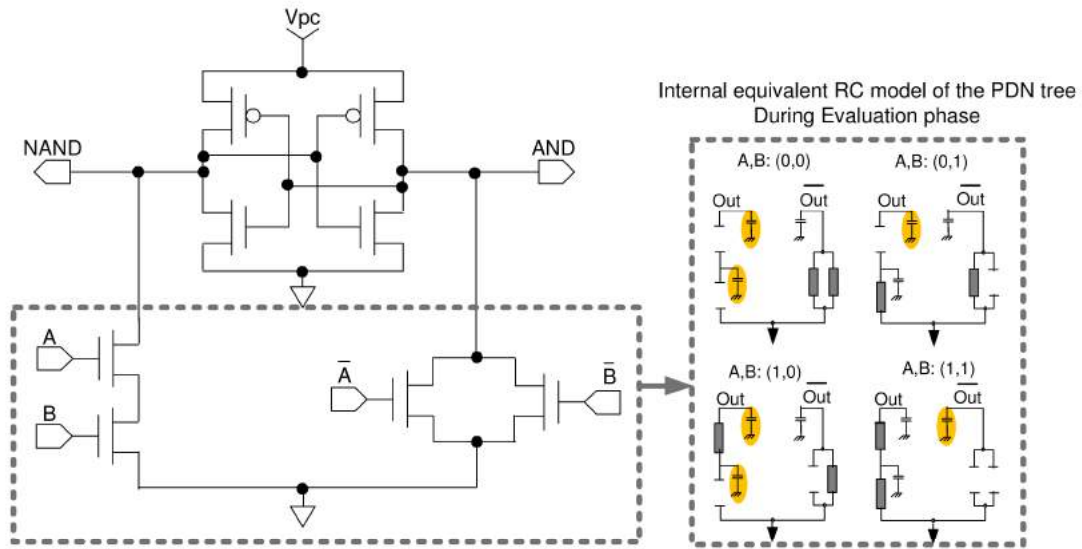
Fig. 3 Conventional 2N-2N2P NAND/AND logic structure and its internal equivalent RC model at pull-down network tree. The yellow marked color is the floating capacitor at each pull-down network condition.
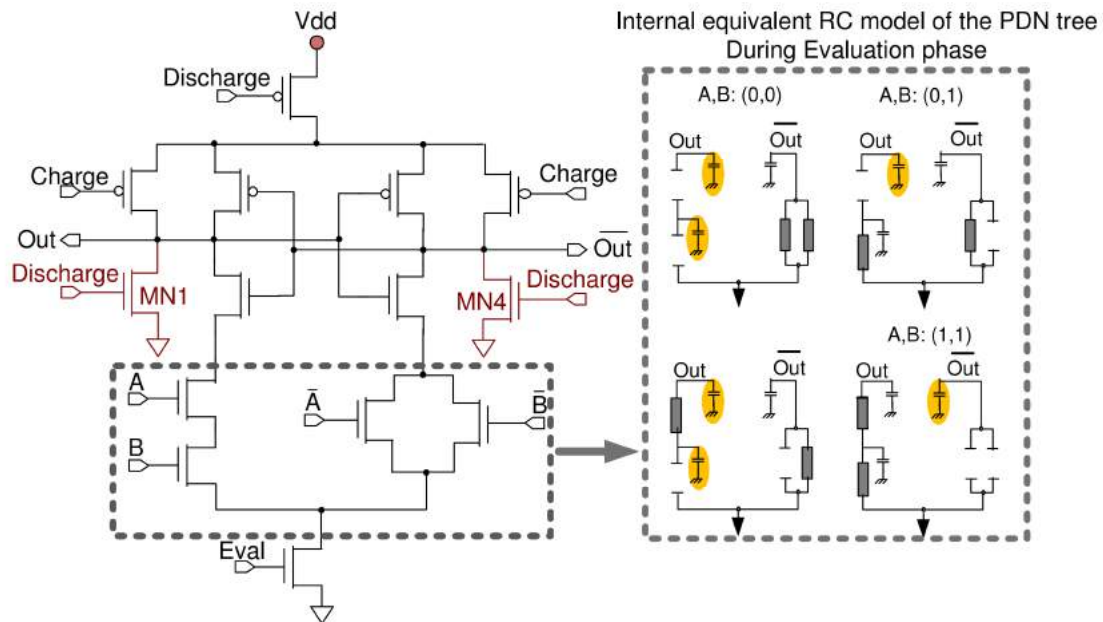

Fig. 4 Conventional TDPL NAND/AND logic structure and its internal equivalent RC model at pull-down network tree. The yellow marked color is the floating capacitor at each pull-down network condition.

4. Simulation and Result

4.1 Simulation Condition

The evaluation provided in this paper was made using the post-layout SPICE simulation with a 0.18 μm, 1.8 V standard CMOS technology. The input signals of proposed CSSAL, SyAL and 2N-2N2P multiplier circuits are all trapezoidal waveforms with adiabatic power clock frequency range from 1.25–50 MHz. On the other hand, the TDPL is supplied with constant 1.8 V of V_{dd}, and the input discharge, charge, evaluation signals' dynamic frequency are 1.25–50 MHz as well. The previous work in [9] reported the pre–layout simulation with active power clock frequency range is 1.25–125 MHz. However, the more accurate information provided in this work shown that the maximum speed of our proposed CSSAL multiplier is 50 MHz. Moreover, the DPA and DEMA attacks analyze the peak current differences and the supply current amplitude to reveal the secret-key during encryption and decryption; hence, our contribution is to analyze the various instantaneous peak supply currents and the various energy consumption per input transition, which will be summarized in the following subsection.
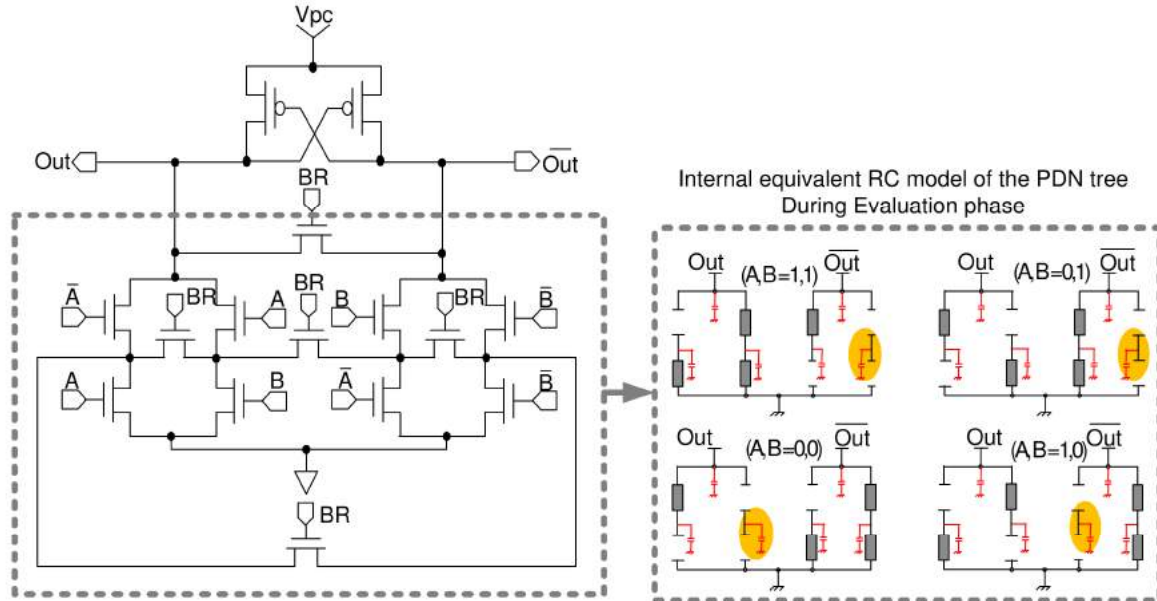
Fig. 5 Conventional SyAL NAND/AND logic structure and its internal equivalent RC model at pull-down network tree. The yellow marked color is the floating capacitor at each pull-down network condition.
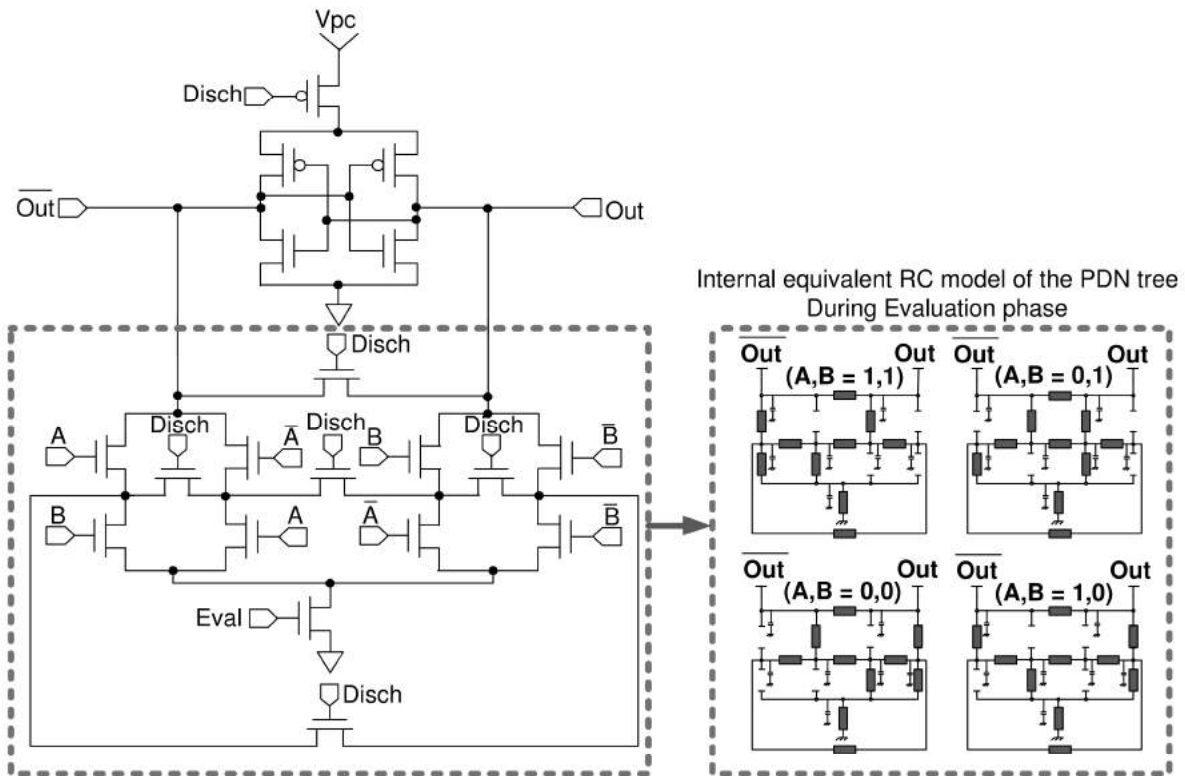

Fig. 6 Proposed CSSAL NAND/AND logic structure and its internal equivalent RC model at pull-down network tree.

4. 2 Results

The comparative results from the security view point are summarized in Table 1. The data of power consumption of each circuit are drawn as:

$$E_{diss} = \int_0^T V_{pc(dd)}(t) I_{pc(dd)}(t) dt, \qquad (5)$$

which is adopted as figure of merit to measure the resistance against power analysis attacks. The calculation for normalized energy deviation (NED) is defined as

$$NED = (E_{max} - E_{min})/E_{max}, \qquad (6)$$
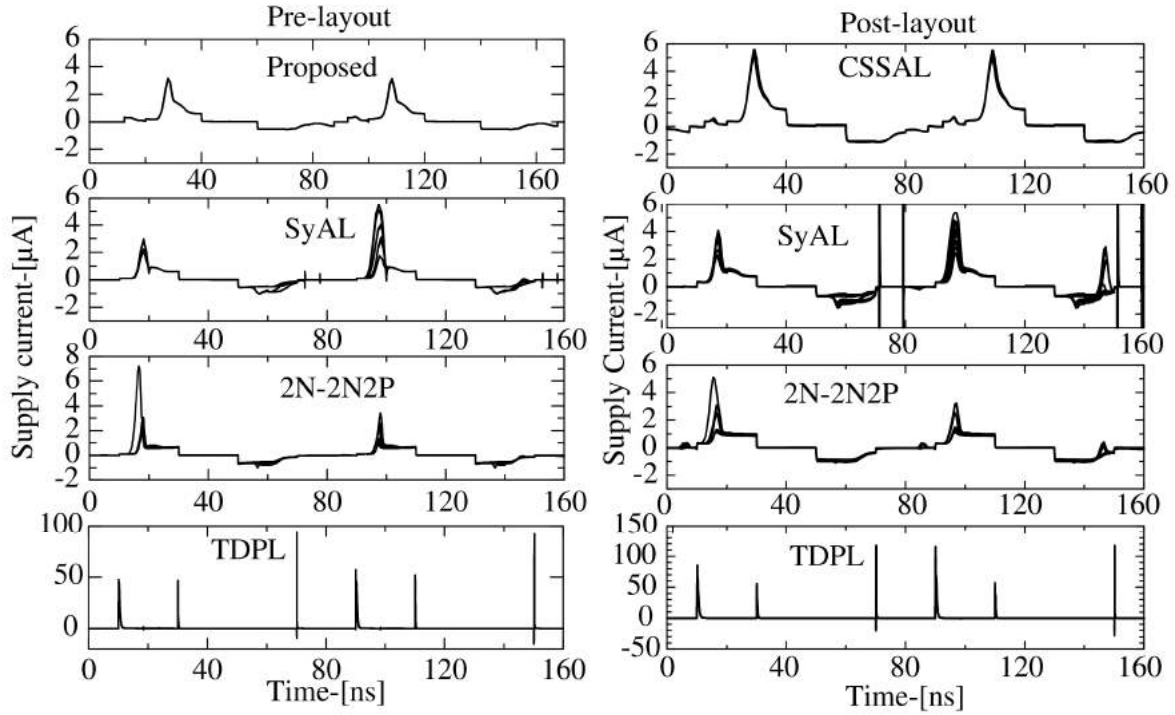
and normalized standard deviation (NSD) [4] is

Fig. 7   Pre-layout and post-layout supply current transition of NAND/AND individual logic at 12.5 MHz power clock frequency.

Gate Counts and Chip Area				
Logics	Proposed CSSAL	2N2N2P	SyAL	TDPL
NAND/AND	19	8	15	14
XNOR/XOR	19	10	15	16
Multiplier	950	450	750	750
Multiplier Chip area (μm^2)	172x155	150x140	110x158	183x173

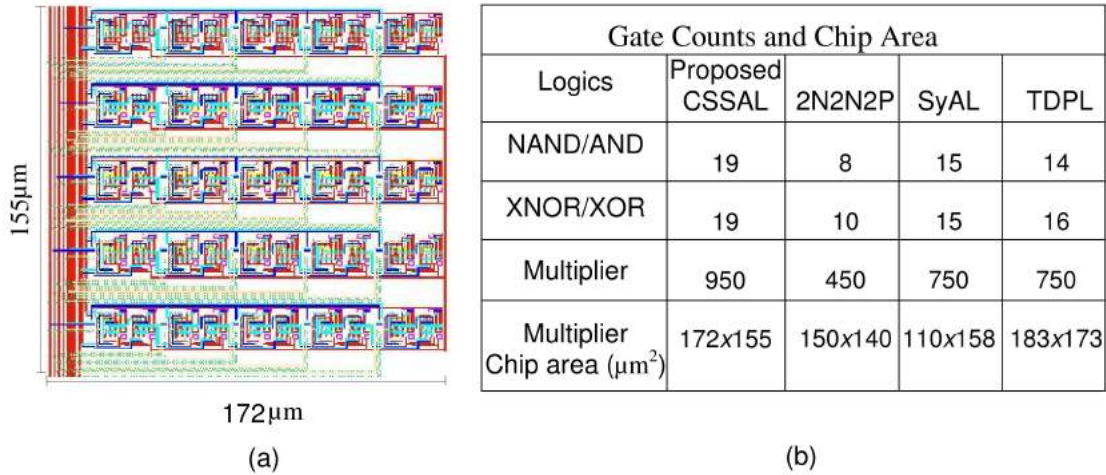(a)   (b)

Fig. 9   Layout of the circuit structure in Fig. 8; (a) The representative layout of the CSSAL multiplier, (b) Comparison table of the gate counts and the chip area of the CSSAL, 2N-2N2P, SyAL and the TDPL.

$$NSD = \sigma_E / \overline{E} \qquad (7)$$

The $\overline{E}$ is the average of energy dissipation over every respective transition, and the standard deviation is define as:

$$\sigma_E = \sqrt{\sum_{i=E_1}^{E_n} (E_i - \overline{E})^2 / n}. \qquad (8)$$

We measure the parameters of NED and NSD which means the ability of the logic resistance against power analysis attack. An important property of NES and NSD explain that the consumed energy is more constant for different input

transition if we achieve more small values. Hence, by observing the result in Table 1, the proposed CSSAL and the conventional SyAL exhibit their ability at low frequency range, because they have the smallest values of NED and NSD at 1.25 MHz. In addition, the SyAL becomes superior at 12.5 MHz power clock frequency. Conversely, the TDPL multiplier is performing its ability at high frequency band. Moreover, the data in Table 1 demonstrate that the 2N-2N2P has drawback in consuming various energy for every input transition.

Apart from the logic ability for resistance against SCA at-

Table 1   The post-layout simulation and the calculation results of the bit-parallel cellular multiplier over $GF(2^4)$ at 1.25 MHz, 12.5 MHz, 50 MHz power clock frequency for the CSSAL, SyAL, 2N-2N2P, and the TDPL multiplier, respectively.

| | Power variation of cellular multiplier over $GF(2^4)$ | | | | | | | | | | | |
| | 1.25 MHz | | | | 12.5 MHz | | | | 50 MHz | | | |
	Proposed	SyAL	2N-2N2P	TDPL	Proposed	SyAL	2N-2N2P	TDPL	Proposed	SyAL	2N-2N2P	TDPL
E_{min} [pJ]	0.4	0.39	0.045	7.04	0.65	0.50	0.08	6.9	0.94	0.27	0.14	6.97
E_{max} [pJ]	0.46	0.46	0.81	35.44	1.24	0.68	0.98	9.61	2.63	1.77	1.91	7.44
$\overline{E}$ [pJ]	0.43	0.43	0.47	14.31	0.88	0.58	0.57	7.67	1.04	1.52	1.09	7.04
σ_E [pJ]	0.015	0.02	0.23	8.4	0.21	0.04	0.79	0.27	0.58	0.36	0.55	0.18
NED [%]	12.04	14.17	94.45	80.13	47.33	26.38	92.13	28.18	64.19	84.51	92.57	8.7
NSD [%]	3.49	4.69	49.08	58.71	24.48	6.93	48.05	10.27	38.06	34.60	50.45	2.49
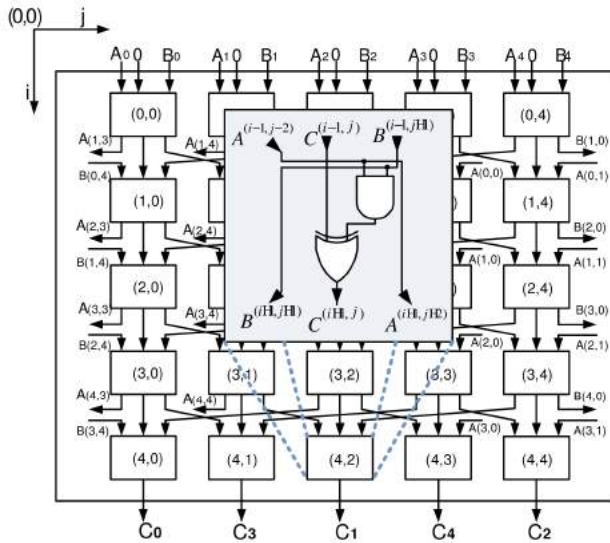
Fig. 8   Configuration of bit-parallel cellular multiplier over $GF(2^4)$.

tacks, the power reduction is also one of the research targets. It is obviously described by the graphical information in Fig. 10 that our proposed CSSAL multiplier has significant energy reduction about nine times lower than that of the TDPL multiplier at 12.5 MHz. On the other hand, in comparison with SyAL and 2N-2N2P, the gate counts of the proposed CSSAL is higher as shown Fig. 9(b); thus, they consume a bit low energy than that of the proposed CSSAL at $\geq$5 MHz power clock frequencies. However, as we indicate in the time expansion from 0.125–5 MHz in the Fig. 10 that the CSSAL has lowest energy than the others.

5.   Measurement and Verification

Photomicrograph of the fabricated LSI bit-parallel cellular multiplier over $GF(2^4)$ is shown in Fig. 11. The LSI measurement result of the input and output signals at 1.25 MHz power clock frequency is shown in Fig. 12. In this measurement technique, we have insufficient available laboratory equipment, thus we combined the connection of the input signals in Fig. 8 as $In1 = \{A0, A1, A2, A3, A4\}$ and the

$In2 = \{B0, B1, B2, B3, B4\} = 1$ (constant V_{dd}); accordingly, the output voltage of a multiplier $\{C0, C1, C2, C3, C4\}$ are correctly produced as $InA \times InB = Out = 1$. To the best of our knowledge, the DPA and DEMA attacks, both are revealing the secure information by statistically analyzing the key dependent differences from the peak current/power differences by respective measurement techniques. Therefore, in this work, we have also measured the Vpc supply current as shown in the bottom of Fig. 12 that the peak current is uniformly plotted which may resistive to DPA and DEMA attacks.

6.   Discussion

We have present here the SPICE simulation results of the pre-layout and the post-layout operating speed, and the power variation in different secure logic style. Then, we have measured the fabricated LSI that the maximum logic speed is decreased to 5 MHz, while the maximum speed of the post-layout is up to 50 MHz and the maximum speed of the pre-layout was up to 125 MHz. Based on the thoroughly investigation results, we have identified that the layout design performance has a great influence in determining the circuit speed, its power consumption and even for logic resistance for SCA attacks. For example, at 12.5 MHz power clock frequency, the pre-layout has 3.32 % of NSD and 5.38 pJ/cycle [8]; however, with the internal impedance of RC extraction of the post-layout simulation resulted 24.48 % of NDS and 14.04 pJ/cycle in the same logic speed. Furthermore, the less accurate equipment for generating the input signals in our measurement also affected the degradation of the maximum logic speed.

7.   Conclusion

In this paper, we have presented the proposed logic operating speed in pre-layout, post-layout and the verification of the fabricated LSI chip. The layout design performance has a great influence in determining the circuit speed, its power
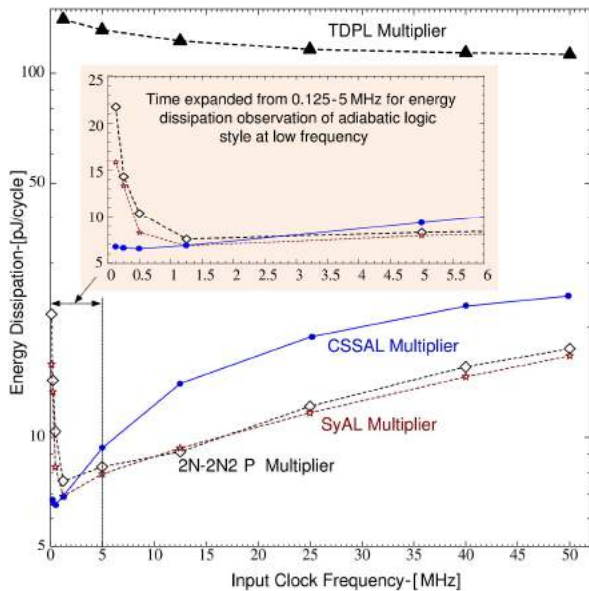
Fig. 10 Simulated post-layout energy dissipation comparison of the bit-parallel cellular multipliers over $GF(2^4)$ in respect to the different input clock frequencies.
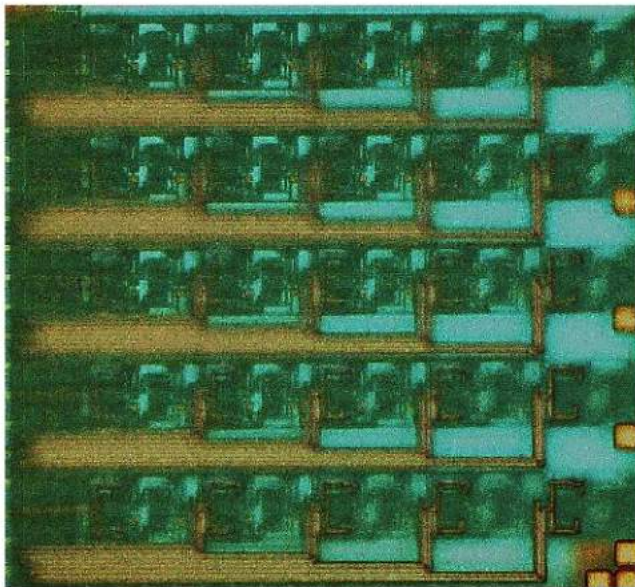

Fig. 11 Photomicrograph of the bit-parallel cellular multiplier over $GF(2^4)$.

consumption and even for logic resistance for SCA attacks. The SPICE simulation has indicated that our proposed logic is resistive and performs power efficiency at low frequency band.

References

1. C.H. Liu, N.F. Huang, and C.Y. Lee, "Computation of AB^2 multiplier in $GF(2^m)$ using an efficient low-complexity cellular architecture," *IEICE Trans. Fundamentals*, vol. E83-A, no. 12, pp. 2657–2663, Dec. 2000.
2. C.Y. Lee, E.H. Lu, and L.F. Sun, "Low-complexity bit-parallel systolic architecture for Computing $AB^2 + C$ in a class of finite field $GF(2^4)$", *IEEE Trans. on Circuit and System–II*, vol. 48, no. 5, pp. 385-393, May 2001.
3. P.C. Kocher, J. Jaffe, and B. Jun, "Differential power analysis", in *Proc. of 19th Int L Advances in Cryptology Conf.–*
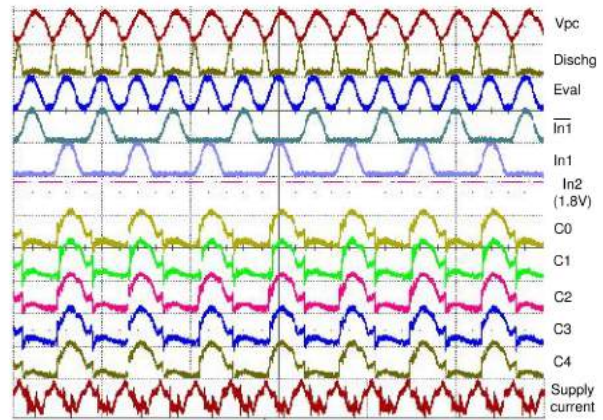
Fig. 12 Measurement result of the bit-parallel cellular multiplier over $GF(2^4)$ at 1.25 MHz power clock frequency. Vertical scale: 2 V/div. Horizontal scale: 2 μs/div.

CRYPTO'99, pp. 388–397, 1999.
4. E. De Mulder, S. B. Ors, B. Preneel, and I. Verbauwhede, "Differential electromagnetic attack on an FPGA implementation of elliptic curve cryptosystems", in *Proc. of WAC'06*, pp. 1–6, Budapest, 24–26 July 2006.
5. M. Bucci, L. Giancane, R. Luzzi, and A. Trifiletti, "Three-phase dual-rail pre-charge logic", in *Proc. Workchop on Cryptographic Hardware and Embedded Systems*, pp. 232–241, Yokohama, Japan, Oct. 10–13, 2006.
6. W. C. Athas, L. J. Svesson, J. G. Koller, N. Traztzanis and E. Y.-C. Chuo, "Low power digital system based on adiabatic switching principles", *IEEE Trans. VLSI System*, vol. 2, no. 4, pp. 398–406, Dec. 1994.
7. A. Kramer, J. S. Denker, B. Flower and J. Moroney, "2nd order adiabatic computation 2N-2P and 2N-2N2P logic circuits", in *Proc. of Int. Symp. on Low Power Design*, pp. 191–196, New York, USA, 1995.
8. B.D. Choi, K. E. Kim, K.S. Chung, and D. K. Kim, "Symmetric adiabatic logic circuits against differential power analysis", *ETRI Journal*, vol.*32*, no.1, pp.*166–168*, *Feb.*2010.
9. C. Monteiro, Y. Takahashi, and T. Sekine, "DPA Resistance of charge-sharing symmetric adiabatic logic", in *Proc. of IEEE ISCAS'13*, Beijing, China, May 19–23, 2013